UNIVERSITÀ DEGLI STUDI DI
CASSINO E DEL LAZIO MERIDIONALE

Corso di Dottorato in
Metodi, modelli e tecnologie per l'ingegneria

Curriculum: Ingegneria elettrica

Ciclo XXXIII

The i-motor: a system for end-of-line testing of electric drives for vehicles

Coordinatore del Corso
Chiar.mo Prof. (Wilma Polini)

Dottorando
(Yassine Boukadida)

Supervisore
Chiar.mo Prof. (Fabrizio Marignetti)

Contents

List of Tables

List of Figures

Acknowledgement

The works synthesized in this dissertation have been developed within a trilateral collaboration involving the University of Cassino and Southern Lazio (Italy), the University- of Sfax (Tunisia), and Loccioni Group (Italy).

I am grateful to God for the good health and wellbeing that were necessary to complete this project.

I would like to express my deep gratitude to Professor Fabrizio Marignetti from the University of Cassino and Southern Lazio, who gave me the opportunity to work under his supervision in Cassino (Italy). I am grateful to him for the valuable discussions, the endless support and availability during the crucial periods of my PhD.

I would like to thank Professor Ahmed Masmoudi from the university of Sfax, who welcomed me in the Laboratory of Renewable Energies and Electric Vehicles (RELEV) and accepted to supervise my works from the Tunisian side, beyond his intensive activities.

I would like to thank Professor Roberto Di Stefano from the University of Cassino and Southern Lazio, for his support and his availability during my research activities.

Special thanks are addressed to the Loccioni Group staff, especially Mr Gino Romiti who is the innovation director and Mr Alessandro Bastari, Mr Vincenzo Fiengo and Irene Luciani for their great interest in my works. Their comments have had a great impact on the scientific merit of my PhD project.

I could not forget the friendly moments I spent with many members of the LEI research group, especially Mr Paolo Conte and Mr Guido Robino .

I express my thanks to professor Rosario Miceli and professor Mohamed Wissem Naouar for agreeing to review my thesis.

My deep gratitude is expressed to professor Lotfi Krichen and professor Giuseppe Tomasso who respectively-accepted to be the president and examinator of the defence Jury of my PhD.

Finally, I would like to express my love and gratitude to my family for its understanding, inspiration, love, and endless support, all along my study years.

General Introduction

During the last decades, in response to the alarming climatic changes caused by the global warming phenomenon, the automotive industry is required to contribute its part by reducing vehicle-based CO_2, by developing new propulsion systems, in the attempt to assist or substitute the internal combustion engine ICE by an electric motor, yielding the to hybrid or the electric propulsion systems.

Within this trend, automotive industries, in collaboration with academic institutions, have been involved in research and development (R&D) projects mainly oriented towards the design of novel propulsion systems and the optimization of their performances during driving cycles, with an emphasis on energy efficiency and the dynamic behaviour.

This increasing demand and the rapid development of the electrification of vehicles and the importance given to energy efficiency lead to the implementation of increasingly complex systems. The complexity of such systems makes them physically hard, time-consuming, and financially costly to be conventionally tested. Especially in power electronics devices where complex circuit and fast operating switches are common.

To overcome these challenges, simulation tools have always been used as a recognized way to develop prototypes, and they are part of all design cycles of all engineering areas. For several years, simulation systems have migrated to the so-called Real-Time (RT) simulations making it possible to couple real devices with simulators. Allowing the exchange of signals between simulations and real components in order to perform test operations. This type of system, is commonly known as Hardware-In-the-Loop (HIL) which allows not only to test the real components, but also their robustness with respect to real constraints.

HIL Simulation refers to the methodology of testing a subsystem where the actual subsystem is hooked up to a simulation environment where the rest of the system is simulated. This methodology is especially useful when it is difficult, expensive, or even impossible to develop a real experimental testing prototype. The HIL technique eliminates the hazards involved in actual testing and the system response to extreme procedures can be safely tested. HIL testing is hence being increasingly adopted in the automotive industry and in several research fields.

Electric and hybrid vehicle powertrains are basically composed of one or more machines, one or more gearboxes, one or more power electronic converters, and an embedded power supply source such as a battery pack. The powertrain operates under tough driving conditions in terms of torque, dynamics, and thermal conditions. Its operation must be evaluated on the basis of standard driving cycles. For such applications, inverters are being asked to fulfil different roles and there is a growing need to decrease the size and cost while increasing the power output. For the sake of achieving high performances, inverter manufacturers need simple and reliable End-of-Line (EOL) testing systems to assess the powertrain functionalities.

The objective of this work is to provide a technical solution for EOL testing of an EV drive through an experimental setup able to predict the drive operation under close-to-real conditions.

From a topological point of view, test benches for the validation of inverters for electric propulsion can be classified into two major configurations. The first, which represents the traditional solution, uses a rotating system consisting of an electric motor mechanically coupled to a brake or a generator emulating the load, resulting in the so-called “dyno test bench”. The second alternative, which is less common, considers a power electronic load emulating the electric machine used to perform test operations in a virtual environment. The dyno test bench is widely used because it is generally considered closer to reality. However, this solution provides lower cost-effectiveness and limited flexibility. While the electric machine emulator test solution is safer, cheaper, space effective, it requires less maintenance and offers more flexibility when testing different drive motors and loads.

The proposal of this dissertation falls in the second class. It overcomes the above limitations by operating the electric powertrain in real driving conditions, although in a virtual environment, minimizing both power loss and cost.

Some previous attempts focused on the machine emulation employing an electronic load performing the electrical validation of a power converter. Instead, in this work, a new HIL test system for electric drives for automotive applications is proposed. The load used in this work is a standard drive controlled in RT emulating at its terminals an electric motor driving the wheels of a vehicle. The control system includes not only the motor model, but also the vehicle and road dynamics, providing the system with the capacity to emulate the real operating conditions of the vehicle during a driving cycle. The vehicle model adds flexibility to the system in comparison to other similar solutions, allowing to implement any kind of EV and road condition by changing the RT emulator parameters.

This has been achieved within a joined PhD program between the University of Cassino and Southern Lazio (Italy) and the University of Sfax (Tunisia). In collaboration with LEDA srl (Italy) and Loccioni Group (Italy)

The developed works are synthesized in the present dissertation which is structure in four chapters, as follows:

- The first chapter is aimed at a state of the art regarding the HIL real-time simulation. It provides an overview of the HIL technique, a special attention is paid to the description of its general architecture, main categories, and advantages. It also presents a literature review exploring the historical development of HIL method and its usage in various sectors such as aircraft, aerospace, and automotive industries.

- The second chapter introduces the importance of test beds in the automotive industry and the main existing configurations of inverter test beds. It presents a literature review of the HIL electric machine emulator test method, and proposes a new motor emulator, dedicated to build a new inverter test bed solution. Then, It describes the architecture of the proposed machine emulator, and provide the analysis of the system aiming to minimize the current ripple in the emulator terminals.

- In the third chapter, a new HIL automotive drive test system is developed and implemented. The NI PXI tool is used to control the electric machine emulator described in the second chapter. A control system includes a motor model and a vehicle dynamics model is implemented in the PXI, in order to provide the control signals to the power system, to reproduce the motor terminal behaviour in the two directions of the power flow, corresponding to the acceleration and regenerative braking. Therefore the test system provides a virtual environment suitable to perform test operations on the inverter under test.

- In the fourth chapter, the potentialities of the developed bench are highlighted through the analysis of the test results obtained considering the emulation of different driving cycles. Tow case studies are operated, and the results are provided. The first case is a reduced scale testing equipment to provide a proof-of-concept to the proposed test system architecture, and the second is an industrial full-scale testing facility developed in Loccioni group.

Chapter 1

Hardware-In-The-Loop Real Time simulation: State Of The Art

Abstract : *Hardware-in-the-loop (HIL) simulation is a rapidly evolving method for control prototyping, system modelling, simulation, and testing. It provides many advantages of both physical and virtual prototyping. This chapter provides an overview of the HIL real-time simulation systems with an emphasis on its general architecture, main categories and advantages. It then describes the historical development of the HIL method and presents a literature review of HIL recent research works in numerous applications.*

Keywords : Simulation,
Offline simulation,
Real time simulation,
Hardware-in-the-loop simulation,
Virtual environment.

1.1 Introduction

Nowadays, as technology continues its rapid development, more complex systems are increasingly introduced in different technological fields. The complexity of such systems makes them physically hard, time-consuming and financially costly to be conventionally tested. Laboratory measurement equipment and digital simulation were invented to help with the design and testing of such complex systems. However, because of increasing complexity in algorithms and hardware implementation for embedded systems, digital simulations were not sufficient as the computation time of the system is simply not fast enough to provide a real-time (RT) output. Therefore, simulation systems have migrated to so-called RT simulations allowing the coupling of real devices with simulators. Such high speed calculations can be reached by utilizing hardware in the loop (HIL) simulation.

HIL is known as a prominent simulation tool before realistic tests of the system and a step after software simulation. First employments of HIL goes back to twentieth-century in flight systems. Recently, this tool has spread in different steps of system life cycle such as design, development, implementation and test of various applications including the automotive industry, aerospace, robotics etc. Utilizing a suitable HIL laboratory, in system design stages is a practical way to increase the system reliability and efficiency as well as the product's value. Also, by proper investigation in this simulation method, many errors can be avoided in the design procedure of software, hardware, and their interconnections which allows engineers to detect failures at an early development stage.

This chapter aims to introduce the state of the art of the HIL technique. An overview of the RT simulation and HIL method is introduced with emphasis on the HIL general architecture, its main categories classified according to the simulation levels, and its advantages in design and development of complex systems. A literature review exploring the historical development and various applications of HIL technique is presented. It is also tried to introduce the latest progress of this effective tool in different applications, by citing some recent works using HIL systems in research and industrial projects, and showing its large contribution in the development of different sectors in nowadays industry.

1.2 Simulation Concept for Development, Verification and Validation

During the last three decades, the evolution of simulation tools has been driven by the rapid evolution of computing technologies. As computer technologies have improved dramatically in performance, therefore the capability of simulation tools to solve increasingly complex problems in less time has improved. Furthermore, the cost of digital simulators has also significantly decreased, making them available to a huge number of users for a wider variety of applications.

From its traditional definition, simulation is the computation of a system's mathematical model in order to study its properties. It plays an important role in verifying that the concept is feasible and that the objectives of the system can be achieved during the concept development of complex systems. The simulation also helps to develop an early estimation of the size, the development effort as well as the cost and time schedule development of the system. In modern industry, it is typically required that simulation software tool should be simple, fast and could be easily adapted to analyse different scenarios in a short time.

Nowadays, simulation systems can interact differently, enabling physical connections with other systems to better address issues like actual power transfer. This implies that the simulated models will interact with real signals, making it possible to analyse different systems in an integrated environment. Therefore simulation tools need to interact with real components in RT which pushes the modern industry to use RT simulations to warranty RT communication with the real world.

1.2.1 Real-Time Simulation

Real-time simulation (RTS) of system model consists on the reproduction of input/output waveforms, with the desired accuracy, that are representative of the behaviour of the real system being modelled. To achieve such a goal, a RT simulator needs to solve the model equations for one time-step within the same time in real-world clock [1], [2], [3]. During the

simulation, time moves forward in steps of equal duration. Therefore, it produces outputs at discrete time intervals, where the system states are computed at certain discrete times and constant step duration. This is commonly known as fixed time-step simulation [2]. It is important to note that other existing solving techniques use variable time-steps during the simulation. Such techniques are used for solving high frequency dynamics and non-linear systems, but are unsuitable for RT simulation [4], [5].

In order to solve mathematical equations and functions at a given time-step, each variable or state is solved successively as a function of states and variables at the end of the preceding time-step. During a discrete-time simulation, the amount of RT needed to compute all functions and equations representing a system during a given time-step can be longer or shorter than the duration of the simulation time-step. Figure 1.1 and figure 1.2 represent these two possibilities. In 1.1, the computing time is shorter than a fixed time-step (also referred to as accelerated simulation) while in 1.2, the computing time is longer. These two cases of situations are referred to as offline simulation. In both examples, the moment at which a result becomes available is considered irrelevant. Generally, when performing offline simulation, the main objective is to obtain the simulation results as fast as possible. The speed of a system solving depends on the available computation power and the system's mathematical model complexity. Conversely, during RTS, the accuracy of computations not only depends upon precise dynamic representation of the system, but also on the length of time used to produce results [5]. Figure 1.3 illustrates the chronological principle of RTS. For a RTS to be valid, the RT simulator used must accurately produce the internal variables and outputs of the simulated model within the same length of time that its physical counterpart would. In other words, the validity of a result depends not only on its correctness, but also on the time within which it is produced taking into consideration the simulated system dynamics.

The main idea using RTS especially in control applications is to make a smooth transition from the non real analysis and simulation to the RT experiments and implementation [1]. RTS is recently used in many engineering field and applications such as: aircraft flight control design and validation, flight simulators, spacecraft development and

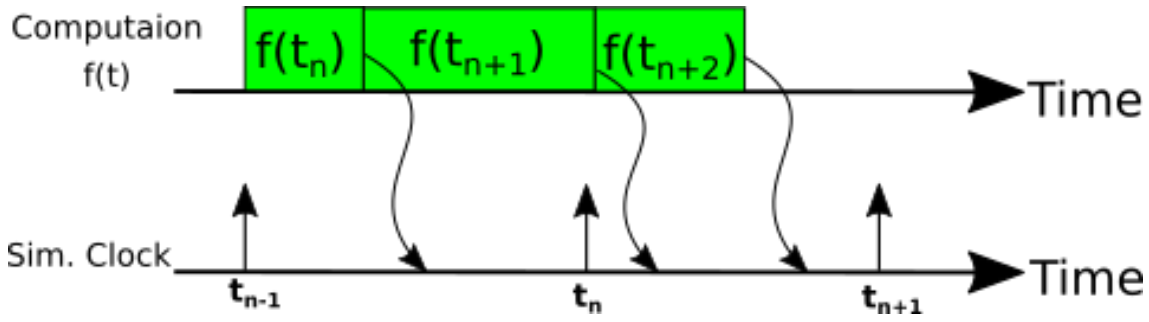

Figure 1.1: Offline simulation: Faster then real-time

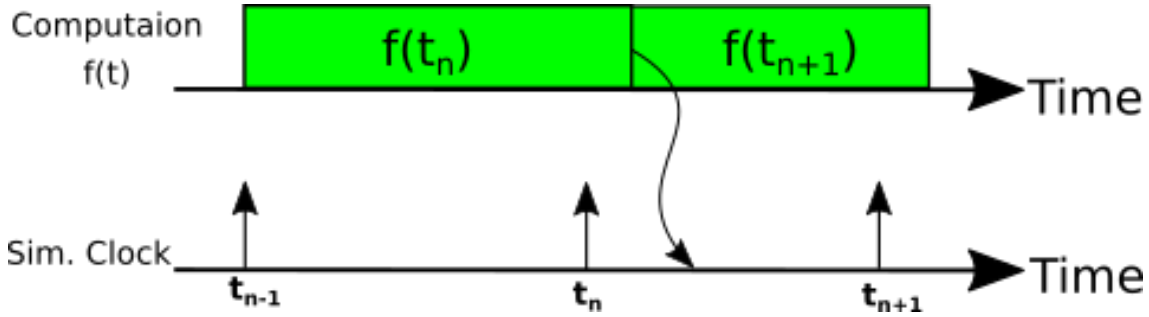

Figure 1.2: Offline simulation: Slower then real-time

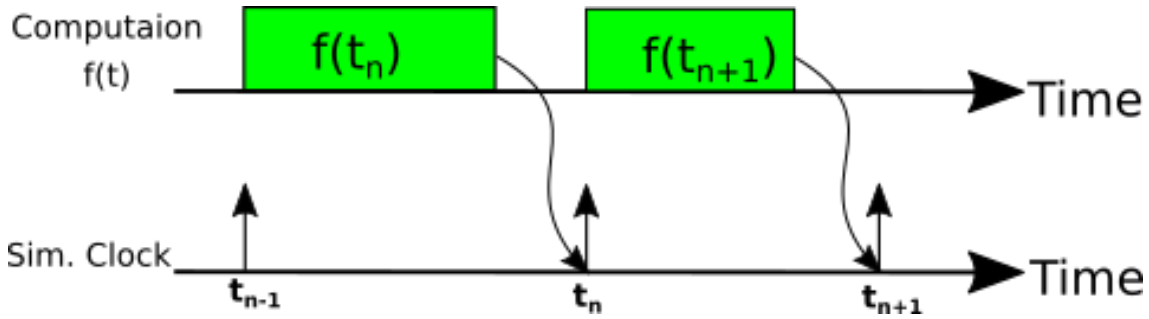

Figure 1.3: Real-time simulation: Synchronized

validation, industrial motor drive design, complex robotic controller design, power grid statistical protection tests, automotive control system and etc. These applications benefit from the use of RT simulators in a number of ways described hereunder:

- It produces a set of requirements and specifications that can be used by all disparate teams involved in a project,
- Development cycle duration is reduced due to parallelization in the workflow,
- It enables testing of simulated devices at or beyond their normal operating limits without the risks involved with testing of real devices, especially when high power levels are present,
- It is easier, cheaper and less risky to test fault responses on a simulated model,
- Testing results are more repeatable since RT simulator dynamics do not change through time the way physical systems do.

RTS can generally be classified into two main categories:

- fully digital RTS (e.g., model-in-the-loop, software-in-the-loop, or processor in-the-loop),
- hardware-in-the-loop (HIL) real-time simulation.

A fully digital RTS requires the entire system including control, protection, and other system components to be modelled inside the simulator and does not involve external interfacing or inputs/outputs (I/Os). On the other hand, the HIL simulation refers to the condition where parts of the fully digital RTS have been replaced with actual physical components. HIL simulation is presented in details in the next subsection.

1.2.2 Hardware-In-The-Loop Simulation

Various definitions of HIL simulation exist in the literature. The most relevant one defines a HIL simulator as "a setup that emulates a system by immersing faithful physical replicas of some of its subsystems within a virtual simulation of the remaining subsystems" [6]. This definition highlights an important characteristic of a HIL simulator, namely, that it must capture the interactions between its virtual and physical constituents. This interaction consists on real signals from the physical subsystem connected to a system that simulates reality, tricking the real subsystem into thinking it is in the real assembled product. Test iterations take place as though the real-world physical system is being used. This technique allows to run easily through thousands of possible scenarios to properly exercise the simulated system virtually without the cost and time associated with actual physical tests. In other words, it creates a virtual environment enabling the simulation and the observation of the behaviour of the system under different operating scenarios that are difficult or even impossible to reproduce correctly in the experimental real environment. It is important to note that not all hardware will be included in the simulation, only those devices considered risky for the successful development of the system are included.

Generally a HIL test system is built around three primary modules which are:

- A RT processor,
- Input/Output interfaces,
- An operator interface.

A bloc diagram presenting the general architecture of the HIL system is shown in figure 1.4.

Take the example of a HIL system used for the validation of tests performed on a car controller. The objective is to test the equipment under various conditions, normal or abnormal, such as during any fault. The simulated part is thus the power electronics, the engine, the various sensors, and the mechanical model of the vehicle which will be simulated in the RT processor. The real part is the electrical control unit (ECU). First,

the appropriate connections are made in order to connect the outputs and inputs of the ECU to the simulator, i.e. the control signals dedicated to power electronics and the various sensor signals, such as encoders, voltage sensors and current sensors. These signals are sent to the ECU via digital/analog and analog/digital converters as if a real system was connected to it as shown in the general architecture in figure 1.4. The simulation parameters and test scenarios can be adjusted or modified in RT by the operator interface.

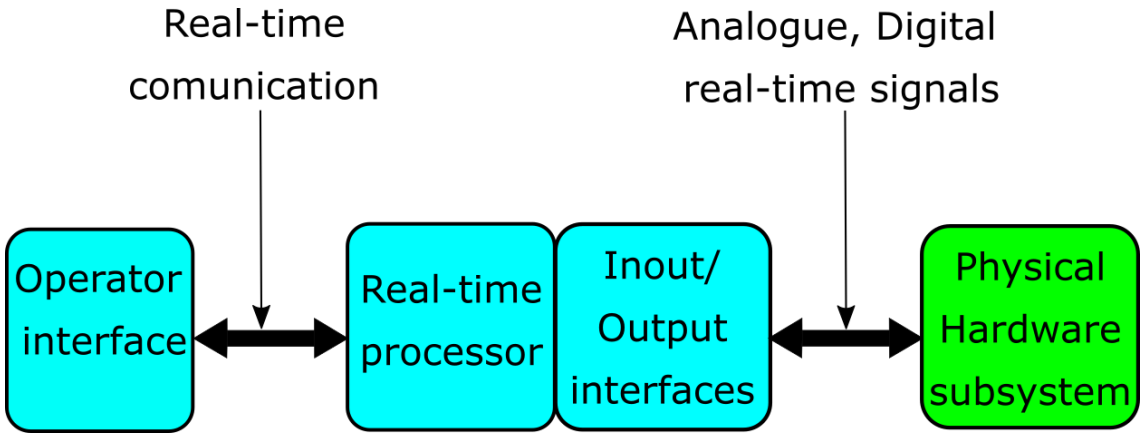

Figure 1.4: General architecture of an HIL Test System

Generally HIL simulations can be categorized into three different levels of simulations [7], [8] which are:

- Signal level HIL simulation
- Power level HIL simulation
- Mechanical level HIL simulation

Signal level HIL

In signal level HIL simulation, RT simulator sends and receives low power signals from the System under test as shown in Fig1.5. The hardware inputs and outputs are managed by the simulation system. Typically the hardware under test is an embedded controller (which contains the process control) The other parts (for example power electronics, electric machine, and mechanical load) are simulated in RT. In this case, only signals are used at the interface between the system under test and the simulation environment, for

this reason, this method is called "Signal level HIL simulation". This kind of HIL has been very often employed for assessment of controller boards in aerospace, wind turbine generator and automotive applications [9], [8].

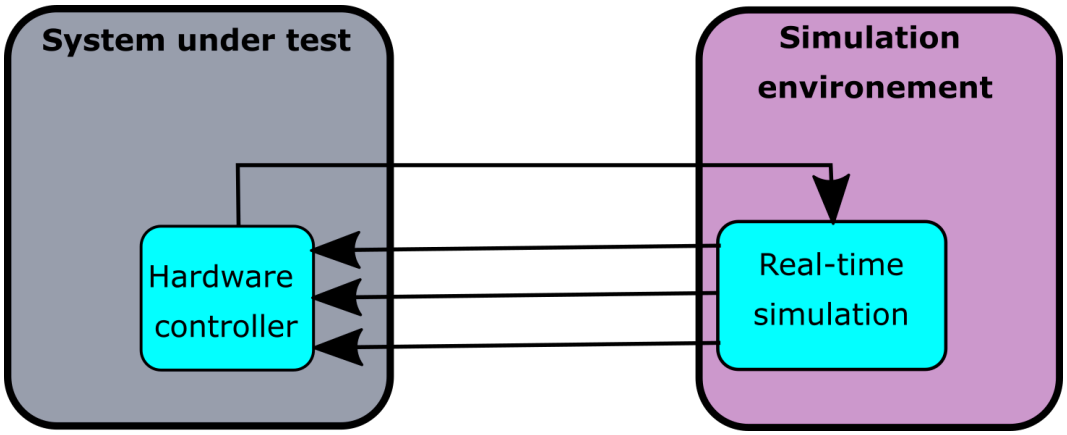

Figure 1.5: Signal level HIL simulation.

Power level HIL

In power level HIL simulations, real power devices outputting power variables are tested, this means that the system under test consists of controller hardware and power electronics hardware which are both tested while the other parts (for example electrical machine and mechanical load) are simulated. The simulation environment is generally composed of a second power electronics set (electric load) and a second controller board simulated in RT as shown in figure 1.6. This method is called "Power level HIL simulation" for its exchange of signal and power variables between the system under test and the simulation plant, it is also called Power Hardware-in-the-Loop (PHIL) [10].

Mechanical level HIL

In mechanical level HIL simulations, and taking the case of an electric machine test bed as shown in figure 1.7, the whole drive (control, power electronics and electric machine) is tested and the mechanical part is simulated. Mechanical inputs and outputs signals are generated by the simulation system to the electrical machine under test. A load machine is typically used in the simulation environment as a controlled mechanical load which is

supplied by a second power electronics set. HIL simulation controls in RT the load machine and sends the mechanical measurements defined by the user to the controller board under test. This method is generally called "mechanical level HIL simulation". Indeed the interface between the system under test and the simulation environment correspond to mechanical variables.

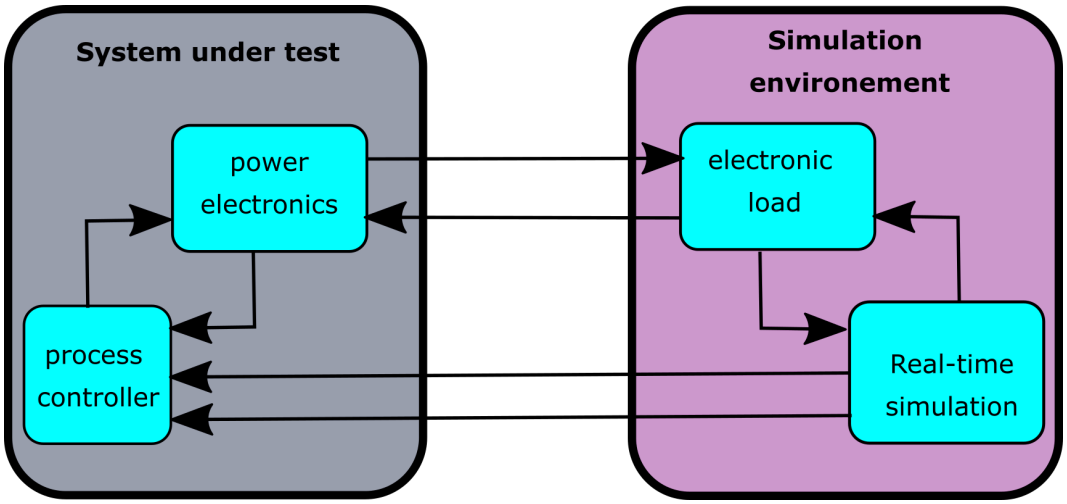

Figure 1.6: Power level HIL simulation.

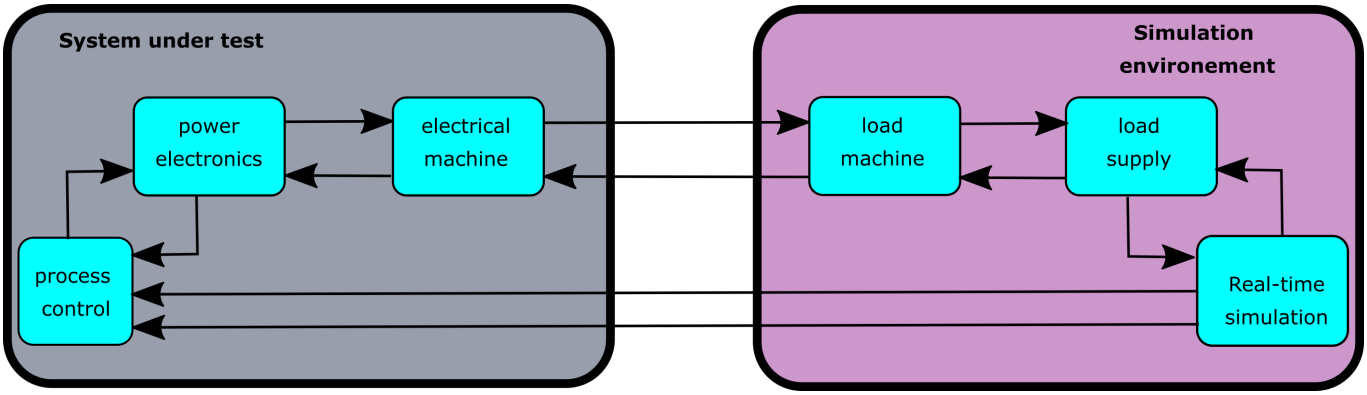

Figure 1.7: Mechanical level HIL simulation.

Advangates of HIL system

The main advantage of using HIL is its operation in RT, meaning that the time step of the simulation is the same as the time step of the actual hardware system in real world. This means that the expected outputs generated by the HIL simulation are almost identical to the outputs of the real hardware. Other advantages are presented hereunder:

- Cost effectiveness: In HIL simulation the most expensive hardware parts are often eliminated from the system and replaced in the simulated environment if required. Therefore it cost less than physical prototyping.
- Rapid prototyping: HIL simulators can also be considerably quicker to build and to develop as they often require less hardware than physical prototypes.
- Simulation speed: HIL simulations of complex physical system run faster than purely virtual simulations of the same system.
- Non-destructive nature: With HIL simulation it is possible to simulate in RT destructive events like a vehicle accidents, or a missile interception without incurring the costly destruction.
- Comprehensiveness: HIL simulation allows to simulate a given system in critical operating conditions over a much broader range than what is feasible in real physical prototyping.
- Safety: HIL simulators is used to train human operators of safety-critical systems in significantly safer environments. for example airplane pilots can be trained using flight simulators which provide a safe training tool.
- Flexibility: HIL simulation provide a virtual simulating environment allowing to modify the simulation test conditions or scenarios in RT by simply tuning parameters with the operator interface, without any hardware modification.

1.3 HIL Simulations Historical Development

In spite of its significant importance, the topic of HIL is less explored in the academic and technical reports, and its general structure is sometimes little known for some academic persons. It has been mentioned in [11] that some HIL examples were locally produced and applied in different industries, however, they are not mentioned in the literature due to confidentiality of applied technology in industry, especially for military and aerospace applications. Therefore it is not easy to provide accurate history in this field.

The first employments of HIL goes back to the second half of twentieth-century and it was probably realized for RT flight simulation, as aircraft systems are considered the mainstream for the evolution of HIL method. The early goals were to simulate the instruments with a fixed-cockpit, and later on improved to move the cockpit according to aircraft motions in order to provide a suitable and secure training environment for pilots. In this case the cockpit and the pilot were real, and the motions were generated by electrical and hydraulic actuators controlled by a simulator. This subject might be firstly mentioned in the NASA documentation in [12].

HIL systems were also used in airspace applications, in [13] it is introduced the HIL simulations as one of the effective factors in the success of the Appolo project during the last century. HIL simulation is applied yet even in the design of Orion, one of the latest spacecraft of NASA [14].

By the end of the twentieth-century HIL systems were built for the dynamic testing of vehicle components with hydraulic or electrical actuators composing testing machines. It was used to test vehicle suspensions, stability, and wheels interactions with the road [11]. Also in vehicle applications, the vehicle driving simulator was an interesting type of HIL simulation, in [15, 16] some of the early attempts to develop a vehicle driving simulator are presented. Furthermore, HIL technique has been used for dynamic motor test bench dedicated for vehicle engines as described in [11], where the engines are real and the vehicles and gears are simulated by some other hardware (an electrical DC or AC motor) together with a digital process computer.

Afterwards HIL became popular in other industries especially in the automotive sector [11]. During the last decades using this technique has spread to many branches of science and its applications considerably have increased. Nowadays, increasing utilization of HIL simulation has attracted academic attentions in different fields. Figure 1.8 shows the multiplicity of publications related to different years in this field, referring to the Scopus database. In accordance with this figure, the number of publications has been increasing since 1970s. This diagram shows that the exponential growth of the publications related to the HIL simulation method is considerable.

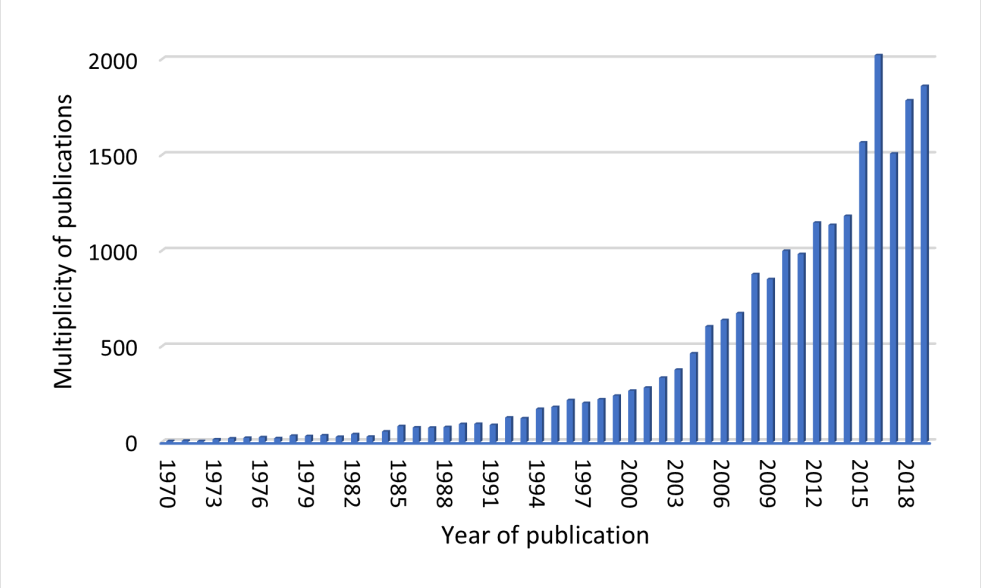

Figure 1.8: Number of publications per year in Scopus database

In recent years technical and scientific centres have paid increasing attention to HIL technology. Which encouraged simulation hardware/software provider companies to develop, design and implement labs dedicated for HIL as their main services. These provider made this technology more accessible for researchers by providing the suitable hardware and software tools to implement the HIL systems. The most famous providers are National instrument (NI), Dspace, typhoon, Operal-rt, Carsim and etc. It is worth noting that that Dspace has mentioned huge companies as its HIL systems consumers including ABB, Audi, BMW, Bosch, Daimler, Diehl Aerospace, Eurospace, Ford, Fujitso, Hitachi, Jaguar, Mazda, Mitsubishi, Motorola, Nissan, Opel, Porsche, Renault, Scania, PSA Peu-

geot Citroën, Siemens, Suzuki, Toyota, Volvo, Volkswagen, Yamaha and etc. The ability to perform HIL simulations is even included in different MATLAB toolboxes which are frequently utilized in practice.

The next section, presents a literature review of the HIL technique citing the latest progress and usage of HIL simulation and different sectors.

1.4 HIL Applications: Literature Review

As mentioned previously, at present HIL simulation is applied in different branches of engineering. New and up to date HIL systems are presented hereunder .

Aircraft and aerospace industries

The aerospace industry has been the main framework for the development and promotion of HIL methodology. First examples go back to 1960s, simulation of the pilot cabin of airplane and Appolo spacecraft software [14]. So far owing to technology development in different aspects of digital electronics, new features are added to this type of simulation and it is exploited in various branches of aircraft and aerospace industry including the design of airplane, spacecraft, missile, helicopter, satellite and etc. Some HIL examples used for aerospace applications are cited hereunder.

In [17], *Karpenko* and *Sepehri* developed a HIL simulation used for the design and test of fault tolerance controller in F16 fighters. Novel fault tolerant control and algorithms can therefore be verified in realistic applications and scenarios. Aerodynamic loads have been emulated using hydraulic actuators. The HIL simulation is supported by the inclusion of a graphical visualization of the aircraft motions. This capability helps the pilot to experience actual flight conditions in total security. A picture of this system is shown in figure 1.9.

In [18], *Spangenberg* and *Friehmelt* presented an HIL lab implemented to simulate and test large airplanes like A380. In order to evaluate new flight control solutions, detailed tests must be carried out to guarantee a safe and comfortable flight. Especially for very large airplanes like A380, as one failure would not only be catastrophic only for this

Figure 1.9: Equipment for HIL lab to simulate flight of F16 fighter

aircraft, but it could have a major influence on the acceptance of aviation in public. The HIL proposed test rig solution can help to solve problems of future flight control systems, and to recognize problems in the early development process. The test rig consists on a cockpit, including the airplanes actuators and sensors necessary to make the virtual test environment. It has been shown that Realistic conditions for the test operations are realised.

Figure 1.10: HIL flight simulators dedicated to pilots training

As mentioned previously, HIL simulations are also used to develop and design flight simulators dedicated for pilots training as proposed in [19]. These simulators provide a virtual environment within a cockpit moving according to aircraft motions. This HIL solution gives a safe training facility for pilots during different flight conditions similar to the real ones. The world's biggest aircraft manufacturers Airbus and Boeing, provide these types of systems to avoid any kind of risks during pilots training. Figure 1.10 shows two examples of a HIL flight simulator.

In [20–23], the HIL method is used for simulation and test operation of unmanned aerial vehicles (UAV). UAV simulations are necessary to ensure stability and performance, due to the delicate and expensive nature of UAV systems, the risk of damage to property during testing, and government regulations. However, offline simulations cannot capture all aspects of a flight control. For this reason, HIL simulation platforms are used. The idea consists on building a virtual environment to produce realistic scenes projected onto a screen. Allowing to test different sensors and actuators of the UAV in real conditions. An example of a UAV HIL test setup developed in [21], is shown in figure 1.11

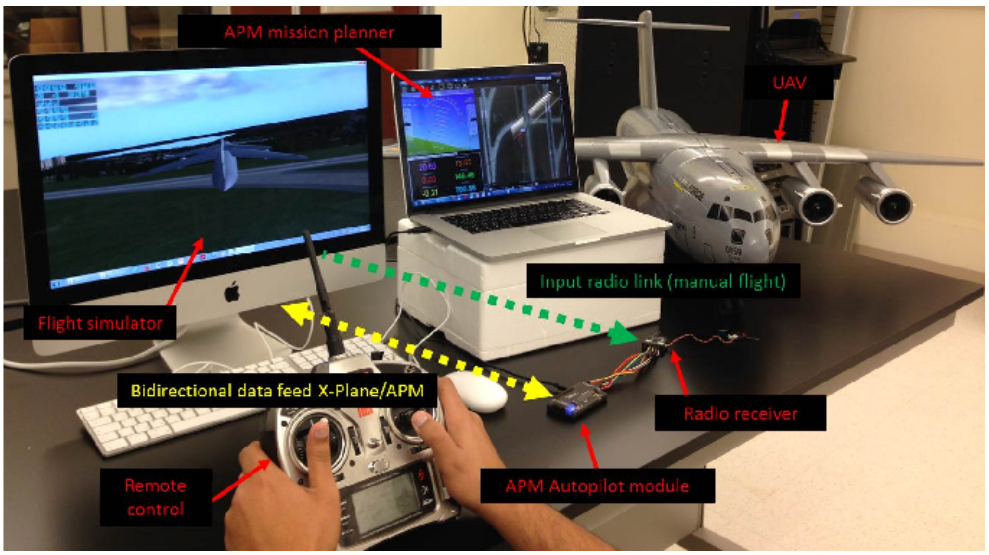

Figure 1.11: HIL simulation setup for UAV testing

In [24], *Min* et al realized a HIL simulation system dedicated for micro-satellite design. The proposed HIL system is based on the mono-axis air-bearing table. It allows to simulate the satellite control system and analyse limit cycle produced by actuators. The

simulation results indicate that the proposed methods are effective and feasible, which can realize the high accuracy attitude control for micro-satellite.

In [25], *Badaruddin* et al shows that HIL lab was also used in the design and development of the Cassini spacecraft. The proposed solution has been realised within a joint effort with NASA to validate the flight software and the sequence programs that govern all spacecraft activity. It is also stated in [26, 27], that NASA has implemented HIL lab structures for testing applications in aerospace research centers, dedicated for NASA space missions.

Considering what mentioned above one may conclude that the HIL simulation technique is vastly exploited in all aspects of the aircraft and aerospace industry including fighters, airplanes, and spacecraft.

Marine systems

Marine engineering has also received benefits from HIL simulation. As novel machinery systems for marine vessels become increasingly more complex, there is a need to develop new and improved methods for their testing and verification. This is important in order to give the vessel owner confidence in the acquired systems, to document sufficient quality, functionality, and performance to vessel contractors, and eventually, it may set a new standard for certification. In this context, testing by HIL simulation of the control and monitoring of marine systems has recently been proposed. In HIL marine systems testing the computer-based system is connected to a RT simulator instead of the vessel. This allows for extensive testing of the control computer system before commissioning and sea-trials. Moreover, the use of HIL testing makes it possible to test the performance of the control computer system under simulated harsh test conditions, that otherwise would compromise the safety of ship and crew, such as high sea-states.

In [28], *Skjetne* and *Egeland* explained through a general approach the HIL and its structure for marine systems, and discussed its testing framework for marine control systems. This reference properly presents the advantages of HIL, using system engineering techniques, as an example for design of a vessel. It introduces HIL simulation as a novel

method for verification and validation of marine control systems.

In [29], *Marouani* et al developed a HIL emulator for electric naval propulsion system. The main objective of the emulator is to reproduce the real system operation. The ship dynamic model is developed and introduced into the realized emulator, allowing the reproduction of the ship propulsion system operation, by generating the different resistance forces using HIL technique. The resulting model is validated by numerical simulations, and then tested on an experimental test bench constituting the emulator. The proposed HIL platform can serve as a test bench for other types of models or teaching emulation techniques of real systems. It has been shown that complex physical systems can be tested easily by this HIL platform, allowing saving in terms of money, time and human resources involved.

In [30], *Hwang* et al proposed a HIL system used to test and evaluate a guidance and control software for an unmanned underwater vehicle (UUV). HIL experiments using 3 axes flight motion simulator have been performed for the verification of control algorithm under real environment. Experimental results have been presented.

In [31], *Woolsey* and *Jarnagin* proposed an HIL system for an autonomous underwater vehicle (AUV) testing. The proposed HIL testing solution has been used to uncover a major system flaw, and to test new vehicle behaviours and subsystems in various conditions. Experimental results have shown that the AUV testes suffered several failures in a traditional experimental test equipment, but, using the developed HIL lab, the cause of failures has been found in the propulsion system.

Power systems

As previously mentioned PHIL simulation represents an extension of HIL, in which the RTS environment is able to exchange not just low-voltage, low-current signals, but the power required by the Devices under Test (DUT). To bridge this gap, it is required to insert power amplifiers between the low-level simulator and the DUTs rated for higher power, all while giving the feedback necessary to close the loop.

PHIL allows also the simulation of high power flows between DUTs, as well as with

the electric circuit model simulated and running on the simulator. This capability permits engineers to test various systems, such as motors, generators, power converters, and photovoltaic systems (PV), while also benefiting from the high-fidelity simulation that provides greater safety and flexibility than typical test benches. Some examples of PHIL applications are cited hereunder.

In [32], *Li* et al presented a newly established RT HIL test facility utilized for the simulation of wind power generation plants. The test site uses two dynamometers and a variable voltage and frequency converter to emulate a realistic dynamic environment, both mechanically and electrically. The facility is controlled by a digital RT electric power system simulator that is capable of simulating electrical networks and control systems of substantial complexity. From the experimental test results presented, it has been concluded that the proposed system shows great potential for the development of a unified wind energy design, test, and research platform

In [33], *Helmedag* et al proposed a test bench for wind turbine enabling system-level investigations. It consists on an electrical and a mechanical PHIL interface emulating the behaviour of the electrical power grid and the wind field, respectively. The HIL test facility allows to speed up the test process for wind turbines as the regular testing procedure takes place outside, and therefore strongly depends on the weather conditions. The motivation for the test bench, as well as the advantages of such a setup and its PHIL interfaces to the RT simulators, have been described. Some experimental results have been presented. a picture of the developed test bench is shown in 1.12.

In [34] Lu et al proposed a RT HIL virtual testing approach for control designs in power electronics applications. It enables the natural coupling between the hardware under test and the simulation environment, which makes the virtual power exchange in HIL simulation possible. In order to validate the proposed testing approach, the RT HIL test facility has been applied in two examples of power electronics applications, namely an H-bridge inverter and a boost converter with their respective control systems, respectively. Experimental results have shown a good agreement with the theoretical ones, which proves the applicability of the HIL test bed and the proposed virtual testing approach.

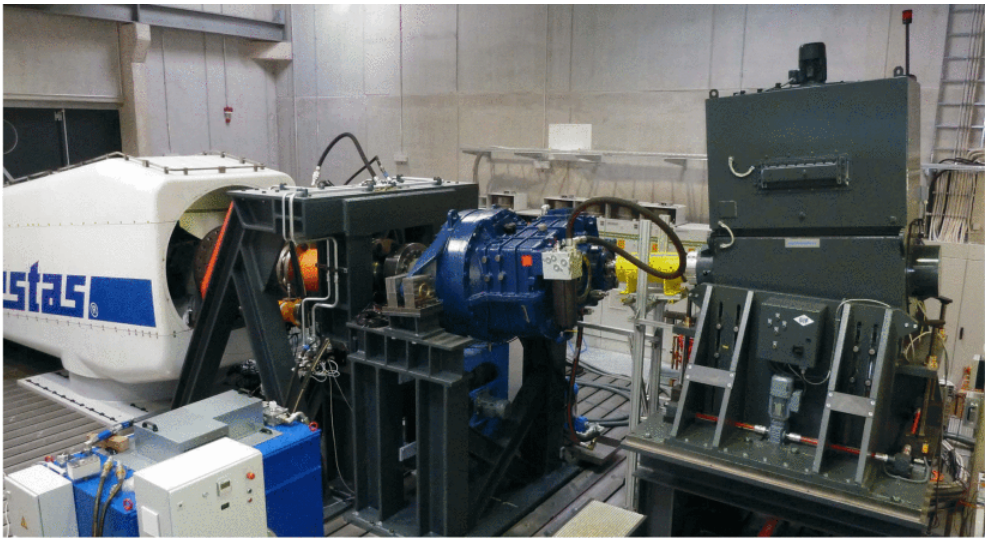

Figure 1.12: Wind turbine HIL test bench

In [35], *Kuperman* et al proposed an advanced HIL test bed system for brushless DC motor. The proposed HIL system allows emulation of external disturbances and parameter uncertainties, without the need of any electrical and mechanical parts supplementary to the electric drive. A RT signal representing the desired changes is created in software and added to the output of the nominal controller, forcing the unperturbed motor output to resemble the output of a motor with actual uncertainties and disturbances. The proposed method allows the emulation of any unpredicted disturbances or parameter variations, and can be used to test and evaluate the performance of advanced control algorithms before mass production. The proposed approach has been validated with simulation and experimental results.

In [36], *Carstensen* and *Biela* presented a novel topology of high power PHIL Simulation for a unipolar arbitrary voltage source Systems. the proposed HIL solution is used for DC circuit breakers system. The developed topology is validated by simulations and a prototype system is designed. It has been shown that with this concept a high current slew rate and a high efficiency can be achieved. The system allows in-depth analysis, research and future developments of circuit breakers for future DC transmission systems.

From what is mentioned above it can be concluded that HIL simulation has had a variety of applications in power system designs that are rapidly enlarging. Due to the

benefits HIL simulation can provide to test new power systems with high-fidelity, high flexibility, and safety.

Robotics

Robotics has gained advantages from HIL simulation as well. Since it combines the advantages of both physical and analytical prototyping of robots. HIL as a prototyping strategy has been successfully applied to the development and testing in a wide range of robotics fields, including advanced mobile robotics, robotic manipulators, and industrial robots. Some examples of HIL systems used for robotics applications are presented hereunder.

In [37], *Temeltas* et al developed a remote simulation of robot manipulators using HIL technique aiming to the development, simulation, and testing of robot manipulators dedicated for mechatronics education. The actual torque components have been simulated in RT on the test-bed using HIL simulation, incorporating a joint actuator-disturbance emulating the load. The required communication and user interfaces are implemented through the use of Internet technologies. Experimental results have been provided to validate the feasibility of the system, thus, the approach motivates the utilization of HIL systems for the manufacturing and the education of robotics.

In [38], *Qi* et al developed a HIL architecture used for robotic simulation. The main contribution of the developed system is the use of a novel HIL simulation distortion compensation approach. Where force measurements delays, dynamic response delays and deformations of the robot are compensated by RT feedbacks using the HIL simulation. Both simulation and experimental results have been presented, showing that the approach can compensate the simulation distortion and improve the simulation fidelity.

In [39], *Martin* and *Emami* proposed a HIL system used for the simulation and design of robot manipulators and their controllers. The platform uses a load emulation mechanism, to apply dynamic loads to the joint hardware, demonstrating suitable performance accuracy despite simplified hardware. Experimental results have been provided, to show the viability of both the load emulation mechanism and the HIL platform. The capability of the HIL system to simulate the performance of a manipulator under normal and

aggressive operating conditions has been also shown through experimental results.

In [40] *Tejado* et al presented a low-cost HIL system for a mobile robot, used for educational or training course to support learning in automatic control and robotics. It consists on a simulator of the robot, which is built by means of physical modelling tools in an Arduino board, and using the MATLAB/Simulink software. Some examples of possible control coursewares carried out using the developed test bed have been shown.

Automotive systems

In the last decades, HIL methodology has gained the widest acceptance in the automotive sector. HIL systems have been used in automotive applications to test and develop Anti-Lock Braking (ABS) systems, Electronic Stability Control (ESC), engine control systems, steer-by-wire systems, advanced driver-assistance systems (ADAS), cameras, radar, Power propulsion systems for electric vehicles (EVs) and hybrid electric vehicle (HEVs) and more.

In [41], *Chu* et al presented A PC-based air-ABS HIL simulation test bench with low cost and high efficiency, which can be used to developed air-ABS for commercial vehicles. A tire model, ABS model, and controller algorithm have been developed in Matlab/Simulink environment, with a rapid prototyping tool to perform RT tests. Experimental results showing the effectiveness and applicability of the developed test bench have been presented.

In [42], *Lee* and *Suh* introduced a PC-based HIL simulator for ABS and traction control system (TCS), in order to analyse their capacities and characteristics. The HIL system includes hardware part which consists of real hydraulic devices, ABS, TCS and brake actuator, and a software part simulating in RT the models of vehicles, tires, and engine dynamics. The analyses of components for ABS/TCS have been successfully accomplished by utilizing the HIL simulator. Furthermore, it has been concluded that the simulator could contribute to the development of more advanced vehicle dynamics control systems.

In [43], *Roh* et al described a HIL system used for ESC performance evaluation. It considers the variation of vehicle parameters influencing ESC performance. The software

part consists of dSPACE control desk conducting RTS, including a vehicle dynamic model and system developed in Matlab/Simulink. A brake unit assembled overall actual brake subsystem has been implemented in the hardware part. Finally, ESC performance tests have been presented for the evaluation of ESC system robustness.

In [44], *Li* and *Hong* introduced the developing process of HIL system for Electronic Stability Program (ESP). The idea combines the virtual model by ADAMS/Car, virtual controller by Simulink and LabVIEW platform, and takes full advantages of each of the three software in different fields of virtual technology. Simulation and experiments have been performed to verify the control algorithm applied. It has been proved from the comparison of the results that the HIL simulation is an effective way in control algorithm design of ESP, which helped to lower the cost, shorten the period of development, and improve the control effects of the ESP system. This method can be applied to the development of other vehicle electronic control systems as well.

In [45], *Yang* and *Zhu* used a HIL system for vehicle combustion engine development. The studied engine is equipped with dual-stage valve lift, external cooled, and electrical variable valve timing systems. A control strategy of the combustion mode transition has been developed and validated using the HIL simulations. The effectiveness of the developed control strategies under both steady state and transient engine operating conditions has been demonstrated with experiments.

In [46], *Jie* et al developed a HIL system for combustion engine model validation. MATLAB/SIMULINK was used to set up the whole engine model based on mean value models and applying it in the ECU HIL testing platform. The comparison between the simulations and test bench experimental results has shown that the engine model could simulate all possible working conditions.

Other HIL application for vehicle combustion engines developments are presented in [47], [48].

In [49], *Bernard* et al developed a HIL test bed dedicated for the full electronic steering system known by "Steer-By-Wire (SBW) systems". The proposed HIL test bed is commonly used at the early stages, or whether a real car prototype was not available for fast

control prototyping. A high dynamic electric drive has been used to virtually reproduce the real non-linear load, represented by the steering chain and other external torque contributes. A HIL simulator has been developed in order to reproduce disturbance torque, like those caused by the road ruggedness. The system architecture as well as the experimental validation of the complete HIL simulator have been presented to demonstrate the feasibility of test bed.

In [50], *Zhu* et al proposed a HIL simulation used to examine the effectiveness of a designed control scheme for a vehicle SBW system. A mathematical model of the SBW has been built in Simulink, then simulated using a HIL simulator. A model controller for the SBW system has been designed in order to track the desired motion states of a controlled vehicle in typical driving scenarios. Simulation results have been presented.

In [51], *Končar* et al proposed a HIL testing solution for automotive video logger device, used in Advanced Driver Assistance Systems (ADAS). View the importance of safety in ADAS systems, many tests with real-life driving scenarios must be conducted before starting mass production. The proposed testing solution presents an improved version of [52], and aims to simplify and reduce time for ADAS algorithms testing and development, which is necessary for autonomous driving. A HIL virtual testing environment has been developed, to conduct test operations without the need for expensive prototypes during algorithm development and testing phase.

In [53], *Zhao* et al proposed a new HIL method for the evaluation of smart cameras used in intelligent vehicle applications. The idea of the developed HIL system consists on replacing the traditional real test environment with a virtual one. The virtual test environment is provided by Carmaker software, to simulate two smart cameras, and obtain the superiority of each camera through the benchmarking of the test results. The test results have been presented showing a great significance of the HIL method to the development and testing of intelligent cameras which is closely related to the development of intelligent vehicles.

In [54], *Sobotka* and *Novak* presented a HIL solution to test radar sensors used in automotive applications. Radar sensors are used for blind-spot detection, adaptive cruise

control, or emergency braking and they have to be thoroughly tested to achieve a high-quality standard. A HIL simulation of static and moving targets, to be detected by the radar sensor, has been presented. The HIL prototype is capable of simulating one target with fully programmable parameters like distance, speed, and dimensions. The absence of mechanical parts significantly reduces the test solution costs. The suitability of the proposed HIL concept for the automotive radar application has been shown through experimental results.

In [55], *Abdelrahman* et al proposed a novel HIL RT experimental verification case study of a hybrid vehicle for power, control, and mechanical systems. All the power train components have been modelled, then a simulation platform has been consequently developed to demonstrate the validity of this mathematical modelling. Typhoon HIL hardware facility has been used in order to provide the experimental verification of the proposed model in RT. The results, from the simulation environment and from the HIL validations, have shown a good agreement, which validated the developed model. The HIL case study can be extended for any electric car, electric trains, and planes, as it provides a generic platform for modelling any propulsion system.

In [56], Joshi developed a HIL simulation for powertrain and chassis of the autonomous vehicle platform. The setup includes actuators, steering controllers, redundant brakes, and powertrain controllers. Ford Fusion Hybrid has been used as the vehicle platform for simulation. The performances of different subsystems in the simulation have been correlated with those on the vehicle in order to understand the fidelity and accuracy of the HIL simulation. Experimental results have shown that testing scenarios and conditions, such as driving across high crosswinds, can be conducted in a simulated environment, which would be otherwise unsafe using physical prototyping.

In [57], *Soltani* and *Assadian* proposed a HIL facility, that can be used in the development and testing of different hardware and software components of the vehicle. The facility can be used for the investigation on the driver-vehicle interaction, at the presence of active brake systems, as well as various ADAS, such as lane keeping or adaptive cruise control systems. The HIL system includes different hardware components of the vehicle

powertrain and a real driver position with a steering wheel, brake, and gas inputs, which constitute drive-vehicle interaction known in the literature as "driver in the loop", and considered very important in the design of vehicle safety systems. Different control algorithms and vehicle models have been simulated in the HIL simulator. Experimental results of vehicle dynamics control have been presented. A picture of the developed HIL system is presented in figure 1.13

Figure 1.13: HIL test facility with the driver in the loop

In [58], *Enisz* et al developed a HIL test bed to facilitates the development of control algorithms, calibration, and verification of ECUs. It has been shown that the system is able to emulate the vehicle dynamics behaviour and to reduce the time required for development and testing. Furthermore, using real vehicles in the test operations can be avoided. The implemented hardware and software environment has been validated and tested, and the experimental results have been shown to validate the test bench.

In [59], *Josef* et al presented a HIL simulator for automotive parking assistant ECU. The described HIL simulator is an electronic device replacing the real ultrasonic parking sensors for the parking ECU under test. The design process has been described in detail. It has been shown that this concept can reduce the cost of the whole device, compared to the traditional solutions, and helps to speed-up the final phase of ECU development.

Other examples of ECU development using the HIL technique are presented in [60–64]

In [65], *Verburg* et al presented a Vehicle HIL simulator, also called in the literature the vehicle-in the-loop test bed. It has been developed for faster and more efficient development and testing, of full scale intelligent vehicles and transport systems. It allows testing the functionality of vehicles by driving the complete vehicle in a relative world. This can be achieved by submitting the vehicle to realistic sensor inputs and actuator loads. The test system technical feasibility has been discussed, and the test results and experiences have been evaluated. It has been shown that the efficiency of the development process is greatly enhanced.

Vehicle-in-the-loop test facility is widely used in automotive industries, where development engineers need testing systems to test powertrains and vehicles in a virtual environment. The complete vehicle is tested in a virtual environment using realistic sensor inputs and real actuators providing the loads. A HIL simulator is generally used to control the test scenarios and conditions in RT. An example of HIL Testing facility, developed by the German company *AVL*, and using the Vehicle-in-the-loop concept is shown in figure. 1.14

Figure 1.14: Vehicle-in-the-loop test system

1.5 Conclusion

Hardware-In-the-Loop (HIL) systems draw more and more attention in different applications of nowadays industry. The first chapter was devoted to a state of the art related to the challenging features offered by HIL real-time simulation (RTS) technique.

As a first step, we have recalled the concept and motivation of RTS and the advantages gained from the interaction of a given simulated model with real components in real time (RT). Then, we have focused upon HIL simulation, presenting its general architecture and its primary modules. The main HIL categories are described, and classified according to their simulation level as follow:

- Signal level HIL simulation
- Power level HIL simulation (PHIL)
- Mechanical level HIL simulation

The main advantages of the HIL method are enumerated.

A historical overview of the HIL method and its evolution is introduced since its first use by the twentieth century in the aircraft industry. Then a literature review of the HIL system is presented, showing the wide number of HIL applications in different engineering aspects found in the literature. Such us Aircraft and aerospace industries, marine systems, power systems, Robotics, and automotive systems.

It has been reported in different works that HIL technique is an effective tool, that could offer a virtual environment suitable for the development and testing of a given system. By reproducing normal and aggressive operating conditions that can be unsafe, difficult or impossible to reproduce in the real world. Which helps to lower the cost, shorten the period of development and provide a test facility with high-fidelity, high flexibility, and safety.

Chapter 2

Developed Electric Drive Emulator

Abstract : *Assessing the operation of electric drives under standard operating cycles is mandatory in production lines of electric vehicles drivetrains. Inverters are a fundamental component in vehicles powertrains. To improve the performance of this component, dyno test beds are used during the process of development. Unfortunately, there are several drawbacks and disadvantages inherent to conventional dyno test beds. In order to avoid these problems, HIL e-motor emulator test beds has been developed. This chapter describes a new architecture of an e-motor emulator dedicated to the performance assessment of inverters used for automotive applications. It consist on a power system made up of two DC-AC converters with their AC sides connected through chokes, this system emulates the dynamic behaviour of the electric vehicle and of its powertrain. System analysis is used to to calculate the current ripple and the optimal values of the chokes and to assess the stability conditions.*

Keywords : Automotive Testing,
Inverter test bed,
Dyno test bench,
Electric machine emulator.

2.1 Introduction

Nowadays, automotive inverters are being asked to fulfill different roles and there is a growing need to optimize their size and power outputs to achieve high performances. However, quality assurance of inverters, and especially their testing solutions, are still poorly supported. Furthermore, the type of test bed solution and its reliability, flexibility, and fidelity to the reality, affects the quality and cost of the inverter, as the end-of-line tests serve to validate a high number of components after the production phase. As a result, inverter makers are increasingly asking for more sophisticated test solutions that guarantees a flexible test facility, and allows manufacturers to save time, energy, and cost.

This chapter introduces test bed systems and their importance for product validation and explains the industrial need to test the automotive powertrain components and especially inverters. A significant amount of work has been done during the last decades into the design, and development of testing facilities for automotive inverters. Among the existing test solutions, one can distinguish two main configurations:

- Classical testing solution: Dyno test bench,
- HIL virtual testing facility: The electric machine emulator test bench.

Much attention is currently focused on HIL machine emulation as a testing methodology, which is increasingly being recognized as an effective approach for simplifying the testing of the drive system. Due to its high flexibility, safety, energy efficiency, and reduced cost, comparing to the classical dyno test bench solution.

The aim of this chapter is to propose a new machine emulator testing apparatus, dedicated to automotive electric drives. Firstly, it presents a literature review of the HIL electric machine emulator test solution. Then, it describes the architecture of the proposed machine emulator, which represents the hardware part of the test system. The proposed emulator is connected by its AC terminals to the inverter under test, it is mainly composed of a second inverter and a three phase inductor, which plays the role of a load emulating a traction electric motor driving the wheels of an electric vehicle.

2.2 Automotive Inverter Testing Solutions

In the automotive industry, the creation of a product follows a number of prescribed stages that can be graphically represented as the so-called V-Model shown in figure2.1. This graph describes the sequence of the stages of a systems development life-cycle:

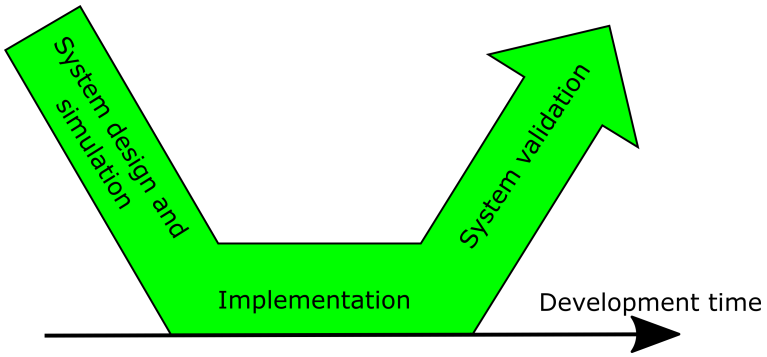

Figure 2.1: V-Model the automotive product creation

The left side of the V-Model works its way from requirements through design to system implementation. The test-bed systems are traditionally employed along the right leg of the V-model, in the stage "system validation", where the product is verified and validated in more complex and realistic testing conditions, and provides proper feedbacks for design correction. Specific types of test-beds are used in the automotive sector for different development tasks, including the manufacture of vehicle components and especially its powertrain. The development of these testing tasks can be classified into three main types which are:

- Mechanical development, including endurance strength testing, optimization of vehicle emissions and fuel consumption, noise, and vibration testing;
- Electrics/electronics development, including power losses optimization, energy circulation, power conversion tests, energy storage capabilities, temperature, and environmental effects, sensors signals compatibility and heating tests;
- Software development, including autonomous driving system tests, emergency time response, ECU, and energy management verification.

To meet the wide diversity of research needs in the automotive industry, and the growing pressure to innovate in shorter development cycles with the lowest cost possible, auto-makers need reliable test beds solutions allowing them to validate complex systems with less cost and time.

Different test bed configurations are used in the development of powertrains in automotive engineering. Some of them focus on the Internal Combustion Engine (ICE) or the electric traction machine, other test beds focus on the remaining components of the vehicle powertrain especially ECU, batteries, and inverters. In this work, we are going to focus on a testing solution dedicated to automotive inverters.

In hybrid/electric vehicles, electric motors, constituting the motion source of the powertrain, are fed by electric drives that combine power electronics with control software in a single device. The inverters controlling traction motors are not only responsible for the electric machine control, but also have other duties, such as battery charging or balancing the high-voltage and low-voltage systems.

Inverters for electric vehicles are built according to very tight specifications and are subject to very tough operating cycles. Little uncertainties in the parameters of the components or assembly tolerances easily lead to overcome some of the operating margins of the converters. As it was demonstrated in [66–68], the temperatures of the powertrain components are subject to complex trends that depend on the driving cycle; therefore, in the dynamic operation, they may differ considerably from those achieved at constant duty operation. For these reasons inverter makers are increasingly asking for sophisticated test solutions that guarantee the inverter functionality.

From a topological point of view, test benches for the validation of inverters can be classified into two major configurations existing in the literature [69]. The first, which represents the traditional solution, uses a rotating system consisting of an electric motor mechanically coupled to a brake or a generator emulating the vehicle, resulting in the so-called "*dyno test bench*". The second alternative, which is less common, considers a power electronic emulator replacing the electric machine "*e-motor*" and connected to the AC terminals of the inverter to be tested. Both testing solutions are described hereunder.

2.2.1 Calssical Testing Solution: Dyno Test Bench

The traditional solution for inverter test beds consists in connecting the powertrain to the electric device interfaces. An electric machine is interfaced to the inverter under test (IUT) through the phase terminals, the current and temperature sensor outputs and the rotor position signals. Generally, the electric machine is mechanically coupled to a mechanical load which is generally another electric machine playing the role of a dynamometer, thus, the test bed solution is so-called "dyno test bench", represented in figure 2.2.1.

The dynamometer can be active or passive depending on the test requirements. A passive dynamometer applies exclusively a braking torque to the coupled electric machine controlled by the IUT against its own direction of rotation. An active dynamometer decelerates the machine controlled by the IUT against its direction of rotation, to test the IUT during the motoring mode, and accelerate it in the direction of rotation to test the IUT during the regenerative braking mode [69].

This test bed solution presented in figure 2.2 must satisfy some additional requirements presented hereunder:

- An adjustable cooling system for the electric machine and the coupled dynamometer,
- DC power supply for the inverter having the possibility of energy recovery,
- Temperature measurement,
- Speed, torque and rotor position measurement at the mechanical coupling,
- Mechanical support for the electric machine and its load to protect against vibration
- speed or torque control for the electric machine and the load dynamometer depending on the test requirement

This test solution is still used in the automotive industry especially when it is required to test the hole drive including the electric machine [70–73]. Figure 2.3 represents a dyno test bench system developed by AVL, one of the world leader company in automotive test equipment.

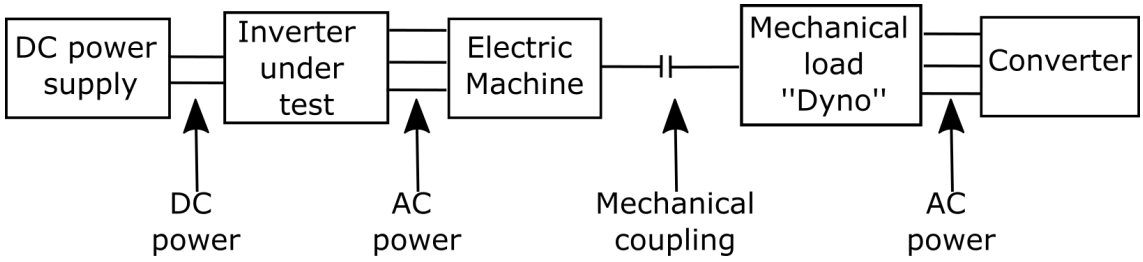

Figure 2.2: Block diagram of a dyno test bed

Figure 2.3: AVL industrial dyno test bench

The dyno test bed solution is considered very close to reality, as it is based on replicating the power train with a real rotating load, which makes the test conditions similar to the real driving scenarios. However, this solution is subject to certain restrictions and especially mechanical ones. The rotating system is dissipative, complex, especially for high speeds, and needs regular maintenance. In addition, there are speed and torque limits for certain driving conditions that are impossible to reach in the experimental environment. Furthermore, this test bed provides low cost-effectiveness and limited flexibility. As a simple modification in the test requirements or changing the IUT type, require redesigning the whole mechanical load and the electric machine.

2.2.2 HIL Virtual Testing Facility: The Electric Machine Emulator Test Bench

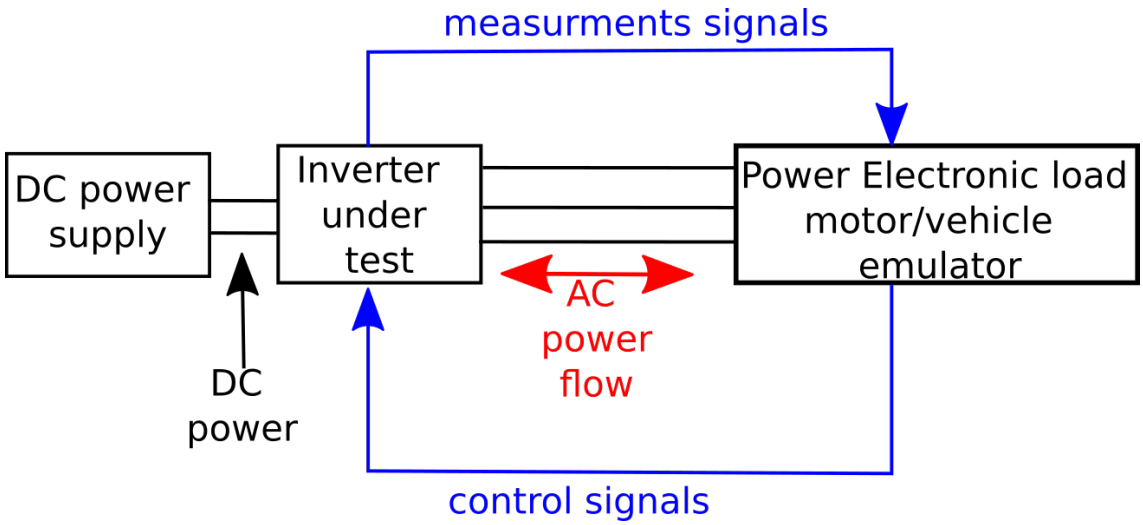

Figure 2.4: Block diagram HIL emulator for inverter test bed solution

In order to circumvent the limitations of the dyno test system, a new type of inverter test solution appeared in the last few years, known as the electric machine emulator test bed (or the "*e-motor*" in some references), and represented in figure 2.4. The basic idea of this test system, is to emulate the moving parts of the vehicle powertrain with a fully digital model of an electric machine without any mechanical components. The *e-motor* emulator aims to build a virtual testing environment simulated in a RT HIL simulator, opening up new possibilities to test the inverter in critical conditions difficult or impossible to reach with a classical experimental environment. While the electric machine remains simulated, the *e-motor* emulator should reproduce in RT the relevant current and voltage signals at the AC inverter terminals, across all four quadrants.

One of the important features of this type of test bed compared to the dyno test bed is its flexibility, achieved thanks to its compact setup and to the absence of the mechanical parts. This becomes evident when choosing the motor to be emulated, as this motor virtually exists in the software as a simulated model, it can be changed or modified in terms of its parameters at the click of a mouse in a software interface, with no need of physical modification. As the test bed has no rotating shafts, the e-motor emulator allows

tests with no mechanical constraints such as speed dynamics or load limitations. In this case, the IUT can be safely subjected to an extensive range of fault modes, while a current safety limitation in the emulator protects the IUT.

This test method aims to overcome the limitations of the dyno test system, especially when the real load is sometimes difficult or even impossible to reproduce correctly in the experimental environment, as cited in [74]. It is also beneficial when the test operation concerns only the inverter, therefore, there is no need to reproduce the remaining components of the powertrain. Most of the *e-motor* emulator test bed solutions existing in the literature use a HIL RTS to create an adequate virtual testing environment. A literature review of these attempts is presented in the next section.

2.3 HIL Virtual Testing Systems For Electric Drives: a Literature Review

One of the early attempts to substitute the electromechanical load with an equivalent solid-state power electronic load was carried out by *Slater* et al [74]. The load could be flexibly-controlled to emulate real systems dedicated to testing the power electronic converters in diverse applications, yielding the so-called "virtual machine" concept. The main objective of the virtual machine is providing a simulated electrical load enabling an inverter test operations at real power levels without the requirement of an actual machine. The virtual machine emulates the real machine during the testing and development stages of the inverter design, thus providing a safer and more flexible development environment. It has been shown that the results yielded by the virtual machine exhibit acceptable accuracy in RT simulation using a dedicated digital signal processor. Furthermore, it has been reported that the virtual machine offers a number of significant advantages over using an actual machine in the testing phase of an inverter. The power electronics of the virtual machine is composed of two back to back, three-phase converters, allowing bidirectional power flow to and from the tested inverter. The virtual machine is controlled by a RT simulator and is programmed to behave like any motor with the possibility to modify its parameters. It has been experimentally demonstrated that the virtual machine is able to

simulate the behaviour of the actual electric machine. Consequently, a virtual machine could be used to test a complete range of inverters, therefore avoiding the need to dispose of a range of motors of different types and ratings to test a range of inverters.

Monti et al [75], introduced a real-life application consisting in the design of an innovative test facility for an electrical drive system using a virtual testing solution. The test bench consider a PHIL system intended to replace electrical machines connected to mechanical loads and having various nominal ratings and electromechanical characteristics. The test platform is composed of a power electronic system and a control system simulated in a RT model. The power section of the testing system is composed of a passive RLC filter, an inverter controlled by a RT simulator, a DC bus, allowing energy recovery. The synthesis of the control laws in different type of electric drives is carried out. Then, an experimental investigation has been carried out considering three drives: (i) a low-power single-phase set-up, (ii) a drive rated below 1kW used as the development environment, and (iii) a drive using a 20kVA inverter.

In [76], *Boller* and *Kennel* proposed an approach to test voltage source inverters for electric drive applications, without the need of a real electrical machine, which has been substituted by a virtual one. A test bench including a power and control systems has been developed. It consists on a second power inverter, an active front end, coupling inductances and a control structure made of a DSP based control system. It has been shown, through experiments carried out on the developed test bench, that the proposed virtual machine has the same behaviour as a real induction motor. The paper demonstrated that different machines and their respective loads could be emulated. The drive inverter under test could be operated in a wide power range without any need for modification of the emulator or its control unit.

In [77], *Monti* et al developed an innovative architecture for a low-cost power hardware-in-the-loop (PHIL) platform, whose structure and operations has been described in [75]. It includes a real-time simulation engine, a power section composed of a filter and a three-phase inverter, a signal interface comprising a field-programmable gate array (FPGA) and a data acquisition systems (DAQ) board. The Experimental tests demonstrated the ability

of the proposed structure to emulate an electromechanical load with sufficient accuracy. They also revealed some design weaknesses. The study introduced the platform and its performances and proposed some guidelines to overcome the design limitations.

In [10], *Grubic* et al proposed a new electronic HIL-based concept for an inverter drive test bench. The machine-load combination in conventional test benches has been substituted by its mathematical model that is implemented in a DSP to control the power electronic section of the load emulator. The coupling network and a suitable inverter topology, the so-called "quasi-Linverter" constitute the system. The paper shows that the proposed inverter topology significantly reduces the output harmonics which enables a better dynamic performance. However, experiments carried out on the developed test bench have revealed that the speed/load profiles are limited by the output capability of the LinVerter prototype. A second generation that enables the reproduction of the speed/load profiles over the whole operating range has been developed.

In [78], *Uebener* et al presented a test bench including an electric machine emulator, reproducing the power flow of a permanent magnet synchronous machine. The performance of an e-machine emulator have been compared to a dyno test bench. It has been shown that an e-machine emulator is an inexpensive alternative to conventional dyno test benches for the test of electric vehicle inverters due to its flexibility and the absence of mechanical moving parts and maintenance. The machine emulator is composed of a multilevel inverter controlled by a current controller and an electric machine model programmed in an FPGA. The terminals of the inverter under test are connected to the machine emulator via coupling inductances. Data from the real e-machine are used to build the flux look-up tables. These data are obtained from a finite element analysis or from measures of a dyno test bench. The flux linkage deviations remain under 1% in the constant torque range which is less than the production tolerances for most electric motors.

In [79], *Casolino* et al proposed an automotive electric drives test system aimed to improve cost-effectiveness. The main idea behind this work is using an electric drive as a load for the drive under test. The test inverter is controlled using three main techniques,

which have been compared by simulation. A RT Software-in-the-loop Simulation (SiLS) of the entire test system has been carried out. Matlab Simulink blocks integrated in the NI-VeriStand (HIL) has been used in the system modelling to allow RT simulation. Special attention has been paid to the architecture of the test system and parameter adjustment. If the parameters of the virtual load are accurately selected, a good agreement of the motor model emulating the electric vehicle behaviour is reached.

In [80], *Saito* and *Akagi* developed a PHIL test bench built around two modular multi-level converters connected in front-to-front configuration without transformer, dedicated to a medium-voltage, high-power, and high-speed synchronous motor drive. The real inverter under test has been used to feed a virtual synchronous motor driving a virtual load. This virtual motor and load consists of a real per-phase auxiliary inductor, a real three-phase rectifier, and a real two-winding common-mode inductor. A three-phase down-sized scaled PHIL test bench has been developed and its performance experimentally demonstrated. A three-phase synchronous motor has been considered as a virtual motor, and a virtual centrifugal compressor with a quadratic torque-to-speed load characteristic has been taken as a virtual load. The validity of the PHIL test bench under steady-state and transient-state conditions has been confirmed by experiments and by simulations.

In [81], *Vodyakho* et al proposed a novel drive system topologies dedicated to prototyping, testing and validation of electric drives using an induction machine emulator without using any real motors/generators. The proposed machine emulator platform utilizes the PHIL concept in conjunction with a high-fidelity machine model and load dynamics, it also include a control strategy in the synchronously rotating reference frame in dq coordinates. The machine and load models have been simulated with a RT simulator generating suitable control commands to a power electronics amplifier that interfaces to the variable speed drive under test. It has been shown through experimental results that the machine emulator is able to closely reproduce the same results of the actual induction machine for a wide range of power level applications.

In [82], *Masadeh* et al proposed an electric machine emulator dedicated for new drive systems testing. The test solution has been designed by utilizing the concept of PHIL

along with an inclusive model of the machine and load dynamics. The emulation system basically comprises two back-to-back, six-switch, bridge-type voltage source converters (VSC). the first VSC runs as an active front-end converter to maintain a fixed DC link voltage of the emulator and also control the bidirectional power flow from and to the second converter. An induction machine model with its control are implemented in a RT simulator to control the two VSC. A coupling transformer is used for isolation purposes and to avoid common-mode circulating currents. The effectiveness of the developed emulator with its control has been shown through experimental and simulated results.

In [83], *Amitkumar* et al presented a PHIL machine emulator system, used to test traction drive inverters. The proposed system uses a power converter to emulate the machine and controlled in RT. The RT simulator uses a synchronous machine model based on look-up table data. The machine emulator has been validated using simulation. Subsequently experimental results have been obtained from the developed machine emulator and a physical machine coupled to a DC dynamometer. A comparison between the results obtained from the physical machine and the results obtained form the machine emulator has been shown to prove the validity of the system.

In [84], *Wu* et al presented a new PHIL architecture for emulation of electric motors. It includes an additional bidirectional dc-dc converter interface between the inverter used for machine emulation and the one used for regeneration. A wide range of machine models can then be emulated with just one PHIL test bench. A 2 kW permanent magnet synchronous motor is emulated and compared with a real motor, to verify feasibility of the proposed method. From experimental results a close match has been shown between the emulator results with that of a real motor, confirming the accuracy of the implementation.

The previous works focus on the electric motor emulation employing an electronic load performing the electrical validation of a power converter. Instead, in this chapter, a new machine emulator used in the development of a RT PHIL inverter test system is proposed [85, 86]. The load used in this work is a standard 4-quadrant drive controlled in RT, emulating at its terminals a real motor driving the wheels of an electric vehicle. In the next section the hardware structure constituting the power system of the e-motor

emulator is presented.

2.4 Hardware Layout of the Test Bench

This section shows the general architecture of the power system, which represent the hardware part of the proposed test bench. The main components of the power system and its mathematical model are described. Then presents the analysis of the system, aimed to choose the value of the choke inductance as a function of the desired current ripple, and finally discusses the stability of the developed system.

2.4.1 Power System Architecture

The power system is made up of two "three leg converters" interconnected by a three phase inductor as shown in figure 2.5. The drive to be tested, including the DC/AC inverter, is connected to the inverter representing the load through a three-phase inductor linking both AC sides, as shown in figure 2.5. The association of the second converter and the three phase inductor plays the role of a load emulating a traction motor driving the wheels of a road vehicle.

In order to emulate an acceleration cycle, the converter under test operates as an inverter which enables a circulation of the power from the DC bus to the load. While the load converter operates as a rectifier, enabling the circulation of the power from its AC side to the DC bus.

The power flow direction is inverted during a regenerative braking mode, that characterizes the operation of electric and hybrid vehicles. In this case the load converter operates as an inverter, enabling the circulation of the power from the DC bus to the converter under test which behaves as a rectifier. Figures 3.9 (a) and 3.9 (b) illustrate the power flow through the test system during acceleration and regenerative braking modes, respectively.

In real automotive systems, regenerative braking enables the conversion of the vehicle kinetic energy into electrical, that is then transferred to the battery pack through the converter (operating as a rectifier).

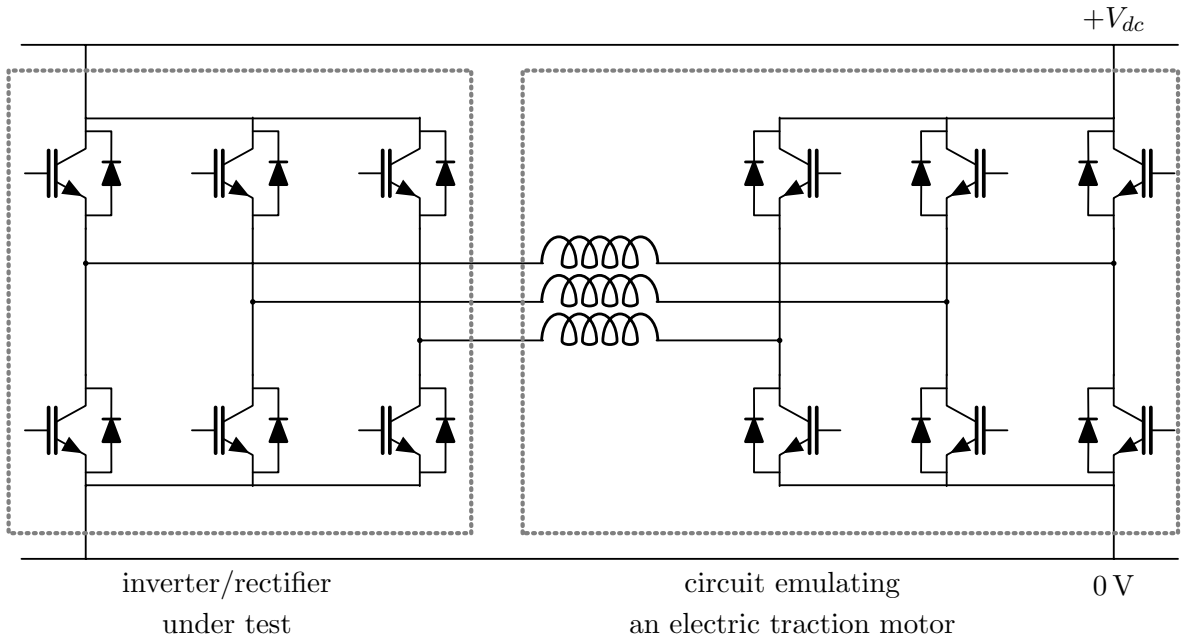

Figure 2.5: Power system connections

Since the two converters constituting the power system have three-phases, the circuit can be treated as three independent single-phase circuits, each one comprising one inverter leg. The corresponding single-phase equivalent circuit model is shown in figure 2.7. The model consists of one leg of the first converter linked to the corresponding leg of the second one through the inductance. The behaviour is the same for the two other phases.

The direction of the currents I_{in} and I_{out} in the DC-link indicate the power flow mode. The direction of the instantaneous currents in the inductances indicate the power flow in the branch. When the left branch provides power, the current path is that coloured in blue shown in figure 2.7(a). The current takes one of the two possible paths through the diodes or the IGBT as in the following equations:

$$\begin{cases} Vs_{22} + V_i + Vs_{11} = V_{dc} \\ Vd_{21} + V_i + Vd_{12} = -V_{dc} \end{cases} \tag{2.1}$$

Where V_{dc} is the dc-bus voltage, $Vs_{i,j}$ the voltages across the power switches and $Vd_{i,j}$ the voltages arccos the diodes as shown in figure 3.9 and 2.7.

During the regenerative mode shown in figure 3.9 (b), the current path is coloured in

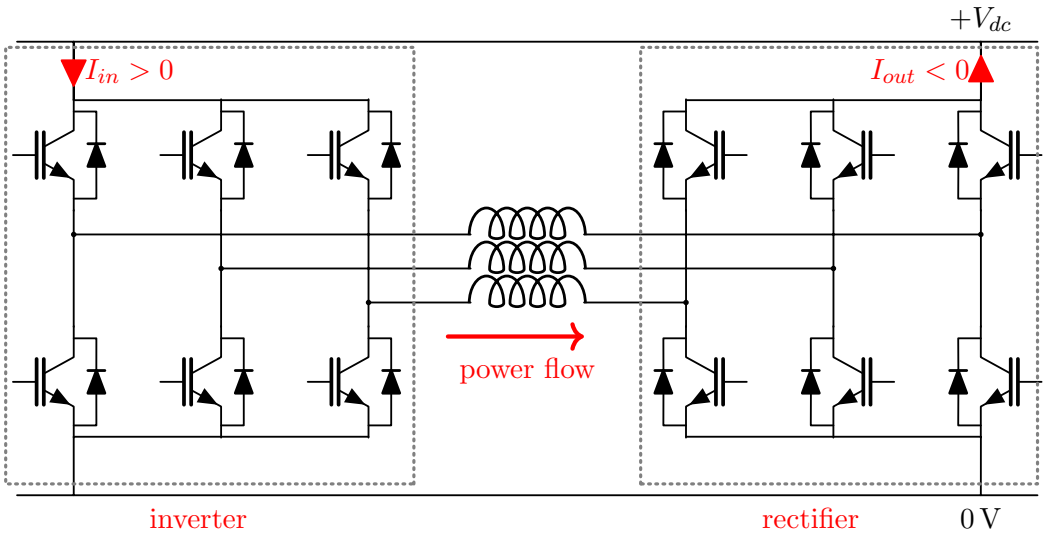

(a)

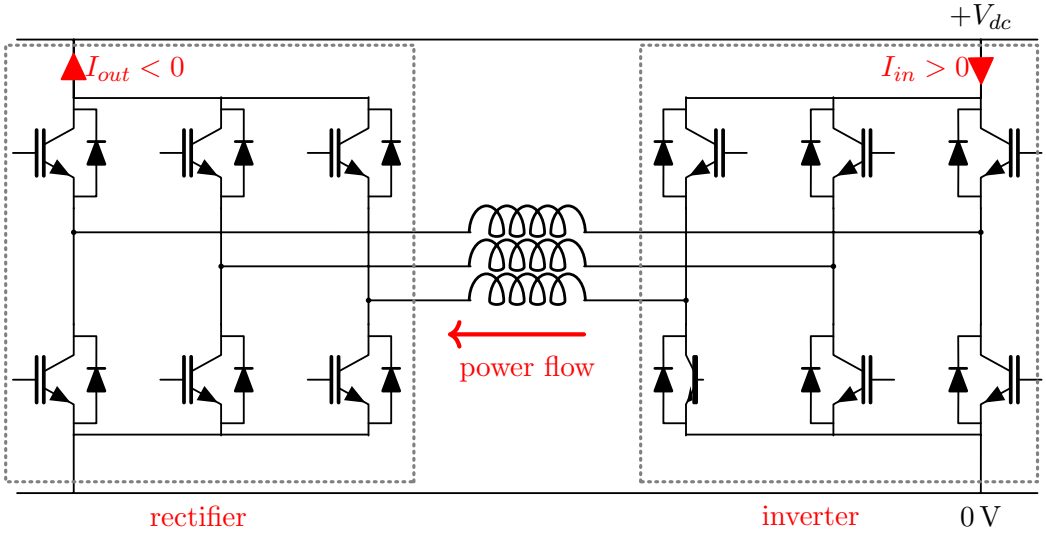

(b)

Figure 2.6: Power flow through the power system: (a) acceleration cycle, (b) regenerative braking cycle

red and shown in figure 2.7(a). The current takes one of the two possible paths through the diodes or the IGBT as in the following equations:

$$\begin{cases} Vs_{12} + V_i + Vs_{21} = V_{dc} \\ Vd_{22} + V_i + Vd_{11} = -V_{dc} \end{cases} \tag{2.2}$$

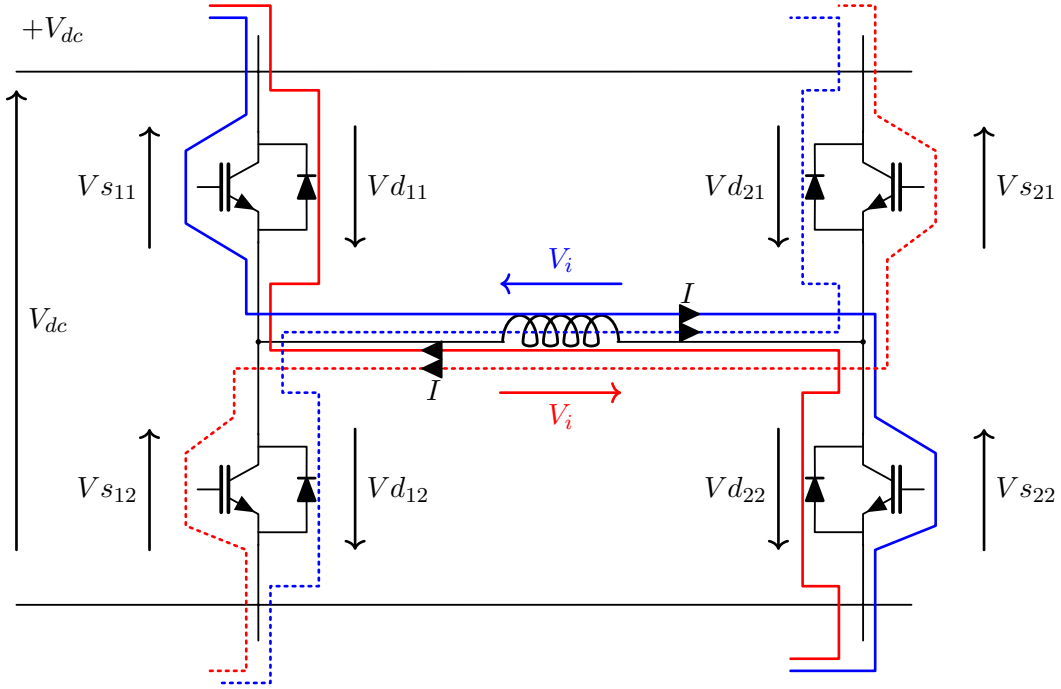

(a)

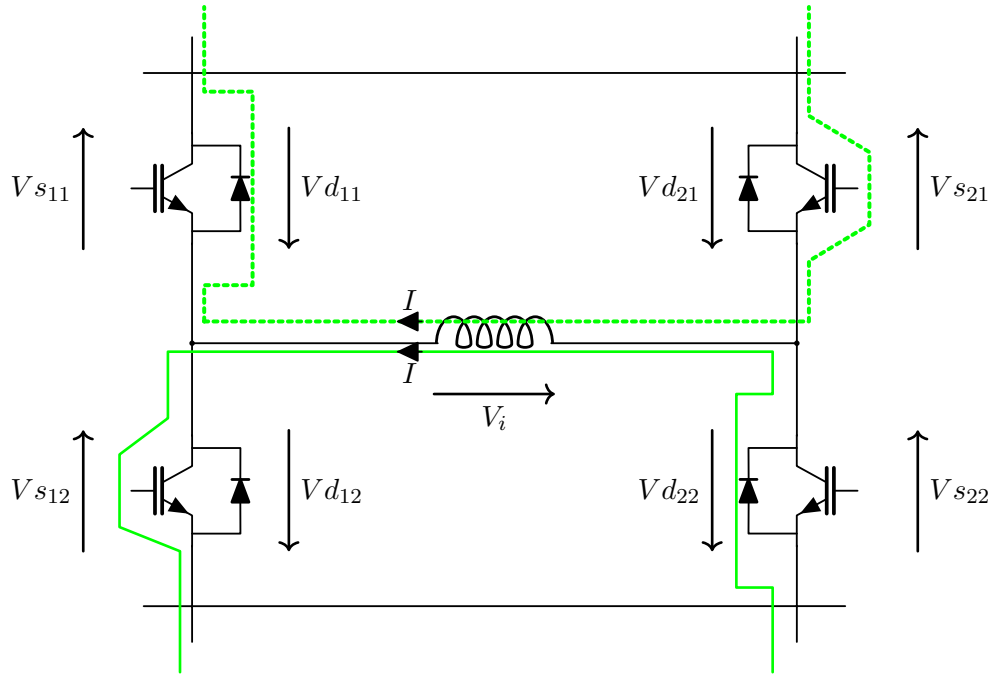

(b)

Figure 2.7: Current flow paths: (a) accelerating and regenerative braking cycle; (b) freewheeling

The current can take four other possible paths, in which the power stored in the inductances is dissipated in free-wheeling nodes. Two of these paths are shown in figure

2.7(b), and analyzed in the following equations. The other two are conceptually the same but in the reverse current direction.

$$\begin{cases} Vs_{21} + V_i + Vd_{11} = 0 \\ Vd_{22} + V_i + Vs_{12} = 0 \end{cases} \tag{2.3}$$

2.4.2 Inductance Computation

Beyond its role in the emulation of the automotive drive train, the three-phase inductance prevents short-circuits between the two converters and reduces the current ripple at the input of the load one. The current ripple should be adjusted to match the real operation of the emulated motor. This subsection is devoted to the prediction of the values of the inductance and the resistance characterizing the circuit connecting both converters, that yield load currents as smooth as possible.

Considering one phase of the inductance, the differential equation describing the RL-circuit represented by Eq.s 2.1 - 2.3 is expressed as follow:

$$\pm V_{dc} - V_{drop} = Ri + L\frac{di}{dt} \tag{2.4}$$

where V_{drop} is the voltage drop over the conducting diodes and switches, i is the RL-circuit current, and V_{dc} is the dc voltage, fixed in our case study to 24V.

Considering an initial value of the current i_0, the solution of equation (3.11) is:

$$i(t) = i_0 e^{-\left(\frac{R}{L}\right)t} + I\left(1 - e^{-\left(\frac{R}{L}\right)t}\right) \tag{2.5}$$

where I is the asymptotic value of i:

$$I = \frac{V_{dc} - V_{drop}}{R}. \tag{2.6}$$

The current variation during a switching period $\Delta(t)$ of the power switches of both inverters is then expressed as:

$$\Delta(i) = i(\Delta(t)) - i_0 = (I - i_0)\left(1 - e^{-\left(\frac{R}{L}\right)(\Delta(t))}\right) \tag{2.7}$$

In order to achieve a ripple-free current in a sinusoidal steady-state, the current variation $\Delta(i)$ should fulfil the following equation:

$$\Delta(i) \simeq I_L sin(\omega_L \Delta(t)) \tag{2.8}$$

where I_L and ω_L are the maximum value and the angular frequency of the load current.

Figure 2.8 and 2.9 show 3D plots of $\Delta(i)$ versus L and R for given values of I_L and ω_L at different switching frequencies of the load inverter. The green plane corresponds to a current variation $\Delta(i)_{sin}$ consequent to a sinusoidal current. Obviously, higher values of the switching frequency of the load inverter lead to lower values of inductances. It must be considered that the switching instants of the two inverters aren't synchronized. Therefore, in the case the two switching frequencies are the same, the average switching period to be considered is one half of the switching time, as each switching interval of one inverter, includes one commutation of the switches of the other inverter. In the case the two switching frequencies are different, the resulting frequency may be taken as the sum of the two. For large power drives, the size of the chokes must be reduced to contain the mass and the cost of the testing equipment. Therefore it would be beneficial to command the load inverter with a higher switching frequency than the tested inverter.

Referring to figure 2.8 and 2.9, one can notice that for each switching frequency there is a set of parameters (R, L), corresponding to the intersection of the 3D plots with the green plane, for which the variation of $\Delta(i)$ has a sinusoidal shape.

For the sake of accurate selection of a combination of (R, L), 2D plots illustrating the variation of $\Delta(i)$ vs. L for different values of R at $16kHz$ switching frequency have been considered. According to figure 2.10, $\Delta(i)$ is close to $\Delta(i)_{sin}$ for inductance values included in the range $0.2 \div 0.4mH$ for a wide range of resistances. However, in order to achieve a value of the current ripple $\Delta(i)$ closer to that of the real drive, L has to be selected in the neighbourhood of $0.3mH$, according to the ripple of the real drive.

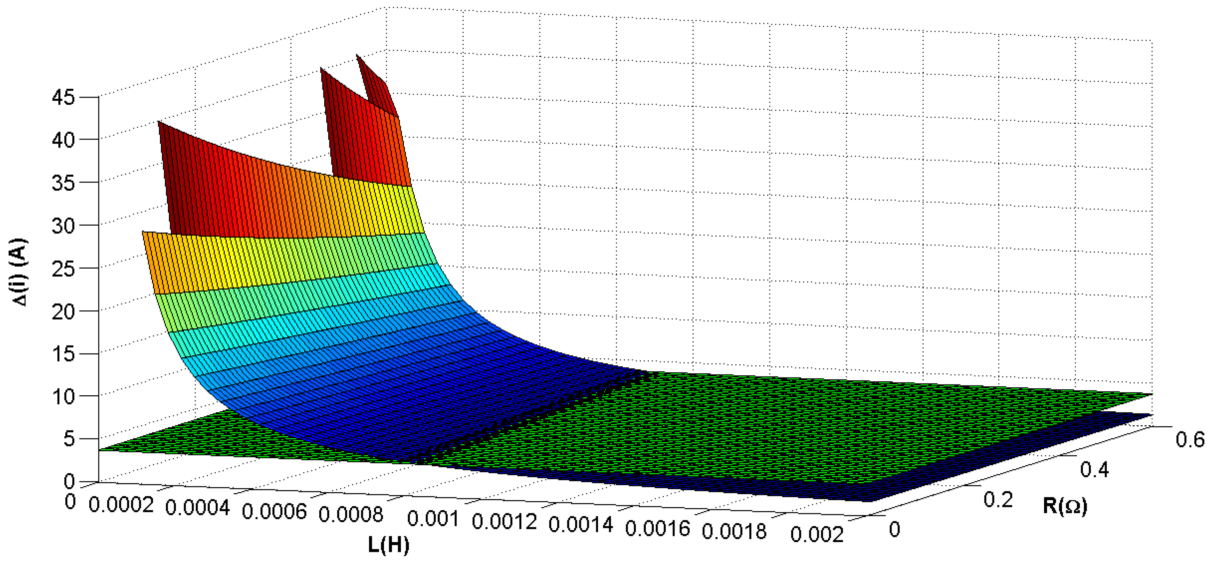

Figure 2.8: 3D plots showing $\Delta(i)$ versus L and R at $8kHz$ switching frequency for given values of I_L and ω_L. The green plane corresponds to a current variation consequent to a sinusoidal current.

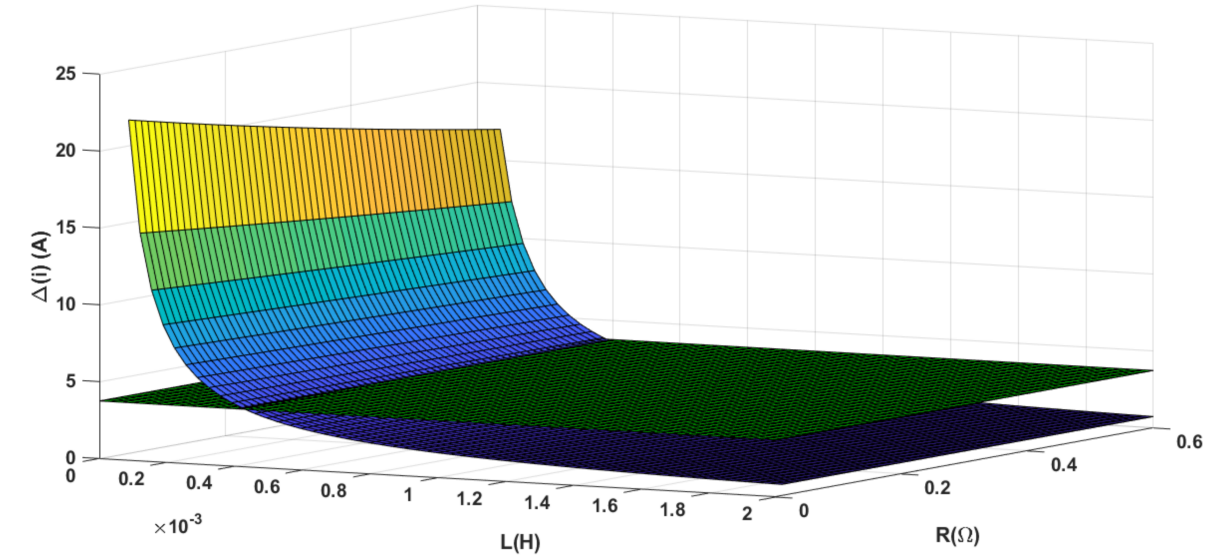

Figure 2.9: 3D plots showing $\Delta(i)$ versus L and R at $16kHz$ switching frequency for given values of I_L and ω_L. The green plane corresponds to a current variation consequent to a sinusoidal current.

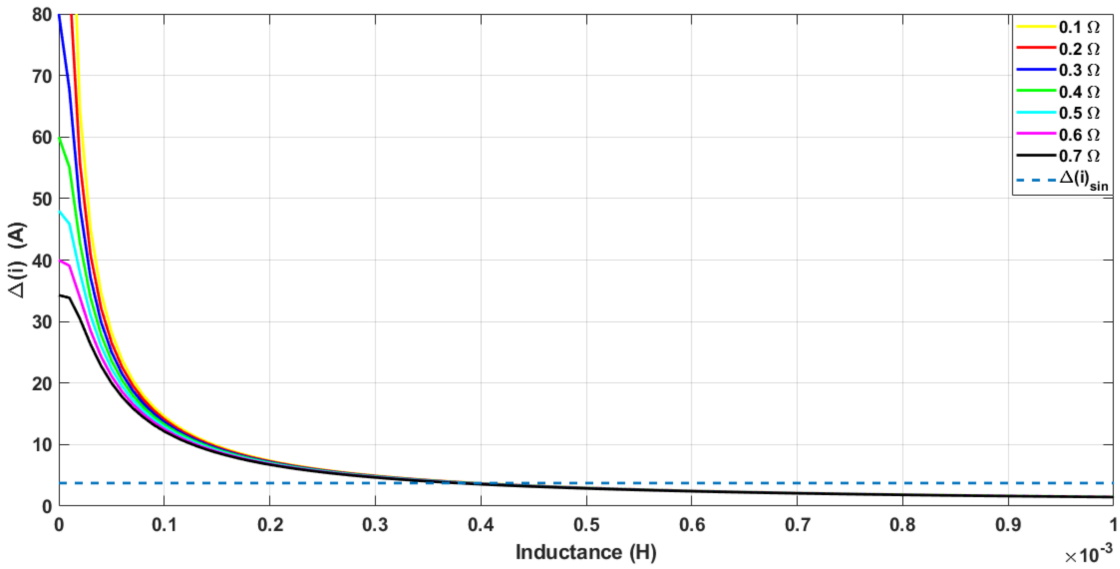

Figure 2.10: Variation of $\Delta(i)$ with L for different values of R at $16kHz$ switching frequency.

2.4.3 Current Ripple Evaluation

Subtracting Eq. 3.13 from Eq. 2.7, and using the parameters of Section 2.4.2, the current ripple is evaluated.

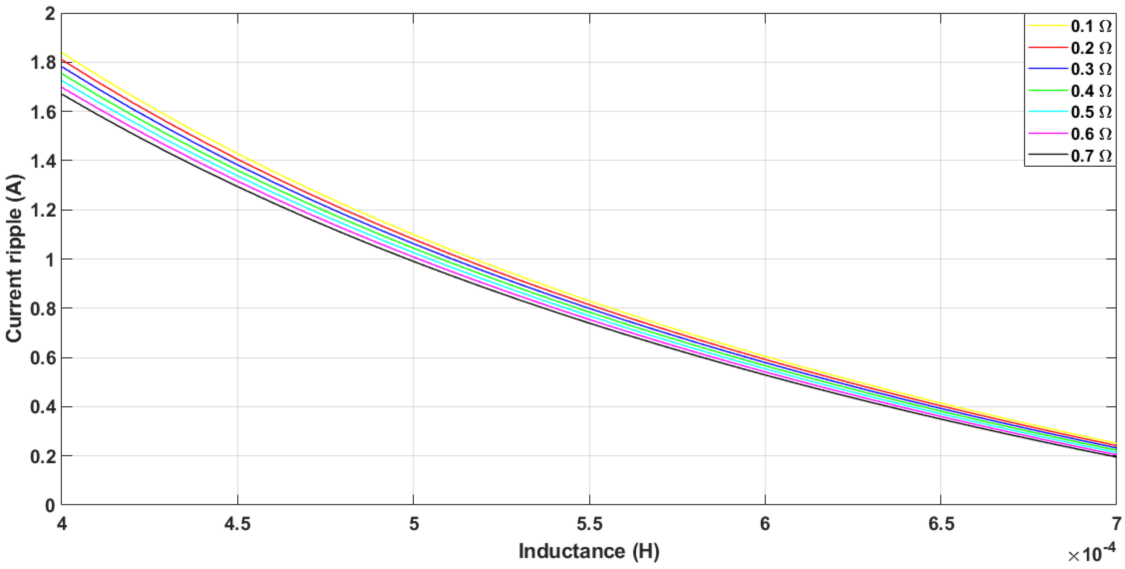

Figure 2.11: Variation of the current ripple at $16kHz$ switching frequency with L for different values of R

The chokes can be optimized on the basis of the behaviour of the current ripple with the inductance values, which is plotted in figure 2.11 with different values of the resistance at $16kHz$ switching frequency. Figure 2.11 shows that increasing the inductance yields negative values, meaning that the current cannot reach the desired setpoint in one sampling time. Finally, figure 2.12 shows the trend of the current ripple with the supply (modulating) frequency. The higher the frequency value, the smaller the ripple.

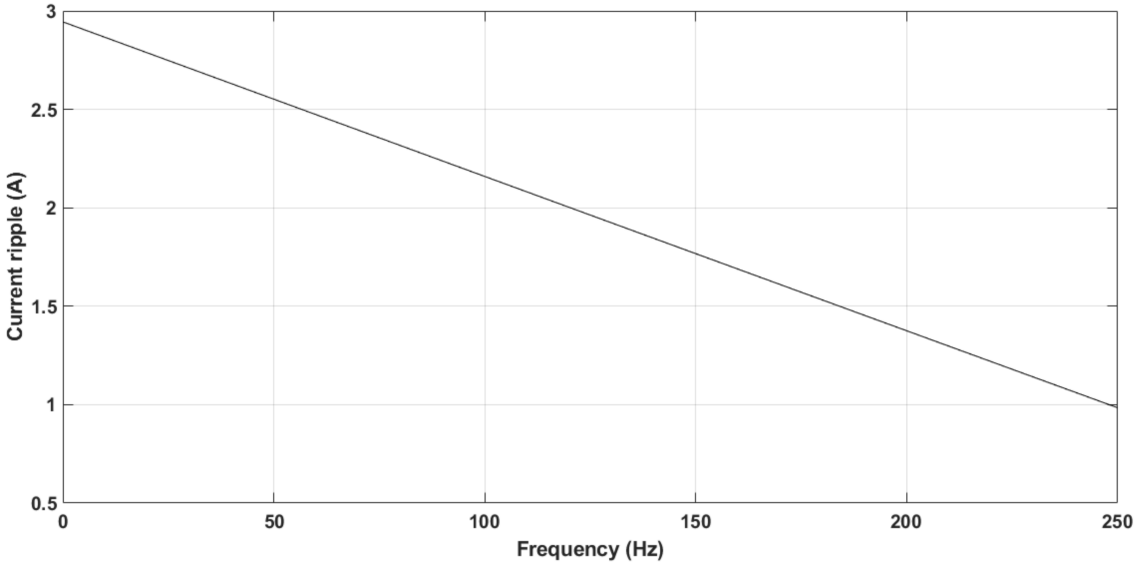

Figure 2.12: Variation of the current ripple with the supply frequency at $16kHz$ switching frequency

2.4.4 Stability Analysis

As described previously the two inverters are connected in cascade through a choke. In this case the whole system may be unstable if the inverters constants, internal PI regulator parameters and switching frequencies are mismatching. Therefore it is important to study the power system stability to avoid future failures due to instability.

The stability of the power system is assessed through the analysis of the roots of its transfer function. The analysed system is composed by the two drives at the current control loop level. The block diagram of the power system is derived by developing the transfer functions of the subsystems, i.e., the two inverters and the inductances (choke).

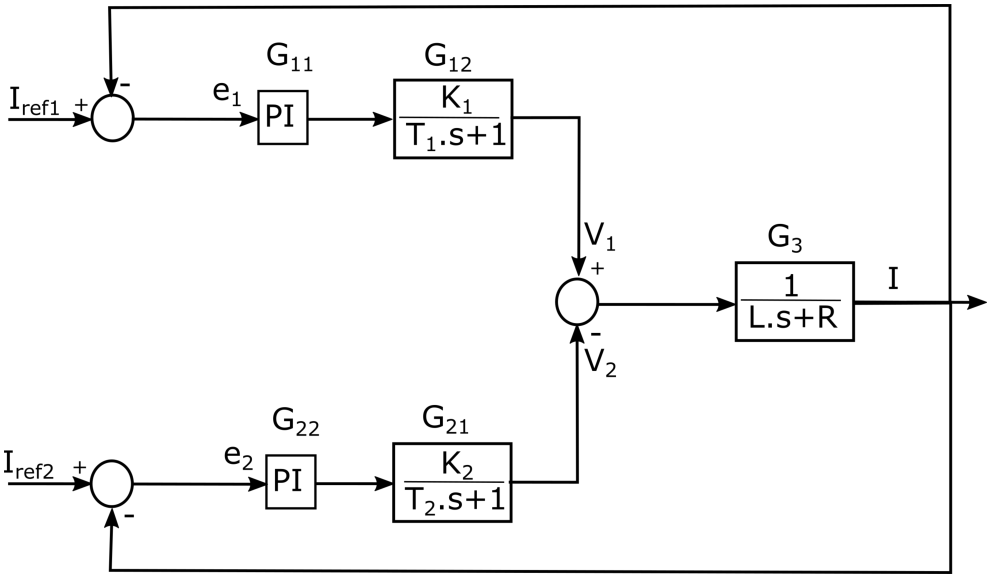

Figure 2.13: Block scheme of the power system

The inputs of the two drives are the direct and quadrature components of the current references. The errors e_1 and e_2 between the references i_d^* and i_q^* and the actual values of the currents i_d and i_q are passed to two PI regulators.

As the i_d and i_q currents are regulated in the same way, it is possible to focus on one component, which will be generically indicated as I as in figure 2.13.

The voltage across the choke is the difference of the inverter voltages. The transfer function of the choke is:

$$G_3 = \frac{1}{L \cdot s + R}. \tag{2.9}$$

with the same meaning of symbols as in Section 2.4.2.

As cited in [87], each inverter can be modelled as a gain K_i , wih a time lag T_i with $i = 1, 2$:

$$\begin{cases} G_{12} = \dfrac{K_1}{T_1 \cdot s + 1} \\ \\ G_{21} = \dfrac{K_2}{T_2 \cdot s + 1} \end{cases} \tag{2.10}$$

The gain can be obtained from the dc-link voltage V_{dc} and the maximum control voltage V_{cm} as:

$$K_i = 0.65\frac{V_{dc}}{V_{cm}} \tag{2.11}$$

The factor 0.65 is introduced to account for the maximum peak fundamental voltage obtained from the inverter with a given DC-link voltage [87]. The time lag in the inverter is equal to the average carrier switching-cycle time, i.e. half the period and is expressed in terms of the PWM switching frequency f_c as:

$$T_{1,2} = \frac{1}{2f_{c1,2}} \tag{2.12}$$

Naming G_{11} and G_{22} the transfer functions of the two PI regulators, the closed-loop transfer function of the system in figure 2.13 can be written in the matrix form:

$$I = \begin{bmatrix} W_1(s) & -W_2(s) \end{bmatrix} I_{ref} \tag{2.13}$$

where:

$$\begin{cases} W_1(s) = \dfrac{G_{11} * G_{12} * G_3}{1 + G_3(G_{12}G_{11} - G_{22}G_{21})} \\ \\ W_2(s) = \dfrac{G_{22} * G_{21} * G_3}{1 + G_3(G_{12}G_{11} - G_{22}G_{21})} \end{cases} \tag{2.14}$$

and

$$I_{ref} = \begin{bmatrix} I_{ref1} \\ I_{ref2} \end{bmatrix} \tag{2.15}$$

To analyse the stability range of the system, depending on the PI regulator constants values, the Routh-Hurwitz criterion was applied to the denominator of the closed-loop transfer functions W_1 and W_2. In the present case, the test inverter is operated at $8kHz$ switching frequency while the load inverter is operated at $16kHz$ switching frequency for the reason described in subsection 2.4.2. The remaining parameters are in Tab. 2.1. Fixing $K_i = 0.6 * K_p$ for both PI regulators (anyway K_i can be varied in a wide range without affecting the stability), the Routh-Hurwitz criterion outputs matrix M (shown in the appendix), whose first column contains five rows made by two positive constants and

three functions in terms of K_{p1} and K_{p2}. According to the Routh-Hurwitz criterion, to achieve stability, the elements of the first column should have the same sign. As the two constants are positive, the sign of the three functions in the first column must be studied, providing three inequations representing the stability conditions in terms of K_{p1} and K_{p2}. The three inequations can be graphically represented by three surfaces in the cartesian space. The values of the gains K_{p1} and K_{p2} ensuring stability are those for which the points of the surfaces have positive z-coordinates. The three surfaces are shown in figure 2.14 and a zoom of the most significant part (within the circle in figure 2.14) is in figure 2.15. The green surface represents the $z = 0$ plane. The points within the hatched area satisfy all three inequalities, i.e. if the K_{p1} and K_{p2} values are taken in that area, the system is stable.

In order to better clarify the procedure, the stability conditions for $K_{p1} = K_{p2}$ are studied. In this case, the Routh-Hurwitz matrix becomes:

$$\begin{bmatrix} 2.4 \cdot 10^{-12} & 7.5 \cdot 10^{-6} - 2.2 \cdot 10^{-4} * K_p & 0 \\ 4.4 \cdot 10^{-8} & 0.3 - 1.3 \cdot 10^{-4} * K_p & 0 \\ 2.1 \cdot 10^{-4} - 2.2 \cdot 10^{-4} * K_p & 0 & 0 \\ 0.3 - 1.3 \cdot 10^{-4} \cdot K_p & 0 & 0 \end{bmatrix} \tag{2.16}$$

The analysis of the first column provides the following stability condition:

$$K_p < 0.9 \tag{2.17}$$

which is consistent with figure 2.15

To verify the stability condition achieved by the Routh-Hurwitz criterion, the pole-zero map of W_1 and W_2 is also shown in figure 2.16 for $K_p = 0.1$ and figure 2.18 for $K_p = 1$,respectively, and using the parameters shown in Tab 2.1.

For $K_p = 0.1$, all the poles have a negative imaginary part which means that the system is stable respecting the stability condition of Eq. 2.17 while it becomes unstable for $K_p = 1$ where there appear two poles with positive real part as shown in figure 2.18.

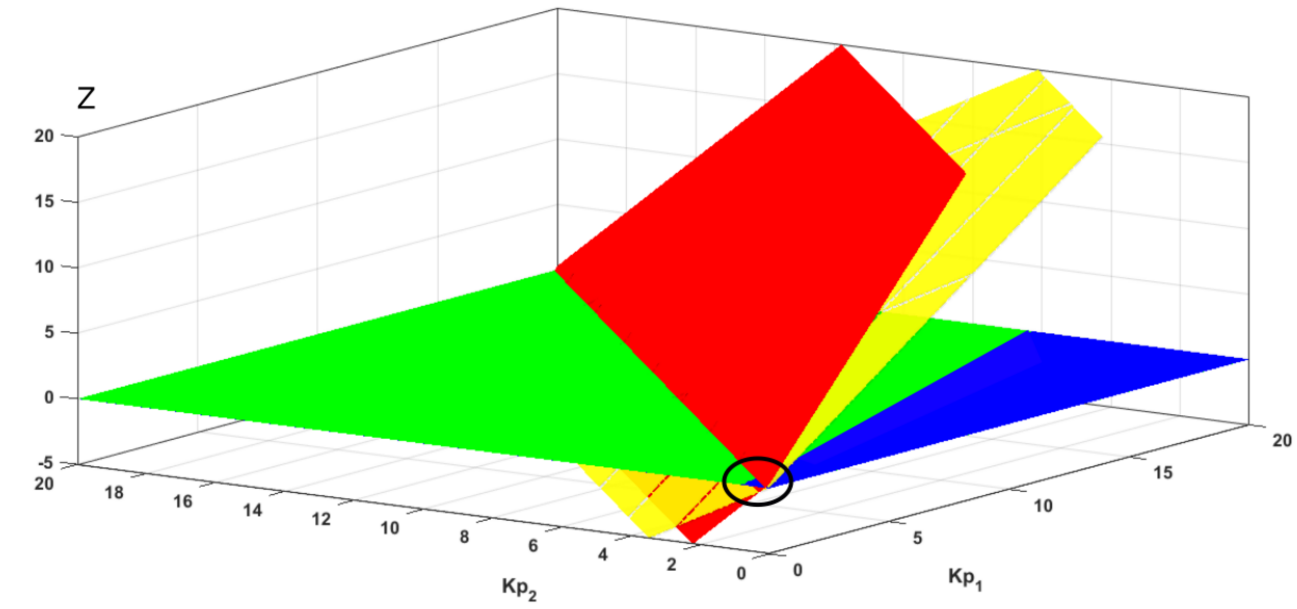

Figure 2.14: Graphical representation of the three last elements of the first column of the Routh-Hurwitz matrix M. The green plan is the $z = 0$ plan. The blue, red and yellow surfaces represent the three functions in the first column in the K_{p1} and K_{p2} variables.

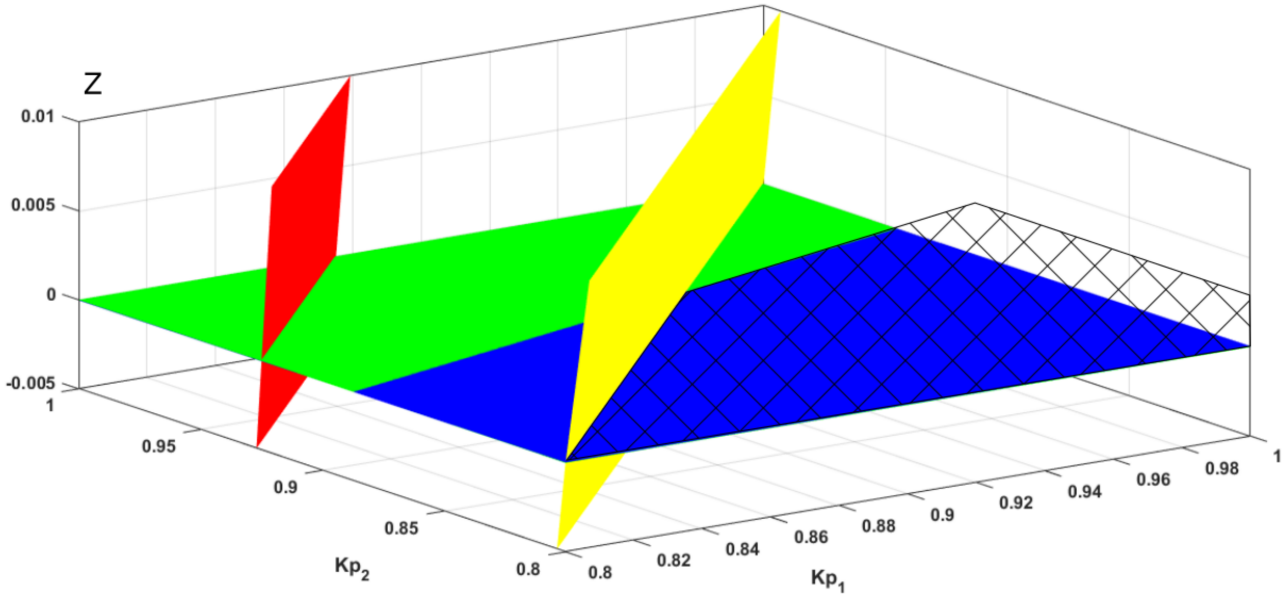

Figure 2.15: Graphical representation of the three last elements of the first column of the Routh-Hurwitz matrix M. Zoom of figure 2.14

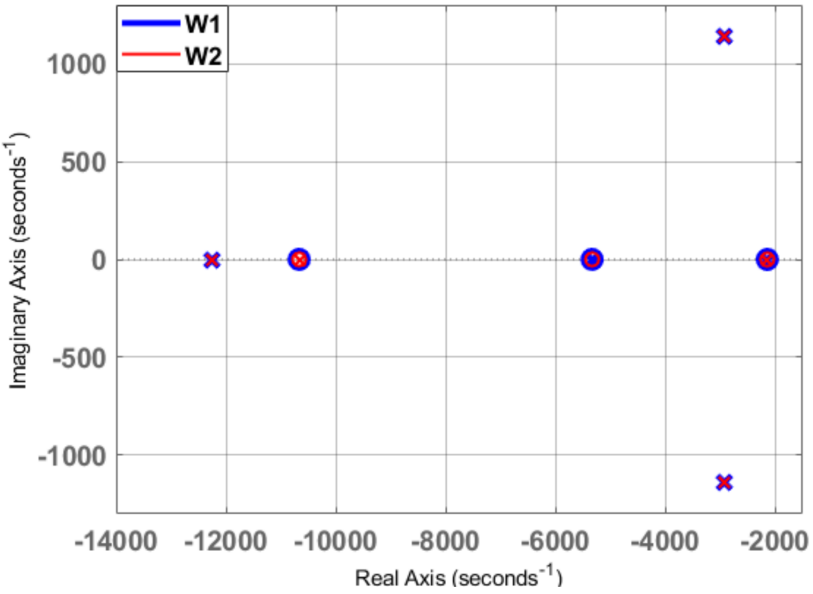

Figure 2.16: pole zero map of the transfer function W_1 and W_2 $K_p = 0.1$, $f_1 = 8kHz$, $f_2 = 16kHz$

Table 2.1: parameters

$K1, K2$	1.56
f_{c1}	8 kHz
f_{c2}	16 kHz
L	0.3 mH
R	0.3 Ω

Step responses are commonly used for the modal analysis, as step functions are able to excite all modes of a system. Accordingly, the step responses of W_1 and W_2 are shown in figure 2.17 for $K_p = 0.1$. The step responses are stable, confirming the aforementioned stability condition.

Step responses were also repeated for $K_p = 1$ as in figure 2.19. As expected, with the new value of K_p, the system response is divergent.

Finally, figure 2.20 shows the poles loci achieved by varying K_p. It is possible to note that increasing K_p pushes the poles towards the positive plane.

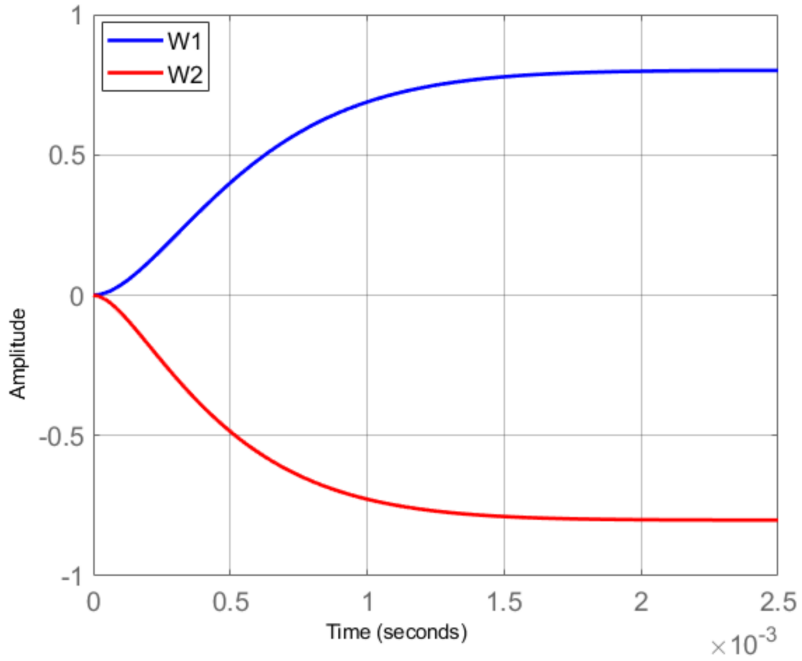

Figure 2.17: step responses of W_1 and W_2, with $K_p = 0.1$, $f_1 = 8kHz$, $f_2 = 16kHz$

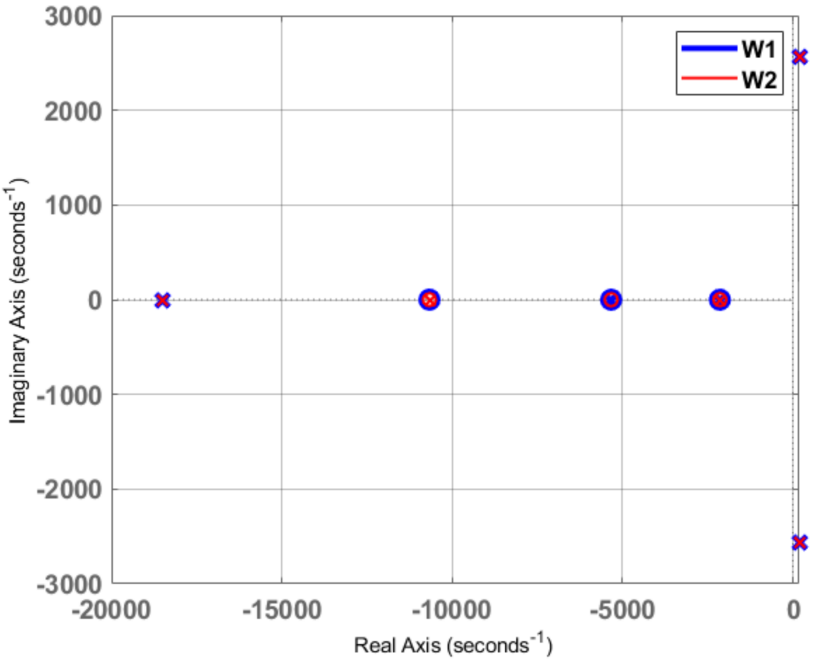

Figure 2.18: pole zero map of the transfer function W_1 and W_2 with $K_p = 1$, $f_1 = 8kHz$, $f_2 = 16kHz$

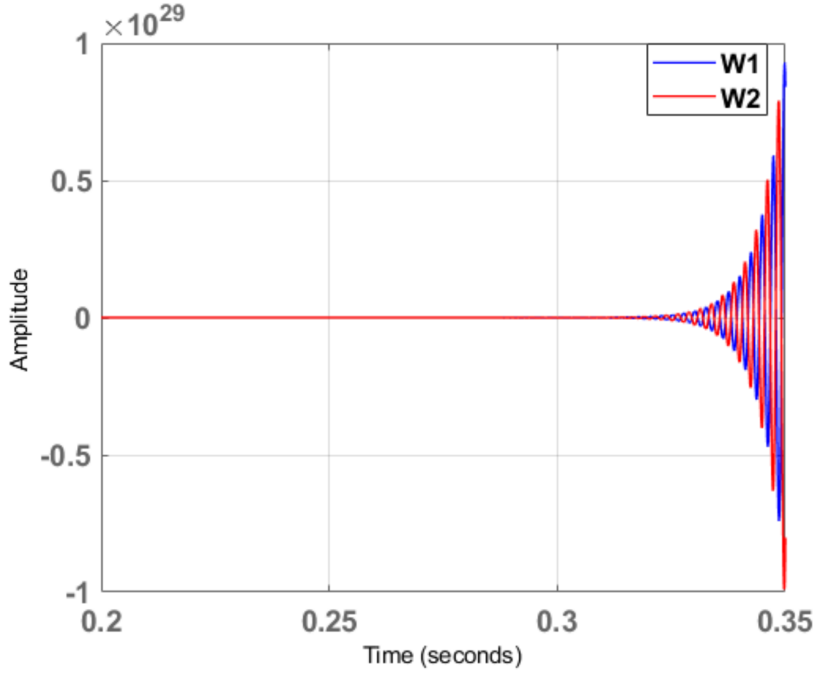

Figure 2.19: step responses of W_1 and W_2 with $K_p = 1$, $f_1 = 8kHz$, $f_2 = 16kHz$

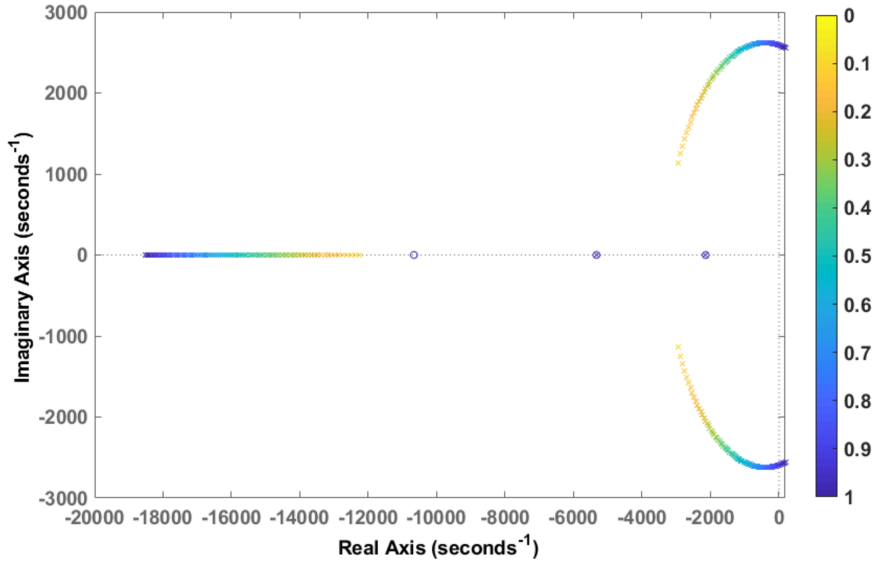

Figure 2.20: Loci of the poles of W_1 for different values of K_p in the range of [0..1].

2.5 Conclusion

In this chapter, the motivations to build test systems in the automotive sector and especially for inverters test applications has been introduced. Then the tow main configurations of inverter test bench and their characteristics has been described.

- The first solution generally called dyno test bench, uses a rotating system consisting of an electric motor mechanically coupled to a brake or a generator emulating the vehicle.

- The second alternative known by HIL e-motor emulator, which is a recent and less common solution, considers a power electronic emulator emulating a traction motor of a vehicle and connected to the AC terminals of the inverter under test.

A literature review of the HIL e-motor test solution, which represent the recent and advantageous configuration has been presented.

In this chapter, a new e-motor emulator dedicated to automotive electric drive tests has been proposed. The hardware part of a PHIL e-motor test solution has been described, it consists in a power system made up of two DC-AC converters connected through their AC sides by a three phase inductor (choke). One among the two converters is playing the role of an automotive inverter to be tested. The second is emulating the traction motor of an electric vehicle.

The analysis of the current ripple has shown the dependence of the ripple on the choke parameters and the speed. The value of the choke has been chosen to minimize the ripple, without introducing excessive delay in the current variation.

The stability of the system has been demonstrated through the analysis of the transfer functions of the power system components. The stability range was assessed in terms of proportional gains of the PI regulators.

Chapter 3

HIL implementation of the test system

Abstract : *A PHIL based machine emulator system, which is essentially power converters controlled to emulate an electric machine behaviour, can be used to test the traction drive inverter. This chapter presents a new PHIL testing technique dedicated to the performance assessment of electric powertrains for automotive applications. A numerically controlled experimental setting is developed, including a power system made up of two dc–ac converters with their ac sides connected through chokes and a control system implemented in a national instrument PCI eXtensions for instrumentation (NI PXI) hardware-in-the-loop testing system. This system emulates the dynamic behavior of the electric vehicle and of its powertrain.*

Keywords : Automotive drive test,
NI PXI system,
Control system model,
Vector control,
Vehicle daynamics,
Virtual testing environment.

3.1 Introduction

A significant amount of work has been done into the design, analysis and testing of inverters for electric traction drive systems. Testing procedures for power electronics devices usually comprise a costly and time-consuming process especially when the inverter have to be connected to electromechanical systems in the case of dayno test solutions.

At present, RT HIL test methodology is increasingly being recognized as an effective approach for simplifying the testing operation of automotive powertrains. In HIL test systems, a simulated model interact with the real hardware being tested, creating a virtual testing environment similar to reality, where test operations can be performed in total safety. This test methodology has been used to build inverter test facilities, yielding the so-called HIL machine emulator, where a power electronic circuit emulates the power flow of the real electric machine, without including any rotating mechanical parts. However, this new testing solution is still poorly supported in research works and industrial applications, and needs further improvement and development.

This chapter proposes a new architecture of a PHIL test system, using the electric machine emulator discussed in the previous chapter, which is a standard four-quadrant drive controlled in RT emulating at its terminals a real motor driving the wheels of an electric vehicle. The NI PXI test devices used to implement the HIL system are presented. A control system (CS) simulated model is implemented in the NI PXI to control the tested drive in RT, and to provide the load drive with the ability to reproduce the same motor terminal behaviour as he simulated motor model in the two directions of the power flow, corresponding to the acceleration and regenerative braking modes.

The CS includes a permanent magnet synchronous motor model used as a traction machine driving the wheels of a vehicle model, allowing the system to create a virtual environment able to emulate real operating conditions of a vehicle during a given driving cycle. The RT simulation of the CS provides the required control signals to the machine emulator and the IUT constituting the power system. The test conditions and driving scenarios can be changed in RT, using graphical interfaces designed in Veristand.

3.2 Implementation of a PHIL Test System

As described in the first chapter, the purpose of the HIL test system is to provide a virtual testing environment simulated in RT, and to achieve an interaction between a real system including the device under test and a simulated plant. The simulated model contains only the devices considered risky for the successful development of system.

In our case the HIL needs to be implemented to provide the suitable control signals to the tested and load inverters, constituting the power system explained in the second chapter. In other words, to provide the virtual testing environment, the proposed machine emulator and more specifically the load inverter, should be controlled in RT in order to reproduce the motor terminal behaviour in the two directions of the power flow, corresponding to the acceleration and regenerative braking.

Once the appropriate architecture for the HIL system is selected, the first step in building a HIL test system is to select the components that suitably-meet the development requirements. A HIL system should be developed in the form of one or more software that allows the model of the system to be simulated, a RT processor to perform the various tasks in a deterministic and appropriate manner, I/O interfaces in order to achieve the communication of the simulated environment with the real one.

In this regard, there are many commercial and industrial equipments to implement HIL systems. RTDS, Opal-RT, and Typhoon are some different types of acknowledged commercial HIL testing equipment, that are used widely in power systems and power electronics emulation and testing. Also, some custom-designed HIL systems [88, 89] have used FPGA as a RT simulator. PCI eXtensions for Instrumentation (PXI) systems has emerged as a major force in the test equipment and instrumentation industry. The PXI system provides a rugged PC based platform for use in automated test, data acquisition and many other applications. It successfully combines different elements and modules with a high electrical performance specification and a low cost. This makes the PXI an ideal platform for HIL applications and RT power system simulation.

The PXI standard was established by the US company National Instruments (NI) [90]

and offers a wide variety of solutions to specifically implement HIL systems, it employs engineering software like NI-VeriStand which is specially designed to handle interactions between all hardware and software included in the test platform. The description of such a technology is presented hereunder.

3.2.1 PXI Instrumentation Platform

PXI is a rugged PC-based platform dedicated to measurement and automation systems. It combines PCI electrical-bus features with the modular, Eurocard packaging of Compact PCI [90]. It includes specialized synchronization buses and key software features. PXI is a high-performance and low-cost deployment platform for applications such as manufacturing test, military and aerospace, machine monitoring, automotive, and industrial test.

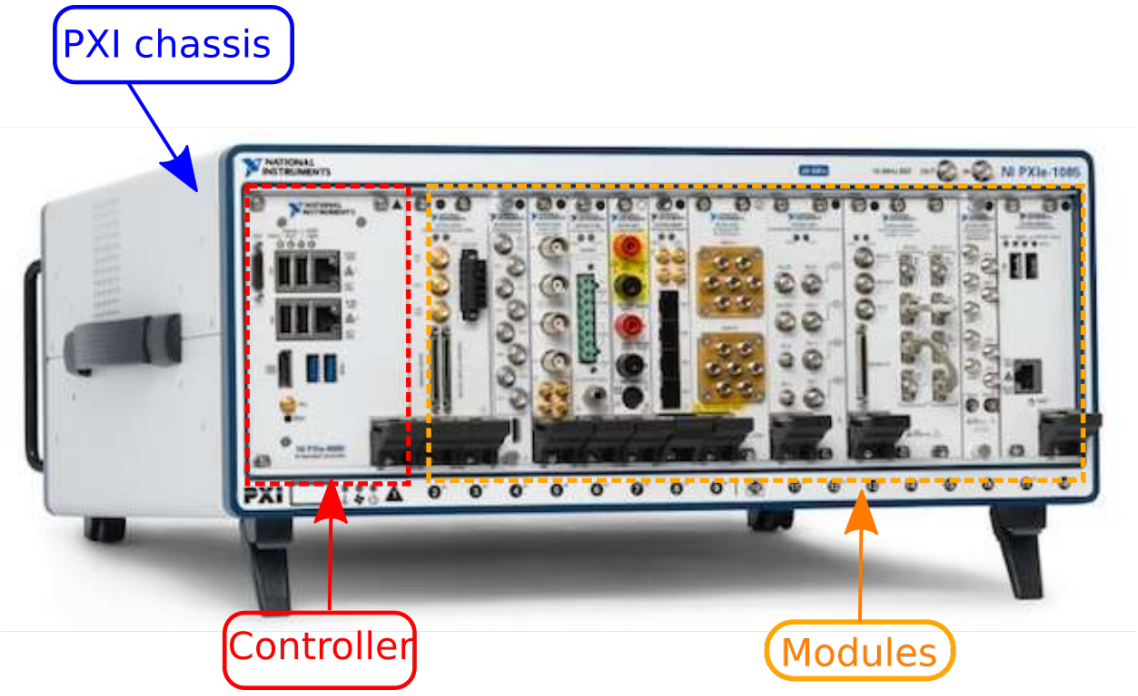

Figure 3.1: Photo of the PXI system

Developed in 1998, it was introduced as an open industry standard to meet the increasing demands of complex instrumentation systems. PXI standard is governed by the PXI Systems Alliance (PXISA), a group of more than 70 companies chartered to promote the PXI standard, ensure interoperability, and maintain the PXI specification.

A further advantage of PXI is that having been adopted by the industry it will remain in use for many years to come, thereby enabling any investment to be protected. These advantages make PXI an ideal standard for use as test equipment.

A PXI system is basically composed of three elements [90] as shown in figure 3.1.

- PXI Chassis,
- System controller,
- Modules or instruments that slot into the chassis.

PXI Chassis

The PXI chassis is the most visible element of the PXI system. It literally provides the framework for the system and it normally can range in size from four slots up to eighteen. As the backbone of the PXI system, the chassis provides the power and cooling to the controller and modules. It also contains a high performance backplane enabling the cards in the system to be able to communicate rapidly with one another.

As regards the application discussed in this work, it was considered a PXI chassis NI PXIe-1062Q shown in figure 3.2 necessary and sufficient for technical characteristics.

Figure 3.2: NI PXIe-1062Q Chassis PXI Express

NI PXIe System Controller

As the specifications of the hardware PXI, PXI chassis all include a slot located in the first slot on the left (slot 1), to the controller.

There is a variety of controllers that could equip a PXI system. The controller should be selected according the specifications required by the HIL system. Figure 3.3 shows a photo of a NI PXIe-8135 controller used in the proposed HIL test application.

Figure 3.3: NI PXIe-8135 Controller

Modules

The National Instruments offers more than 200 different PXI modules and because PXI is an open industry standard, more than 1,500 modules are available from more than 70 vendors. Each of these forms has different characteristics and functions suitable for any development needs, which give the PXI Platform a high level of flexibility.

In order to create the HIL test system, a module is required to process the signals, whether they are inputs or outputs. This is achieved by peripheral modules among which, one can select the NI PXI-7853R R Series with Virtex-5 LX85 FPGA, shown in figure 3.4. It consists in a multifunction reconfigurable input/output (RIO).

Figure 3.4: NI PXI-7853R multifunction RIO module LX85

The NI PXI-7853R Multifunction RIO LX85 has three connectors. Each one has a specific reference label that provides assignments information and the pins address. For the purpose of using these pins in the mapping process.

For the sake of simplicity and safety, National Instruments recommends shielded cables and plugs compatible connectors as accessories, as the one shown in figure 3.5. It enables the connection to one among the three connectors of the RIO module.

3.2.2 Measurement and Automation Explorer

The PXI system has to be connected to the host PC, so that the NI Veristand software can recognize it as a possible target, in which the virtual environment model will be simulated in RT. This is achieved by a connection to one of the two Ethernet ports on the controller while configuring the software NI MAX (Measurement & Automation Explorer). The NI MAX is installed by default in the host PC.

The NI MAX allows:

- The access and the configuration of all NI hardware and software detected by the host PC,
- Creates and edit channels,

- Run system diagnostics,
- Keep NI software updated.

Figure 3.5: NI SCB-68 connector

3.2.3 NI VeriStand

The PXI modules are able to operate independently which makes them usable for other purposes. For this reason, it is essential to involve an additional software that make these modules working together, manage the data flow, and the timing of the entire system.

The NI Veristand is a software package distributed by National Instruments which is designed specifically for developing advanced RT testing applications, such as HIL simulations. This software achieves actions which depend on its execution mechanism using the so-called "NI VeriStand Engine".

In the proposed test bench system, NI Veristand allows to import simulation models and control algorithms into the PXI system. It is also used to design an editable user interface that allow engineers to interact with the simulated model, modify model parameters, change test conditions or scenarios, and monitor application data in RT without the need of any programming knowledge.

3.3 Real Time Control Model Simulated in the PXI

The NI PXI provides a virtual test environment suitable for RT simulation and control of complex systems. In the proposed test bench, a control model is simulated in RT inside the PXI, providing a virtual environment to test the inverter under different driving conditions, by emulating all possible automotive cycles. The PXI provides the required control signals for both converters within the power system described in the second chapter. It also communicates with a host PC allowing the variation of the system parameters and of the operating conditions in RT, giving more flexibility of the test solution.

The control system (CS) includes not only the motor model, but also the vehicle and road dynamics models, providing the system with the capacity to emulate the real operating conditions of the drive in simulated driving cycles. The vehicle model adds flexibility to the system in comparison to other similar solutions, allowing to implement any kind of EV and road condition by changing the RT emulator parameters.

The CS provides the control signals to the power system in order to reproduce the motor terminal behaviour in the two directions of the power flow, corresponding to the acceleration and braking modes. The parameters of the road, vehicle and motor model can be changed in RT to implement different types of vehicles and driving cycles.

The models implemented in the CS are non-linear and tightly connected, as they contain the speed and the load torque as variables and must therefore be solved together. A general structure of the control scheme is shown in figure 3.6.

The load inverter must be commanded to absorb the same power as the simulated drive during the driving cycle, i.e. it must generate the same torque at the same speed. To guarantee that the real drive operates at the same speed as the simulated one, the rotor angle θ_m is computed through the integration of the simulated speed Ω_m.

The simulated speed Ω_m is produced by solving the vehicle model and the mechanical section of the electric drive model as shown in figure 3.6. The simulated value of the rotor angle θ_m is converted into a real signal by the virtual resolver. This signal provides the resolver input to both real drives: the load and the test converter.

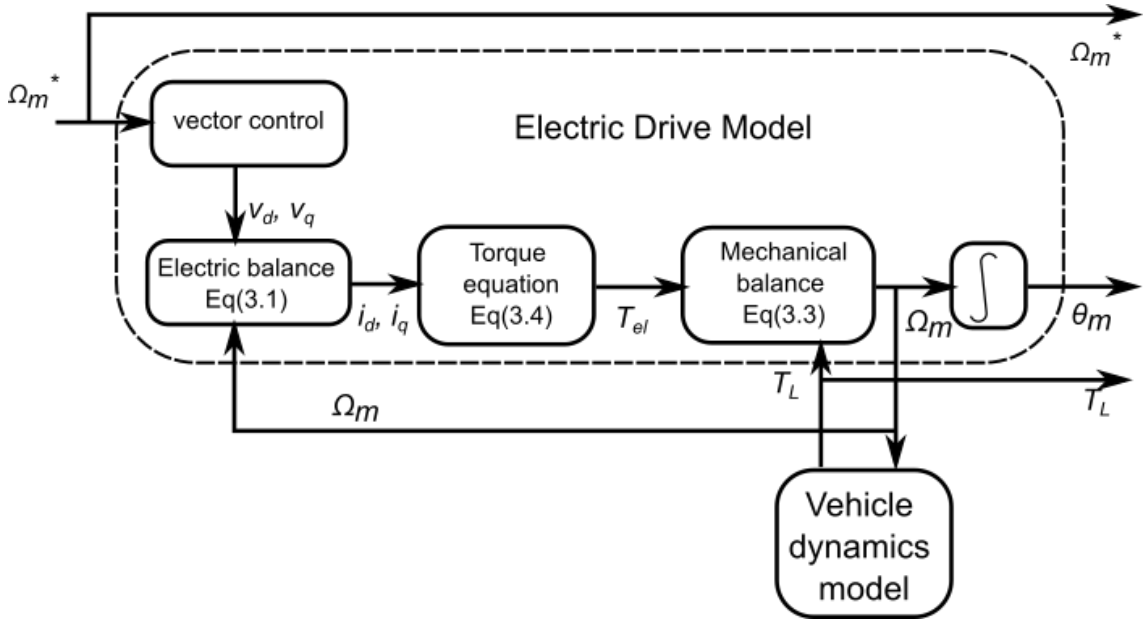

Figure 3.6: Control system block scheme

The torque reference to the load drive is the load torque T_L. Even this signal must be generated through simulation. The load torque is achieved through the integration of the road/vehicle model. It serves as an input to the mechanical balance equation, to produce the speed, as shown in figure 3.6. The other input to this equation is the electromagnetic torque of the simulated motor T_{el}.

The simulated drive, as the tested drive are speed-commanded in this test bench and their speed reference signal Ω_m^* is generated internally in the CS.

The CS model is implemented in a NI PXI system, and it is interfaced to the power system through three analog output signals:

- The speed reference signal to be applied to the drive under test;
- The computed rotor angle;
- The torque reference signal applied to the drive emulating the traction motor.

The models composing the control system, their Mathematical equations and schemes are described hereunder.

The control scheme implemented in the PXI is in figure 3.7, this scheme is the graphical detailed representation of the block scheme in figure 3.6.

It considers a permanent magnet synchronous motor (PMSM) fed by a current-regulated voltage source inverter and driving the wheels of an electric vehicle. A vector control strategy is implemented in the electric drive model.

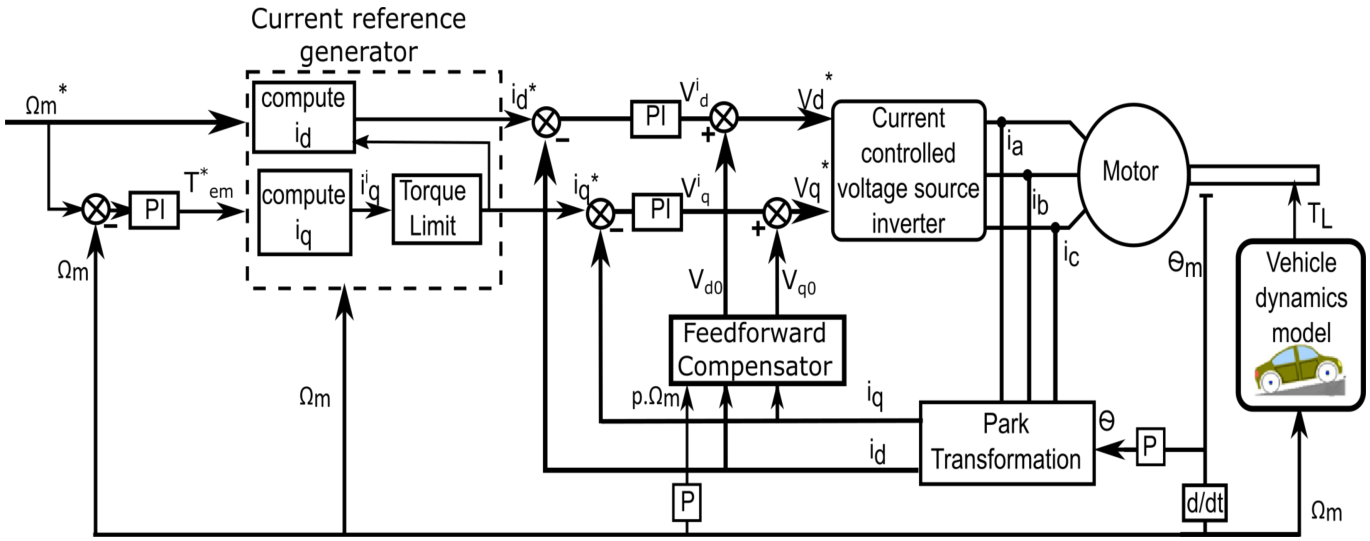

Figure 3.7: Vector control scheme implemented in the NI PXI

3.3.1 Electric Motor Model

The selection of the PMSM is motivated by its higher performance especially in terms of energy efficiency compared to the induction motor. The PMSM voltage equations are expressed as follows:

$$\begin{cases} v_d = ri_d + \dfrac{d\lambda_d}{dt} - p\Omega_m\lambda_q \\ v_q = ri_q + \dfrac{d\lambda_q}{dt} + p\Omega_m\lambda_d \end{cases} \tag{3.1}$$

where:

- v_d and v_q are the direct and quadrature components of the armature phase voltages,
- i_d and i_q are the direct and quadrature components of the armature phase currents,
- λ_d and λ_q are the direct and quadrature components of the armature phase flux linkages,

- r is the armature phase resistance,
- Ω_m is the rotor speed,
- p is the number of pole pairs.

The direct and quadrature components of the armature phase flux linkages are expressed in terms of i_d and i_q as follows:

$$\begin{cases} \lambda_d &= L_d i_d &+ &\lambda_{pm} \\ \lambda_q &= L_q i_q \end{cases} \tag{3.2}$$

where:

- L_d is the armature inductance within the d-axis,
- L_q is the armature inductance within the q-axis,
- λ_{pm} is the PM flux linkage, also called no-load flux.

The mechanical equation of the model is expressed as follows:

$$T_{em} - aT_L = \frac{J}{a}\frac{d\Omega_{wh}}{dt} + D\Omega_{wh}\frac{1}{a} \tag{3.3}$$

where:

- J and D are the inertia and damping coefficient, respectively,
- T_L is the load torque of the motor, which is in fact the traction torque at the wheels shaft,
- T_{em} is the electromagnetic torque developed by the PMSM, with:

$$T_{em} = \frac{3}{2}p(\lambda_d i_q - \lambda_q i_d) \tag{3.4}$$

- a is the reduction ratio of the gearbox,
- Ω_{wh} is the drive wheel speed.

The D'Alembert Equation Eq. 3.3 provides the wheel speed as an input to the vehicle dynamics system. The vehicle dynamics model provides the value of the load torque T_L

3.3.2 Vector control

A standard IPM motor vector control has been implemented [91]. However, the same scheme can be used to control an SPM motor by selecting $i_d = 0$ and $L_d = L_q$. The control technique is different in the constant torque and in the flux-weakening regions. The block scheme of the control technique is in figure 3.7. Below base speed, the Maximum Torque per Ampere (MTPA) control is used. The i_d component is computed as:

$$i_d^* = \frac{\lambda_{pm}}{2(L_q - L_d)} - \sqrt{\frac{\lambda_{pm}^2}{4(L_q - L_d)} + i_q^2} \tag{3.5}$$

The maximum torque is achieved with this control technique when the i_d^* current reference reaches

$$i_{d,a}^* = \frac{\lambda_{pm}}{4(L_q - L_d)} - \sqrt{\frac{\lambda_{pm}^2}{16(L_q - L_d)} + i_{max}^2} \tag{3.6}$$

with i_{max} maximum current:

$$i_{max} = \sqrt{{i_{d,a}^*}^2 + i_q^2} \tag{3.7}$$

The intermediate voltage commands v_d^i and v_q^i are provided by two PI regulators. To cancel cross-coupling effects and linearize the current control loops, a feedforward compensator is considered, as shown in figure 3.7 [91, 92]:

$$\begin{cases} v_{d0} = -p\Omega_m L_q i_q \\ v_{q0} = p\Omega_m(\lambda_{pm} + L_d i_d) \end{cases} \tag{3.8}$$

The reference voltages v_d^* and v_q^* are then achieved as:

$$\begin{cases} v_d^* = v_d^i + v_{d0} \\ v_q^* = v_q^i + v_{q0} \end{cases} \tag{3.9}$$

Above base speed, if the torque limit is reached, the flux weakening control is activated. The reference id^* is calculated as:

$$i_d^* = -\frac{\lambda_{pm}}{L_d} \pm \frac{1}{L_d}\sqrt{(\frac{V_{out}}{p\Omega_m})^2 - (L_q i_q)^2}. \tag{3.10}$$

where V_{out} is the limit value of the phase voltage. Eqs. 3.5 and 3.10 are used to compute i_d in the MTPA and field-weakening region. Considering the reference torque

T^*_{em} as an input, the system consisting of Eqs. 3.4 and 3.5 or Eqs. 3.4 and 3.10 provides the current references i^*_d and i^*_q . In commercial drives, the relations linking i^*_d, i^*_q to the torque reference are implemented through lookup tables.

3.3.3 Vehicle dynamics

The vehicle model plays a key role in the system, as it allows to implement the dynamical behaviour of a given vehicle. The formulation is made in terms of the wheel angular speed, taking into consideration the vehicle and the road parameters which can be modified in RT. A simplified vehicle model has been developed in [93], based on [94].

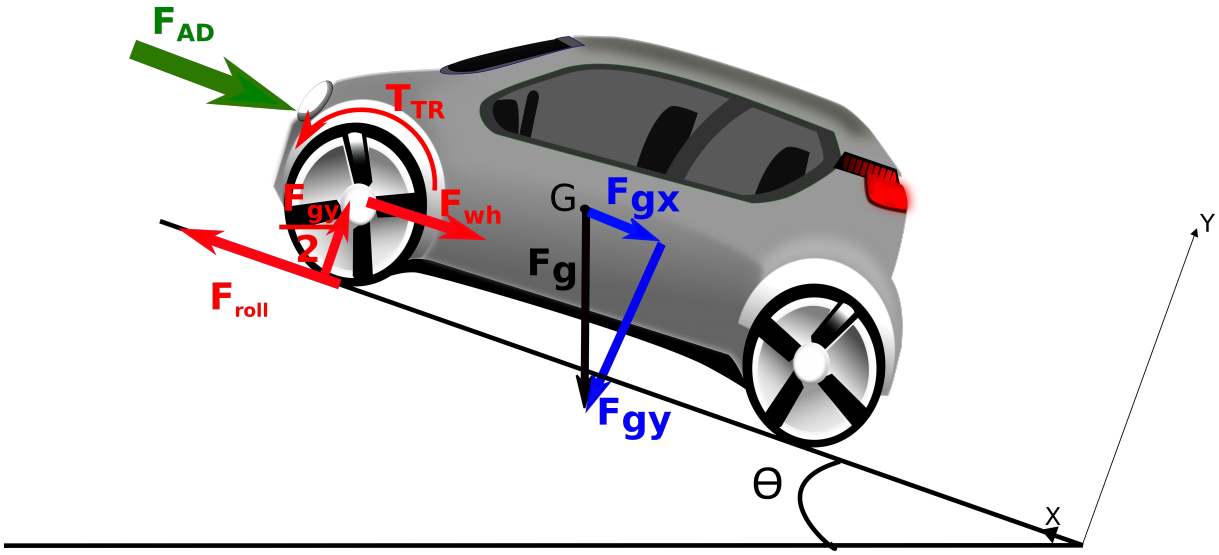

Figure 3.8: Forces applied on the vehicle

Prior to develop the model representing the longitudinal dynamic of the vehicle, the following assumptions have been considered:

- The forces applied to the vehicle right-side half are assumed to be identical to those applied to its left-side one. Consequently, the model could be limited to one half of the vehicle,
- The motion is limited to the longitudinal direction,
- The vehicle is a two-wheel drive type that is to say the model limited to the half of the vehicle considers a traction force applied to one wheel (for instance the front wheel).

The model developed here under considers the external forces acting on the vehicle which are classified into two types, as cited:

- Forces acting on the vehicle chassis,
- Forces acting on the vehicle wheel which arises from the physical interaction between the tire and the road.

Forces Acting on the Chassis

Let us consider a system of orthogonal axis, namely (G; x, y, z) with its origin G located in the center of gravity of the vehicle, the so-called "body axis". The motion directions are indicated by the vectors (i, j, k), as illustrated in figure 3.8, where the invisible z-axis is perpendicular to (x, y) plane and is pointing to the driver right side.

Accounting for just the longitudinal motion of the vehicle, so only the (x, y) plane is considered, figure 3.8 shows the typical forces acting on chassis, which are:

- The gravitational force F_g with its two components (F_{gy}, F_{gx}),
- The aerodynamic force F_{AD},
- The traction force F_{wh}.

Gravitational Force The gravitational force F_g represents the weight of the vehicle acting at its center of gravity, with a magnitude equal to its total mass m multiplied by the acceleration of gravity g.

Considering the general case of a sloped road, the gravitational force has two components: (i) a longitudinal component F_{gx} which is proportional to the sine of the slope and parallel to the road, and (ii) a vertical component F_{gy} which is proportional to the cosine of the slope and perpendicular to the road surface. These are expressed as follows:

$$\begin{cases} F_{gx} &= mg\sin\theta \\ F_{gy} &= mg\cos\theta \end{cases} \tag{3.11}$$

where θ is the angle characterizing the road inclination, the so-called "road slope angle". The longitudinal component acts on the vehicle going uphill and downhill. In order to

account of the two directions, a sign (+) or (-) is affected to this force depending on whether the vehicle is going down or uphill.

Aerodynamic Force The aerodynamic force F_{AD} is a force that resists to the motion of a body through a fluid like air or water. If the motion of the body is in a fluid like air it is called air resistance. The aerodynamic force always acts in the direction opposite to the flow velocity. F_{AD} is a function of the square of the speed as expressed here under [95]:

$$F_{AD} = 1/2(\rho C_x S_t (V + V_w)^2) \tag{3.12}$$

where ρ is the air density which is equal to 1.225kg/m^2 , C_x is the drag coefficient depending on the body shape, V is velocity of the vehicle, V_w is the air velocity, and S_t is the maximum vehicle cross area in m^2.

Traction Force The traction force is applied from the wheels axis to the vehicle chassis. During acceleration, the traction force plays the main role to push the vehicle forward. During braking, the kinetic energy of the vehicle is taken down by the brakes. In this case, the traction force turns to be negative, reducing the speed of the vehicle (braking effort) which is known as the longitudinal force. In this model the traction force is calculated using the *Pacejack* tire model developed here under.

Forces Applied to the Wheel

The forces acting on the wheel are shown in figure 3.9, where:

- F_{wh} is the traction force,
- F_{roll} is the longitudinal reaction force applied by the ground on the wheel. Under steady state operation, F_{roll} is balanced by F_{wh}
- F_{gy} is the force counteracting the weight of the vehicle applied in the center of gravity G. The sum of the forces F_{gy} applied to the wheels is constantly equal to the vehicle weight.

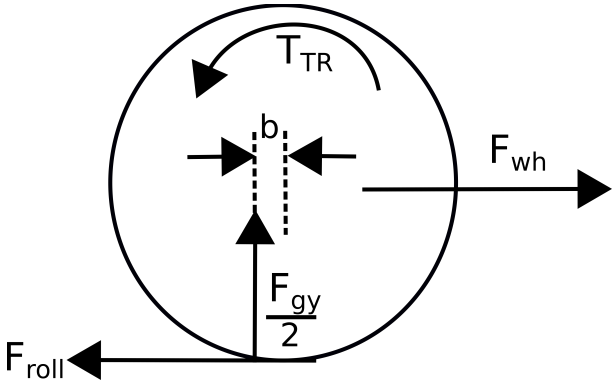

Figure 3.9: Forces applied to the wheel

Tire Model

Dealing with vehicle dynamics, the tire model has a great importance for the investigation of the behavior of a moving vehicle. It is the only link between the vehicle chassis and the road. Several models of the tire are available in the literature, among which one can distinguish the so-called "magic formula tire model" proposed by *Pacejka* [96].

Fundamentally, the magic formula tire model is not based on a physical background and does not involve the dynamics fundamental principle equation. It is an experimentally-assisted analytical model that considers mathematical approximations of curves which are recorded during experimental tests of the vehicle. The developed model includes scaling factors that are predicted using the data based obtained from the carried out experimental tests.

The *Pacejka* model calculates the friction coefficient μ as follows:

$$\mu(\sigma) = D\sin(C\arctan(B\sigma - E(B\sigma - \arctan(B\sigma)))) \tag{3.13}$$

where B, C, D, E are parameters that specify the road conditions. Their values, for different road types, are provided in table 3.1.

and where σ is the slip ratio which is expressed in terms of the wheel radius R and rotating velocity ω (in rad/s), and the vehicle linear velocity V (in m/s), as follows:

$$\sigma = \begin{cases} \dfrac{(R\omega - V)}{R\omega} & \text{during acceleration} \\ \\ \dfrac{(R\omega - V)}{V} & \text{during braking} \end{cases} \tag{3.14}$$

Table 3.1: B, C, D, E parameters for different road types

	B	C	D	E
Dry Road	10	1.9	1	0.97
Welt Road	12	2.3	0.82	1
Snow	5	2	0.3	1
Ice	4	2	0.1	1

Accounting for the value of σ, one can establish a relation linking F_{roll} and F_{gy} as follows:

$$F_{roll} = \mu(\sigma)\ \frac{F_{gy}}{2} \tag{3.15}$$

Model Formulation

Generally speaking, the modelling of a system is an approach to formulate its behavior by a set of equations. The model allows, for a given domain of validity and a given accuracy, the prediction of the system outputs in terms of its inputs.

The model to be derived in this paragraph is dedicated to reproduce the dynamic behavior of a road vehicle. It is based on the *Alembert* equations. These represent the equilibrium between the active and reactive forces applied to the wheels. This model takes into account the vehicle weight as well as the road slope, the traction, the friction, and the aerodynamic forces. The derived model involves some constants which are the characteristic parameters of the vehicle and of the road.

The developed model is initiated by the dynamics fundamental principle equation. It consists in expressing the equilibrium of the forces acting on the vehicle chassis in the longitudinal direction parallel to the direction of the motion, as follows:

$$F_{wh} - F_{AD} - F_{gx} = (m/2 + 2M_{wh})\frac{dV}{dt} \tag{3.16}$$

F_{gx} is the weight force component in the motion direction referred to half of the vehicle. Refering to figure 3.8, F_{gx} is expressed as follows:

$$F_{gx} = (m/2 + 2M_{wh})g\sin(\theta) \tag{3.17}$$

where θ is the road slope angle.

The equilibrium of the forces causing the linear motion gives:

$$F_{roll} - F_{wf} = M_{wh}\frac{dV}{dt} \tag{3.18}$$

The equilibrium of the torques causing the wheel rotation is expressed as:

$$T_{TR} - F_{roll}R - \frac{F_{gy}}{2}b = J_{eq}\frac{d\omega_{wh}}{dt} \tag{3.19}$$

where T_{TR} is the traction torque, b is the distance between the wheel axle and the center of the pressure curve as illustrated in figure 3.9, and J_{eq} is the equivalent moment of inertia of the total wheel drive system.

The above derived model involves four unknowns which are: F_{wf}, F_{roll}, V, ω_{wh}. However ω_{wh} is an input of the model which directly linked to the rotor speed of the traction motor model.

Accounting for equation (3.18), F_{wf} can be expressed as follow:

$$F_{wf} = F_{roll} - M_{wh}\frac{dV}{dt} \tag{3.20}$$

Rewriting equation (3.16) taking into account equation (3.20) has led to:

$$F_{roll} - F_{AD} - F_{gx} = (3.M_w + m/2)\frac{dV}{dt} \tag{3.21}$$

The integration of equation (3.21) yields the velocity V. Furthermore, the wheel rotational speed could be directly measured. Hence, the slip ratio σ can be calculated using equation (3.14) accounting whether the vehicle is accelerating or braking. Then, the friction coefficient μ can be predicted using the magical formula (3.13).

F_{roll} and F_{AD} are predicted applying equations (3.15) and (3.12) respectively. Then, the resistant torque T_r is obtained applying the following relation:

$$T_r = F_{roll}R + \frac{F_{gy}}{2}b \tag{3.22}$$

Finally, the vehicle load torque T_l is predicted as:

$$T_l = 2T_r \tag{3.23}$$

The vehicle model calculates the resistant torque from the angular wheel speed, taking into account the road slope angle and the vehicle and road parameters. A block diagram of the quarter car is in figure 3.10

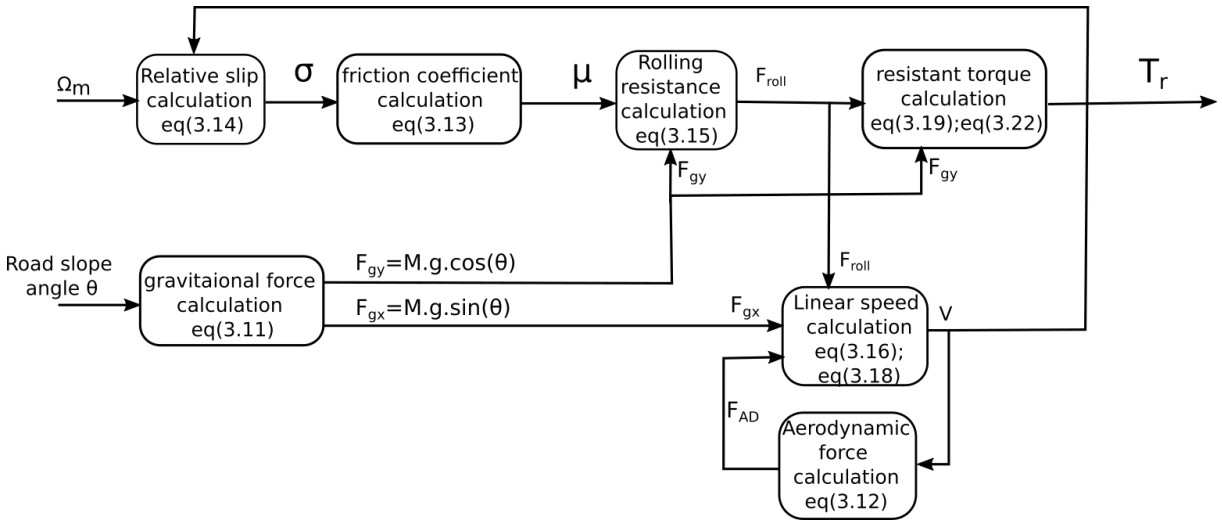

Figure 3.10: Vehicle dynamics quarter car model block diagram

3.4 Interfacing the Power System to the Control

As described in the previous chapter, the power system replicates the operation of a drive train consisting of the converter under test feeding the three-phase load converter. The load converter emulates a PMSM driving the wheels of an electric or hybrid vehicle.

The power system is simply interfaced to the control through two analogue signals, as shown in figure 3.11 :

- The reference speed, which is the input to the speed loop of the drive under test, shown in figure 3.12;
- The load torque T_L provided by the vehicle dynamics model to control the torque loop of the load drive, shown in figure 3.13.

For the sake of simplicity and cost-effectiveness, the rotor angle is passed to the virtual speed transducer, which is a custom-made hardware transforming the digitally-computed

angle into an analogue signal compatible to that of a real encoder/resolver interface. The virtual speed transducer is interfaced to the encoder/resolver input of the test and the load inverters. The PMSM rotor position θ_m is provided by the encoder emulator to both drives. A general block scheme of the system is shown in figure 3.11.

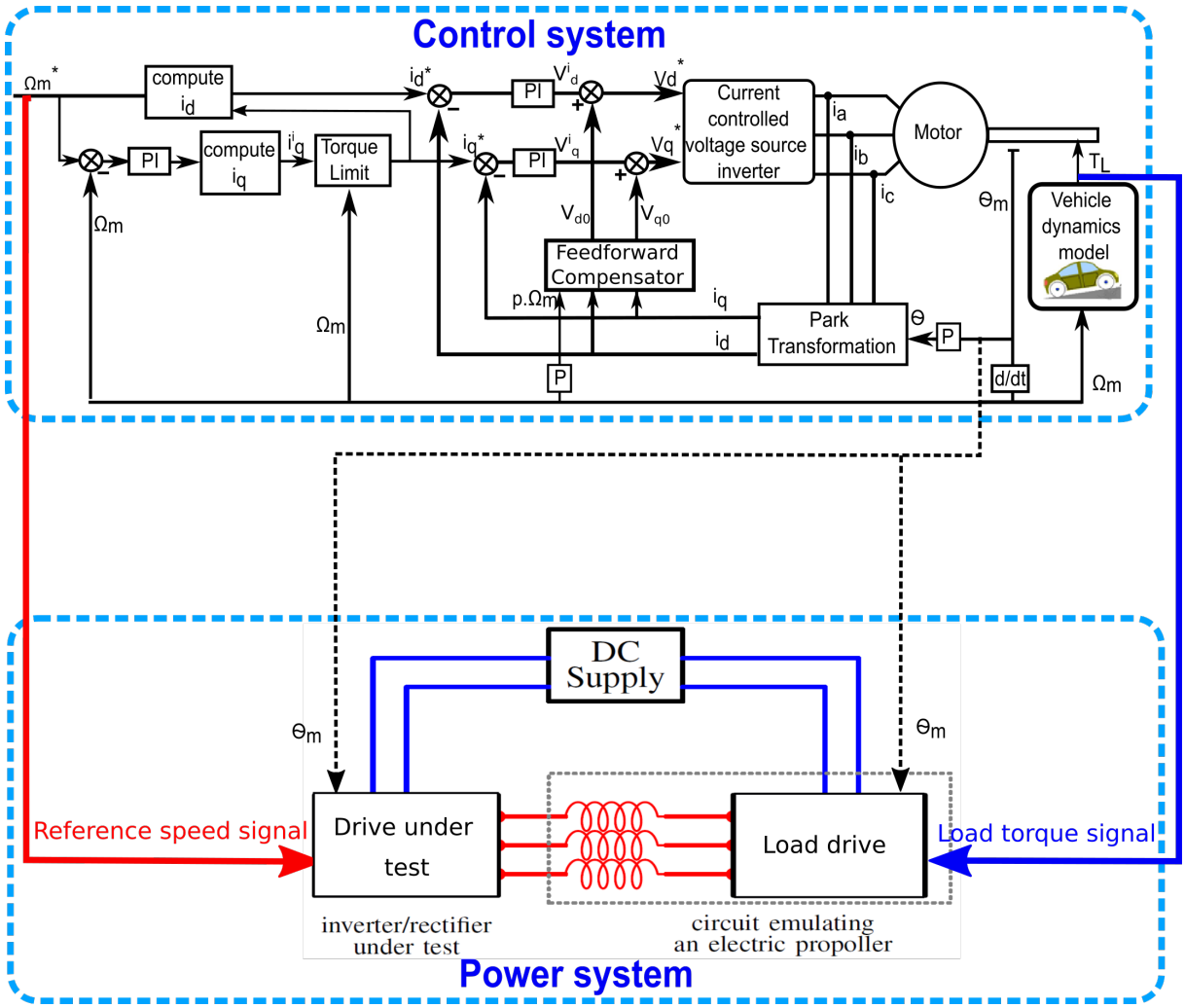

Figure 3.11: Schematic diagram of the developed test bench. The lower section contains the physical drives, the upper part is the structure of the control scheme.

It is important to remark that EVs are usually controlled in torque mode, although most EV drives also include a speed command for cruise control and for implementing other special functions. To achieve stability, one drive must be speed controlled and the other should be torque controlled. In the present implementation of the test bench

we chose to provide torque reference to the load drive, to allow the tested drive to be commanded to replicate a given driving cycle.

The inverter under test is speed controlled, the speed control scheme shown in figure 3.12. The speed error is fed to a current reference look-up-table in order to generate the current command i_q^* and i_d^*.

The load inverter is torque controlled, the torque control scheme shown in figure 3.13. The torque commend is fed to a current reference look-up-table in order to generate the current command i_q^* and i_d^*.

In both control scheme shown in figures 3.12 and 3.13, the reference currents i_q and i_d are compared with their respective actual currents. The resulted errors are used to generate the voltage commands v_q^i and v_d^i. a feed forward compensator is used to compensate the voltage commands after measuring the respective actual voltages. The voltage references v_q^* and v_d^* are used as inputs to the SVPWM block to generate the PWM gate signals to control the inverter. The rotor position is used to achieve the Park transformation of the measured currents and voltages. The parameters of the control loop are the same used in the simulated model implemented in the PXI.

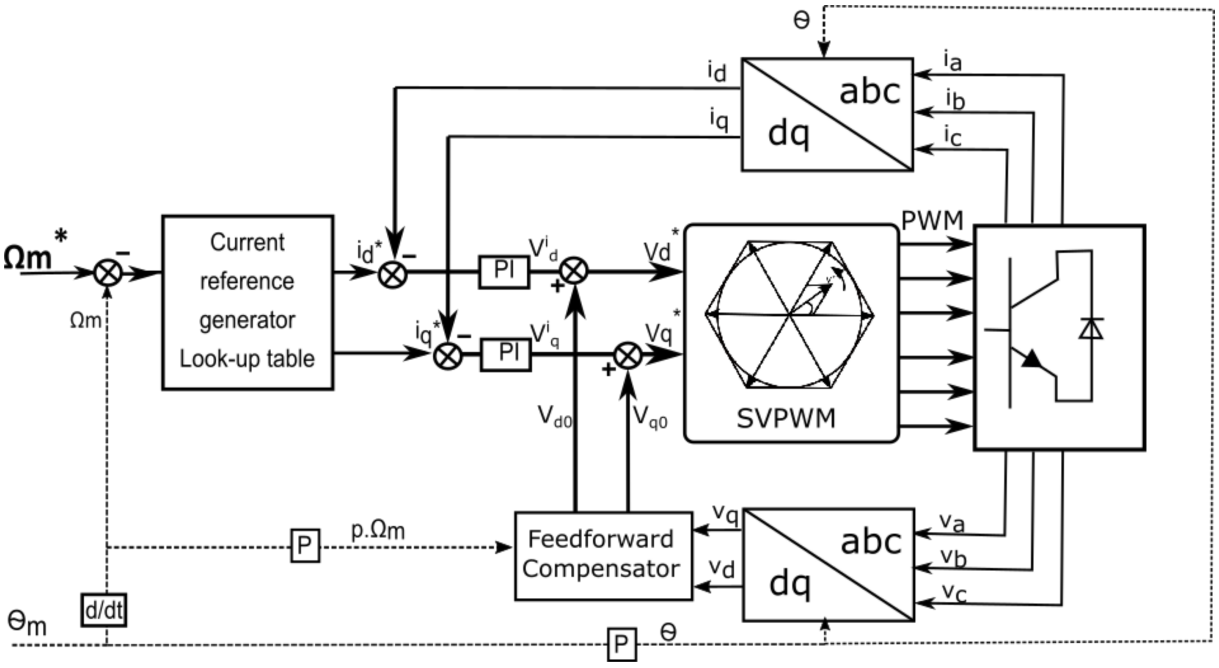

Figure 3.12: Control scheme of the drive under test

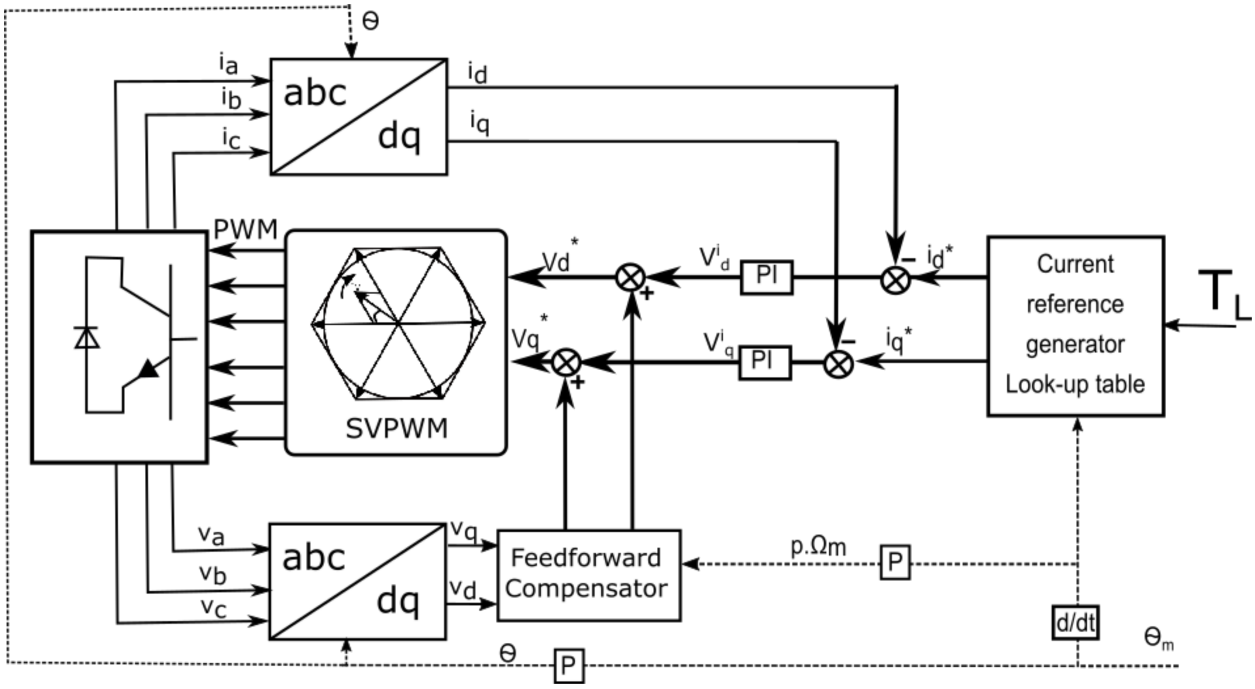

Figure 3.13: Control scheme of the load drive

In order to achieve the RT control of the test system, two graphical interfaces have been designed which are described hereunder:

- *The main dashboard* whose layout is shown in figure 3.14. It enables RT control of selected drive variables such as the inputs (the reference speed and the road slope angle). It also enables the display of the speed in both rpm and rad/s (circular scales), the armature phase current, the load torque, the mechanical power demanded by the load,

- *The vehicle control dashboard* whose layout is illustrated in figure 3.15. It offers the possibility of modifying some variables in the vehicle model, such as the mass, the wheel radius, the road parameters. Moreover, it enables the on-line supervision of the aerodynamic drag, the rolling resistance, and the gravitational forces, as well as the vehicle speed, which are taken into account in the vehicle dynamics model.

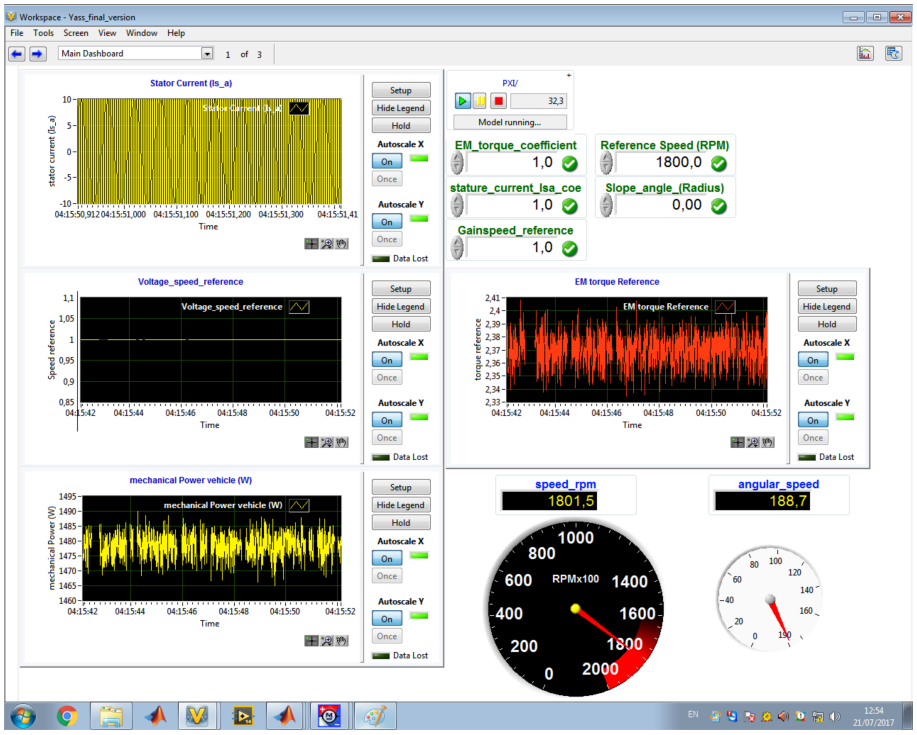

Figure 3.14: Designed main dashboard layout

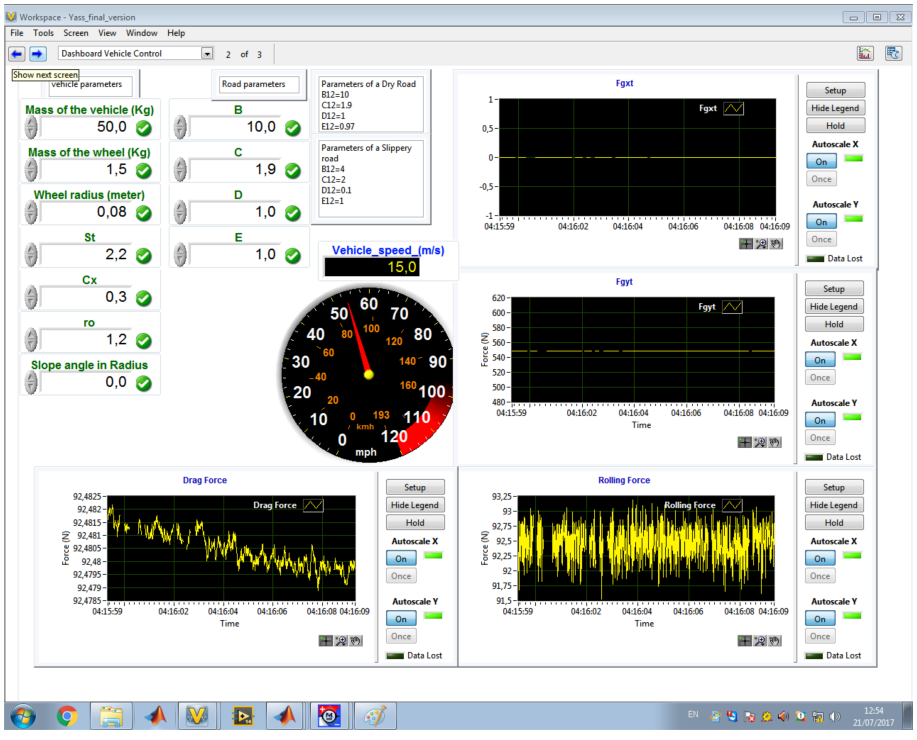

Figure 3.15: Designed vehicle control dashboard layout

The HIL test system is implemented using the NI PXI system components described in section 3.2. Two Unitek DC/AC commercial converters are used in the test bench system to provide a proof-of-concept. The first converter is the one to be tested and the second converter is playing the role of a load as explained in 2.4.1. The control scheme described in the previous chapter (section 3.3) is modelled with Matlab Simulink, then implemented in the NI PXI system using NI Veristand, to be simulated in RT. NI Veristand is used to import the simulated model into the PXI system, to manage the input/output signals, and to assure the communication between the power system and the simulated model representing the virtual environment. Therefore the HIL test system can provide a virtual testing environment able to emulate different driving scenarios similar to the real life. NI Veristand is also used to design user graphical interface that allows to interact with the simulated model, modify the model parameters, change test conditions and scenarios in RT, as the two interfaces shown in figures 3.14 and 3.15.

A picture of the developed test bench is given in figure 3.16.

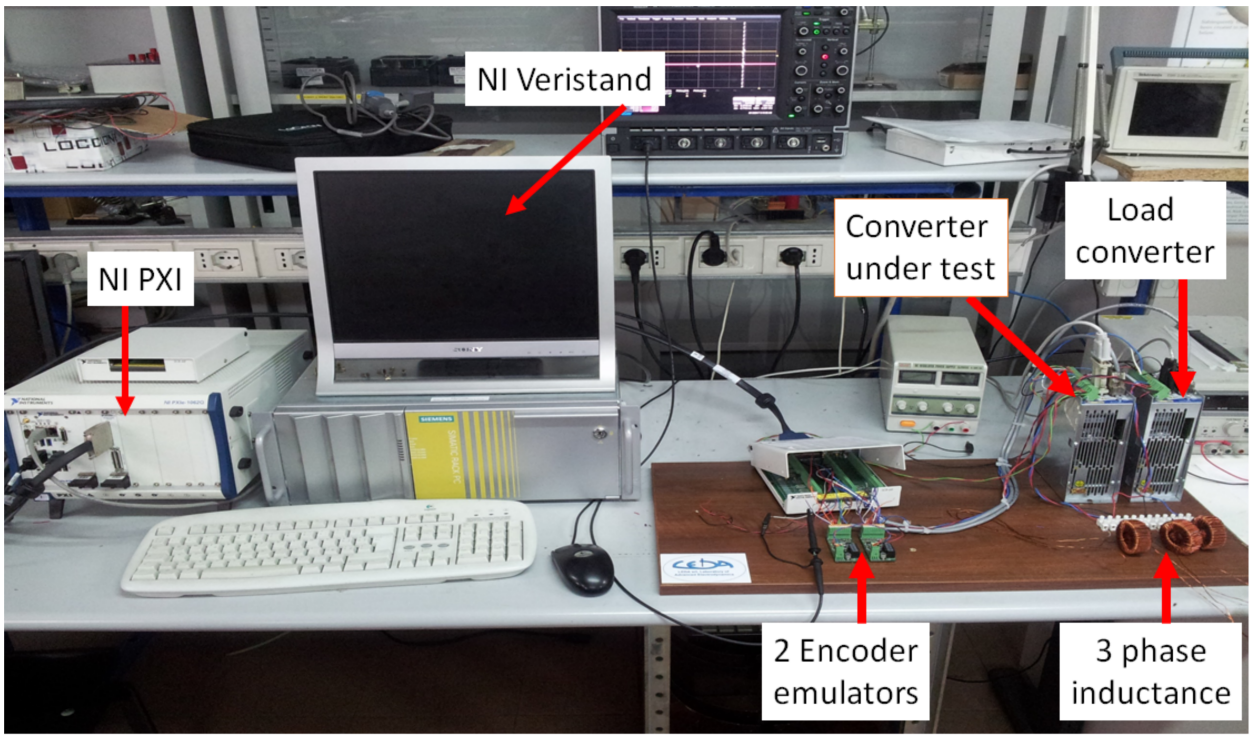

Figure 3.16: Photo of the developed test bench

3.5 Conclusion

The chapter presents the development of a PHIL test facility for automotive electric drivetrain testing. The HIL instrumentations used to implement the test system have been described, it consists on a NI PXI system equipped with a RT controller and an input/output module. The PXI system used in this work is able to simulate a given model and communicate with the real system under test in RT.

The test system consists of:

- The electric drive to be tested,
- An electric drive acting as a load. connected to the tested drive through a three-phase choke and emulates a traction motor driving the wheels of an electric vehicle,
- A control system implemented in a NI PXI RT simulation HIL system. The control system integrates in RT the equations of three models:
  - The synchronous motor;
  - The vector control;
  - The vehicle dynamics.

The simulation program implemented in the NI PXI interface considers a permanent magnet synchronous machine (PMSM) fed by a vector-controlled voltage source inverter. The load torque considered in the mechanical equation of the PMSM is provided by the vehicle dynamics model. The simulated model implementation allows performing all control tasks in RT.

The power system is controlled through two analogue signals generated from the PXI:

- The reference speed, to control the inverter under test,
- The load torque T_L provided by the vehicle dynamics model to control the load inverter.

User graphical interfaces have been designed using Veristand software allowing a RT interaction with the simulated model. Therefore it is possible to modify the model parameters and to change test conditions in RT.

The experimental validation of the proposed test are treated in the next chapter.

Chapter 4

Real Time Test Results Analysis of the Developed System

Abstract : *After the description of the concepts, architecture and structure of the PHIL inverter test facility, the accuracy of the test bench should be examined through experimental tests. The experimental emulation of automotive driving cycles in two case studies highlights the effectiveness of the developed automotive testing system. The power flow is analysed during the motoring and the regenerative braking phases.*

Keywords : Machine emulation quality,
Acceleration,
Motoring mode,
Braking,
Regenerative mode.

4.1 Introduction

The primary objective of this chapter is to perform a RT experimental tests that are able to reproduce the behaviour of the PMSM machine. The previous chapters expose the concepts, structures and preferred topologies of the HIL inverter test facility, to get the best results for the desired application. For its part, this chapter encompasses all these studies and accomplishments to finally achieve the inverter test application using electric machine emulation.

In the following investigations, the proposed PHIL test bench is carefully analysed in order to obtain a representative statement about the quality of the machine emulation. To evaluate the test system emulation quality, it is important to check the behaviour of the machine emulator during steady state and transient operations, and verify if the machine emulator reproduce at its terminals the same behaviour as the PMSM machine model simulated in RT. For this reason, various, systematic and comparative measurements are carried out on the HIL test bench. The experimental study investigates significant technical aspects, like the power balance and regeneration capability of the drive.

To provide a proof-of-concept, a reduced scale testing equipment described in the previous chapters and shown in figure 3.16 was assembled and operated for different driving conditions. An industrial full-scale testing facility has also been built in the Loccioni group research laboratories using the same testing concept and architecture, and the results are provided. To validate the approach, the drive is commanded to carry out a standard european driving cycle. In both cases the whole control system, including the motor and the vehicle dynamics model, is integrated into the NI PXi to be simulated in RT. The integration of the system equations is performed in the NI PXI within a sampling time of $0.1ms$. The accuracy and reproducibility of the measurement results on a HIL test bench is of central importance for later use in the development of electrical drive systems.

4.2 RT Test Results

Once the PHIL test system is implemented, experimental tests can be caried out in order to examine the accuracy of the PHIL electric machine emulation. In other words it is necessary to ensure a good correlation between the behaviour of the RT simulated motor model and the machine emulator in the real hardware component of power system. Hence it is important to check the current of the simulated motor model against the measured current in the terminals of the machine emulator during RT experimental tests.

Electric drives have been tested using the proposed technique. Case study A relates to a powertrain involving an axial flux Surface mounted Permanent Magnet (SPM) PMSM. This system is a laboratory equipment which served to validate the concept, to verify the choice of the inductances and to assess the power flow in normal operation and in the regenerative braking. Case study B represents a full-scale industrial test bench for an EV powertrain with an Interior Permanent Magnet (IPM) PMSM. This test equipment was built and installed in the Loccioni company and is designed to test commercial drives for EVs using real parameters. The parameters of the vehicles and the road for Case study A are in Tab. 4.1, the parameters of the motors for both Case studies are in Tab. 4.2.

Table 4.1: Vehicle parameters for both case studies

Vehicle mass	50 Kg
Wheel mass	1.5 Kg
wheel radius	6 cm
maximum vehicle cross area	1.2 m^2

Table 4.2: Electric motor parameters for both case studies

	SPM	IPM
V_{dc}	24V	475V
L_d	0.7mH	0.194mH
L_q	0.7mH	0.292mH
Rs	0.3Ω	0.0.008Ω
p	8	4
λ_{pm}	0.01Vs	0.021
J	0.0035 Kg m^2	0.044 Kg m^2

4.2.1 Case Study A

This section discusses the results obtained following different tests carried out on the developed bench for Case A. Two UNITEK drives model DS2420 have been used as shown in figure 3.16. In order to limit both the power supply power and the choke size, the weight of the vehicle and the dimensions have been reduced. The scaling factor for the weight is $s_1 = 0.05$ and for the dimensions is $s_2 = \sqrt[3]{s_1} = 0.37$. All other parameters are real. These tests cover operations emulating:

- Start-up cycle,
- Constant driving conditions (speed and slope),
- Constant speed and variable road slope,
- Constant road slope angle and variable speed.

The variation of the traction motor armature currents with time is recorded in the driving cycles above summarized.

Start-up

Let us consider a start-up period of $10s$, from standstill to a constant speed reference equal to $1000rpm$, as shown in figure 4.1. The road slope angle has been kept constant equal to zero in the vehicle model embedded in the control system. In other word the simulated vehicle is being driven on a horizontal road.

Figure 4.2 shows the waveforms, of the simulated phase current of the motor model generated by the PXI, and the emulated one measured at the input of the load inverter. One can notice a quite acceptable agreement between the simulation and the emulation results, in terms of frequency and amplitude, during the start-up as well as at steady-state operation.

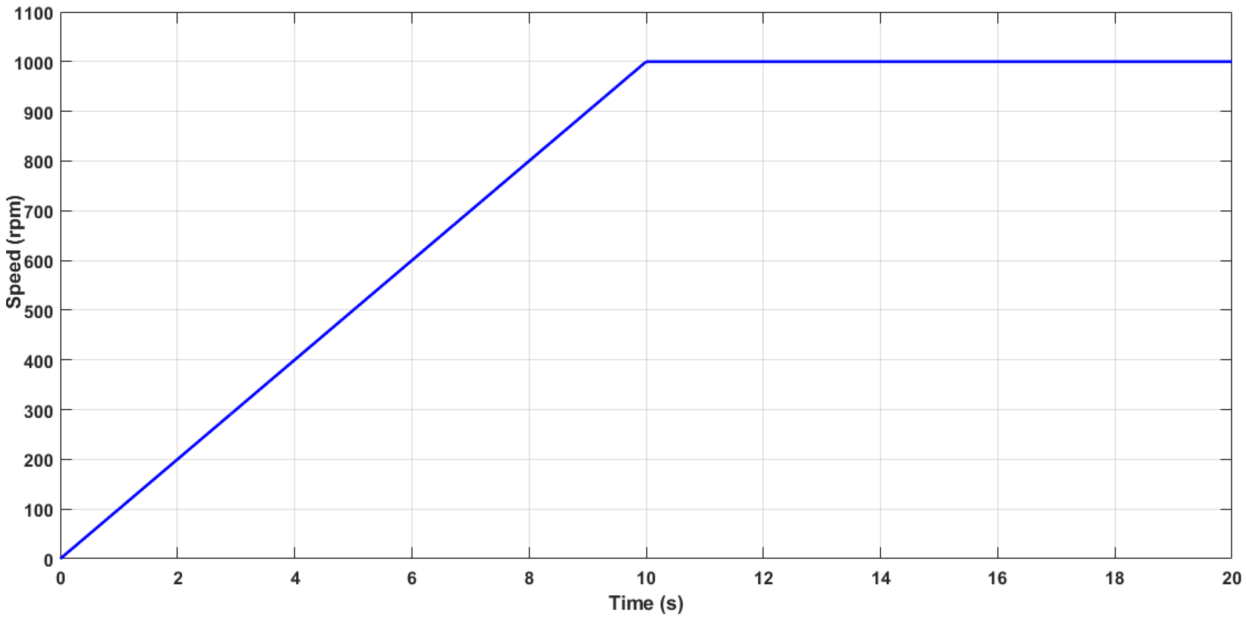

Figure 4.1: Start-up, reference speed

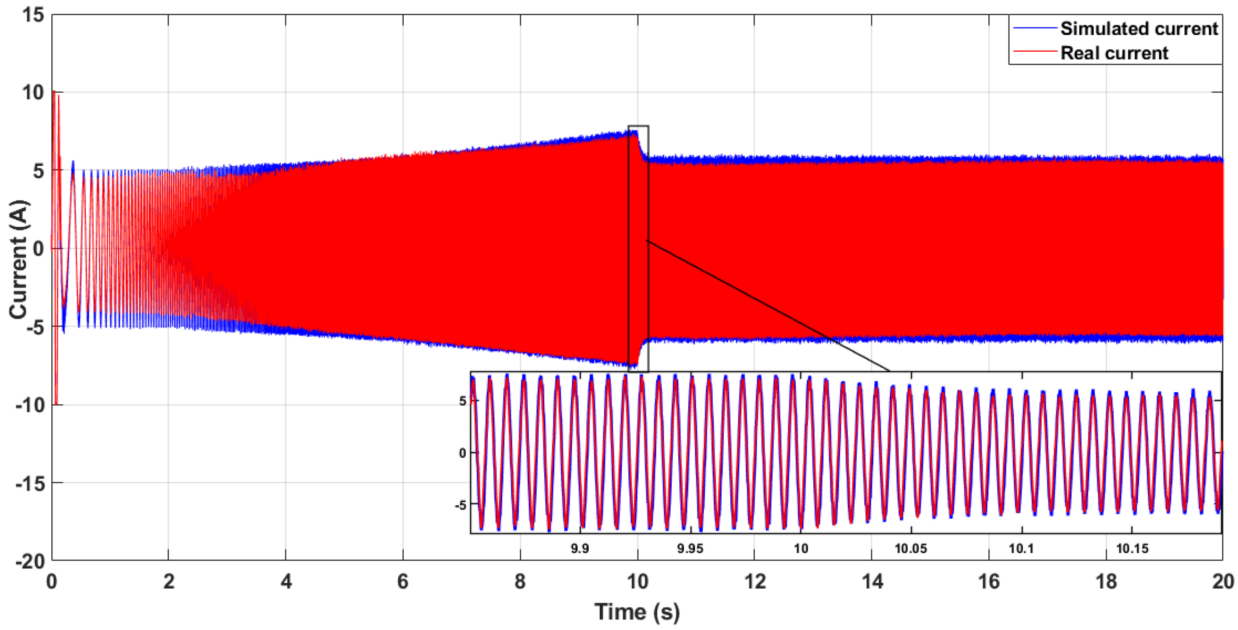

Figure 4.2: Simulated and emulated phase current variation during the start-up cycle: (blue) simulated current generated by the PXI, (red) measured current at the load inverter terminals

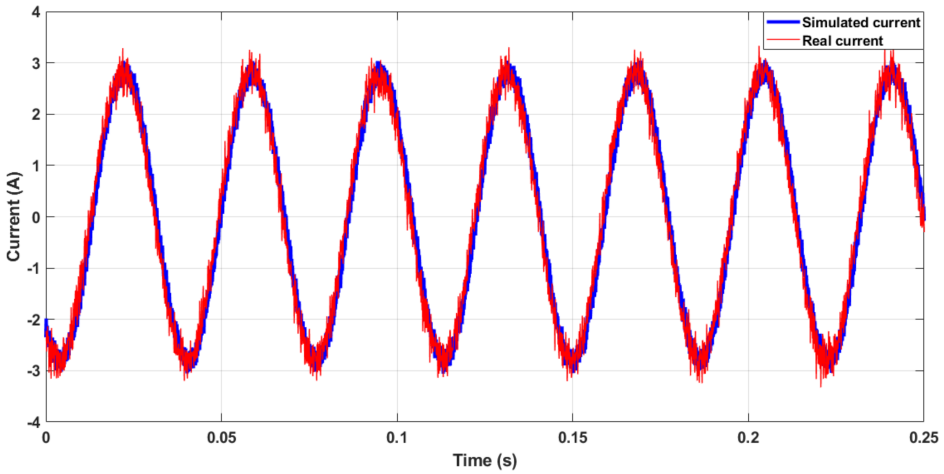

(a)

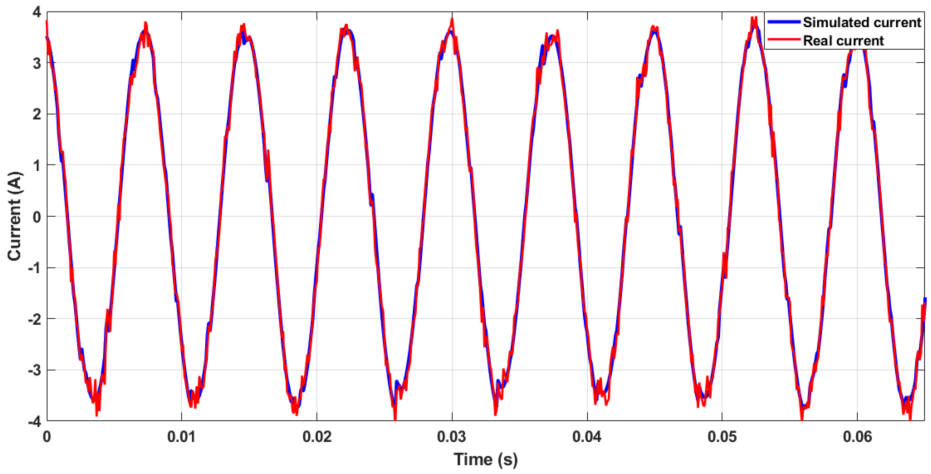

(b)

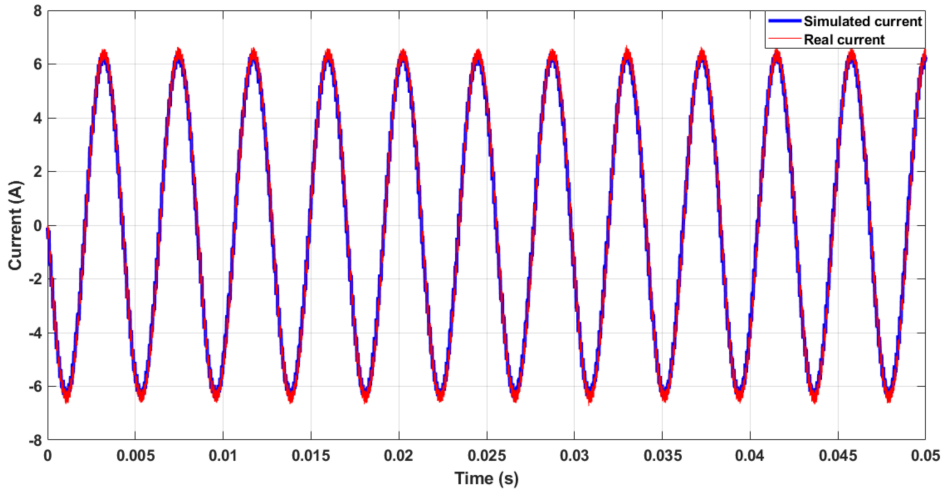

(c)

Figure 4.3: Simulated (blue) and emulated (red) phase currents for a road slope angle of 0.1rad for different speeds N_m. **Legend:** (a) N_m=200rpm, (b) N_m=1000rpm, (c) N_m=1760rpm

Operation at constant driving conditions

Let us consider the case of a positive road slope angle $0.1\,rad$. The simulated vehicle is climbing a hill that is 12% sloped, the EV drivetrain operates in motoring mode. Figures 4.3.(a), 4.3.(b) and 4.3.(c) show the traction motor phase current for the speeds of 200rpm, 1000rpm and 1760rpm, respectively. From the analysis of these results, and as expected taking into account the load torque exhibited by the vehicle, the motor phase current increases non linearly with the speed. A quite acceptable agreement between the simulation and emulation results is noticed.

Both in the simulated and in the measured waveforms, the current ripple reduces while the speed increases. For the simulated currents, this behaviour is obvious: as the speed increases, the back EMF increases and the difference between the back EMF and supply voltage reduces. Moreover, the reactances increase and therefore the current ripple is reduced. For the measured waveforms, the ripple reduces, as analyzed in Secection 2.4.3.

Operation at constant speed and variable road slope

Following a start-up transient at zero road slope angle $\theta = 0$, the vehicle reaches a steady-state operation characterized by a constant wheel speed equal to $800\,rpm$ starting from t=1s as shown in figure 4.4. At t=3s, the road slope has been varied positively then negatively according to the cycle illustrated in figure 4.5. The road profile according to the road slope variation is shown in figure 4.6. The vehicle load torque and the demanded mechanical power are shown in figure 4.7. The resulting simulated and emulated PMSM phase currents are shown in figure 4.8.

From the analysis of these results, one can notice the following remarks:

- During climbing ($\theta > 0$), the load torque is positive and the mechanical power takes positive values. The system emulates an acceleration driving cycle as illustrated in figure 3.9(a),
- During downhill operation ($\theta < 0$), the load torque turns to negative and consequently the mechanical power takes negative values. The system emulates a regenerative braking cycle as illustrated in figure 3.9(b).

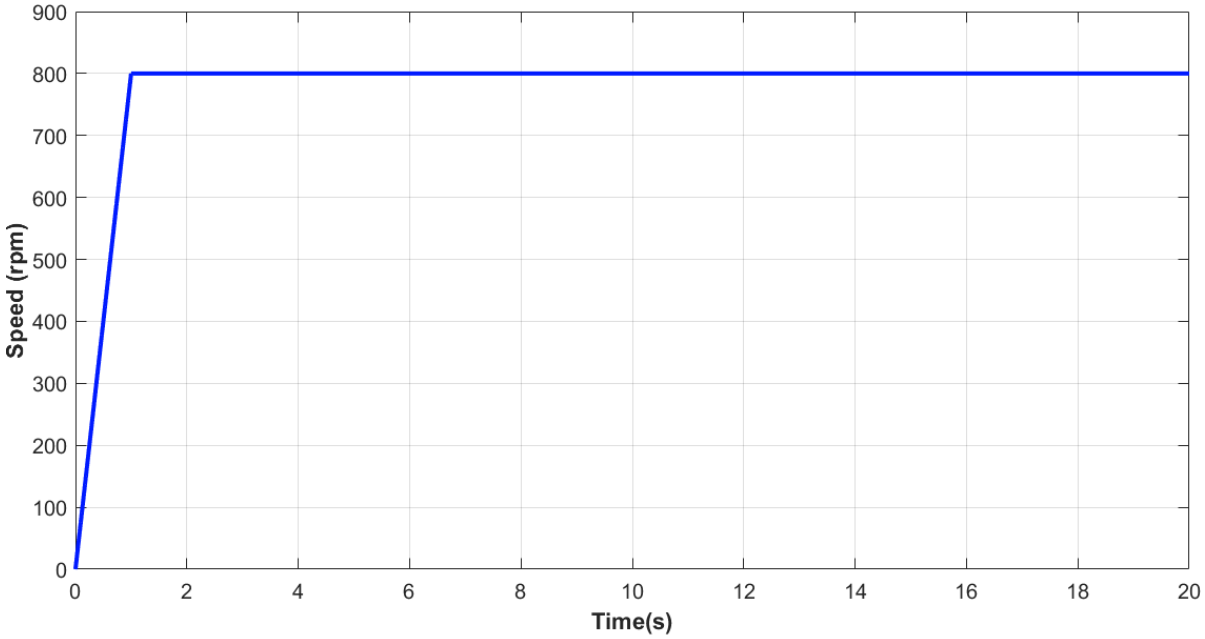

Figure 4.4: reference speed

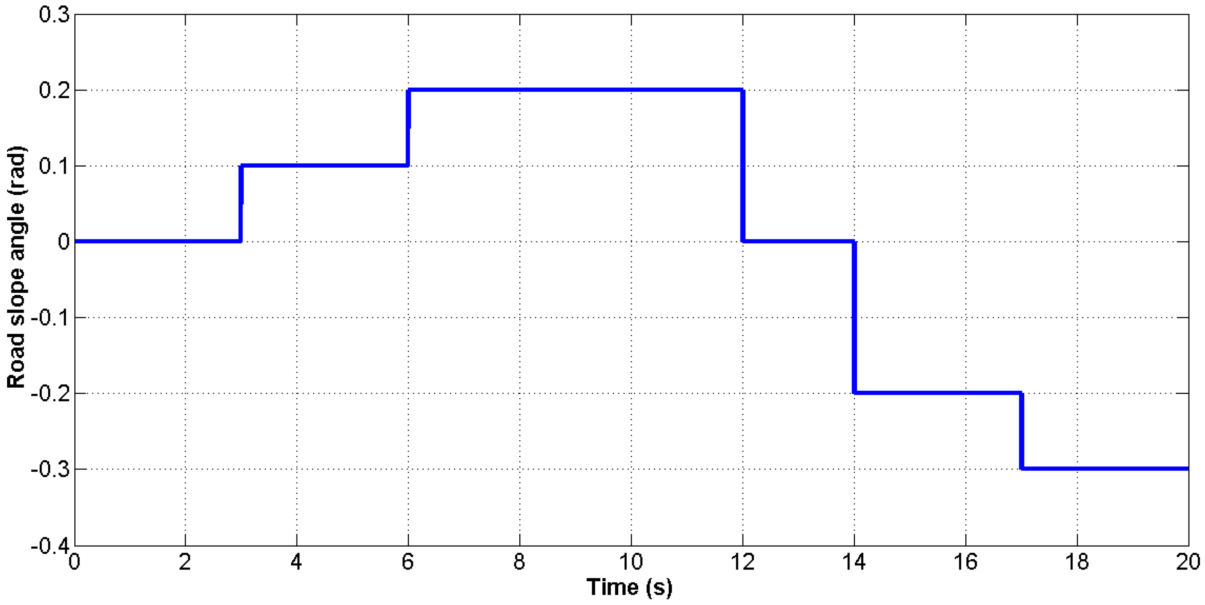

Figure 4.5: Road slope angle variation profile including up- and down-hill operations

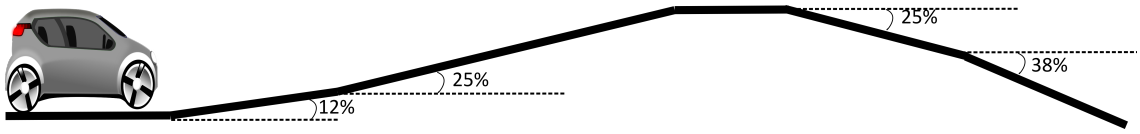

Figure 4.6: Road profile

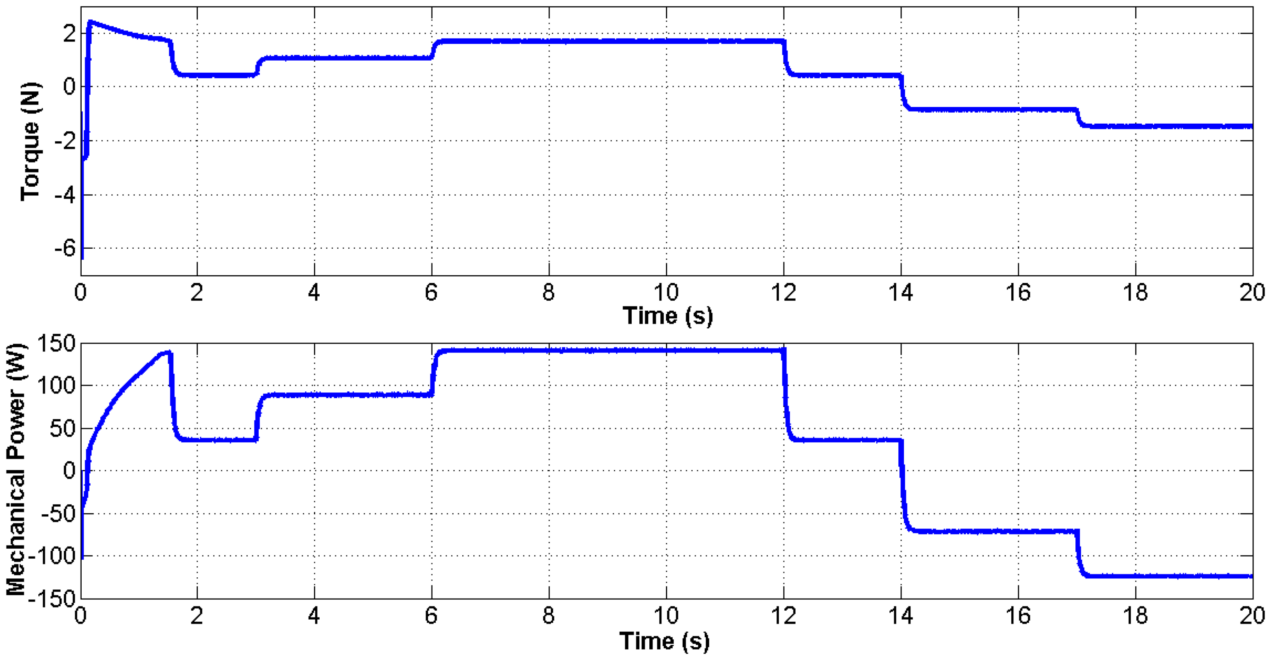

Figure 4.7: Load torque (top) and mechanical power (bottom) waveforms obtained under a constant speed (after t=1s) and a variable road slope angle according to the profile shown in figure 4.5

Moreover, it is to be noted that the simulated and emulated armature phase currents are in good agreement and that their amplitudes are proportional to the absolute value of the load torque shown in figure 4.7.

For the sake of a deeper investigation of the capabilities of the developed emulating system, the DC currents at the inputs of both converters as well as the DC voltage have been recorded and are shown in figure 4.9.

From the analysis of figure 4.9, it appears that:

- For a positive slope (roughly meaning the system is applying a positive torque), the tested converter operates as an inverter with a positive DC bus current at its input, while the load converter operates as a rectifier that has a negative DC bus current. This scenario emulates the acceleration cycle shown in figure 3.9(a);

- For a negative slope (starting from $t = 14s$), the tested converter operates as a

rectifier that has a negative DC bus current while the load converter operates as an inverter with a positive DC bus current. This scenario emulates the regenerative cycle shown in figure 3.9(b);

- In both phases, power losses in the system produce a difference in the DC current magnitudes.

In order to explain the last consideration, the power balance can be computed. The power balance of the system in motoring mode can be expressed as:

$$P_{in} = P_{losses} + P_{out} \tag{4.1}$$

where

- P_{in} is the input power from the DC link of the test inverter;
- P_{loss} is the total power loss in the test system;
- P_{out} is the output power regenerated to the DC bus from the load inverter.

As an example, at $t = 4s$ in figure 19 the input power is calculated as:

$$P_{in} = I_{in}V_{dc} = 2.5 * 24 = 60W \tag{4.2}$$

where I_{in} is the instantaneous value of the DC current and V_{dc} is the DC-link voltage. The total power loss in the system P_{loss} is mainly dissipated in the two converters and in the inductances. It can be calculated as follows:

$$P_{loss} = P_{conv1} + P_i + P_{conv2} \tag{4.3}$$

Where P_{conv1} and P_{conv2} are the losses in the first and second converter (the sum of conduction and switching losses) and P_i is the loss in the inductances.

The power loss in the inductances is caused by the Joule loss in the copper and in the iron core of the inductances. The copper wire resistance R_i and the core equivalent

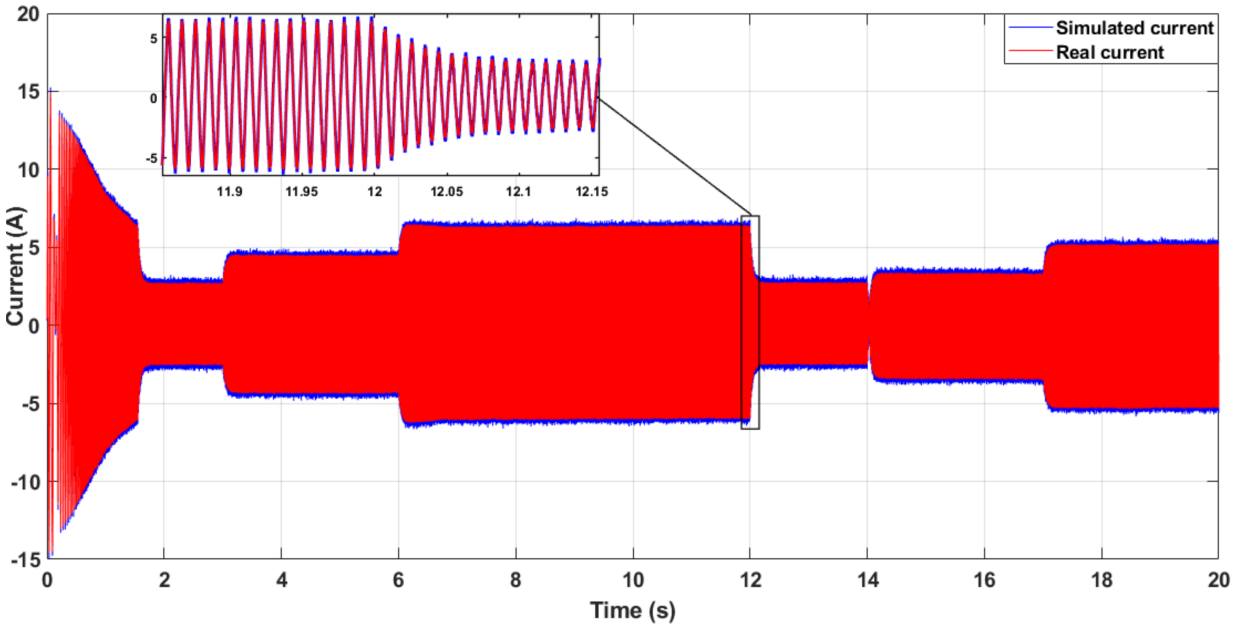

Figure 4.8: Simulated and emulated phase current variation during the road slope angle variation cycle: (blue) simulated current generated by the PXI, (red) measured current at the load inverter terminals

resistance R_μ have been experimentally calculated. Their values are:

$$\begin{cases} R_i = 0.3\Omega \\ \\ R_\mu = 4.58\Omega \end{cases} \tag{4.4}$$

Naming I_i the rms value of the AC phase current in the inductance, and I_a the active component of the current in the inductance, both measured experimentally. The power loss in the 3-phase inductance is:

$$\begin{aligned} P_i &= 3 * (R_i I_i^2 + R_\mu I_a^2) \\ \\ &= 3\left[0.3 * (3.18)^2 + 4.58 * 0.7^2\right] = 15.8W \end{aligned} \tag{4.5}$$

The measurement of P_i is in agreement with the value computed in Eq.4.5.

The losses in the two inverters have been measured and their values are:

$$\begin{cases} P_{conv1} = 4.2W \\ \\ P_{conv2} = 4.7W \end{cases} \tag{4.6}$$

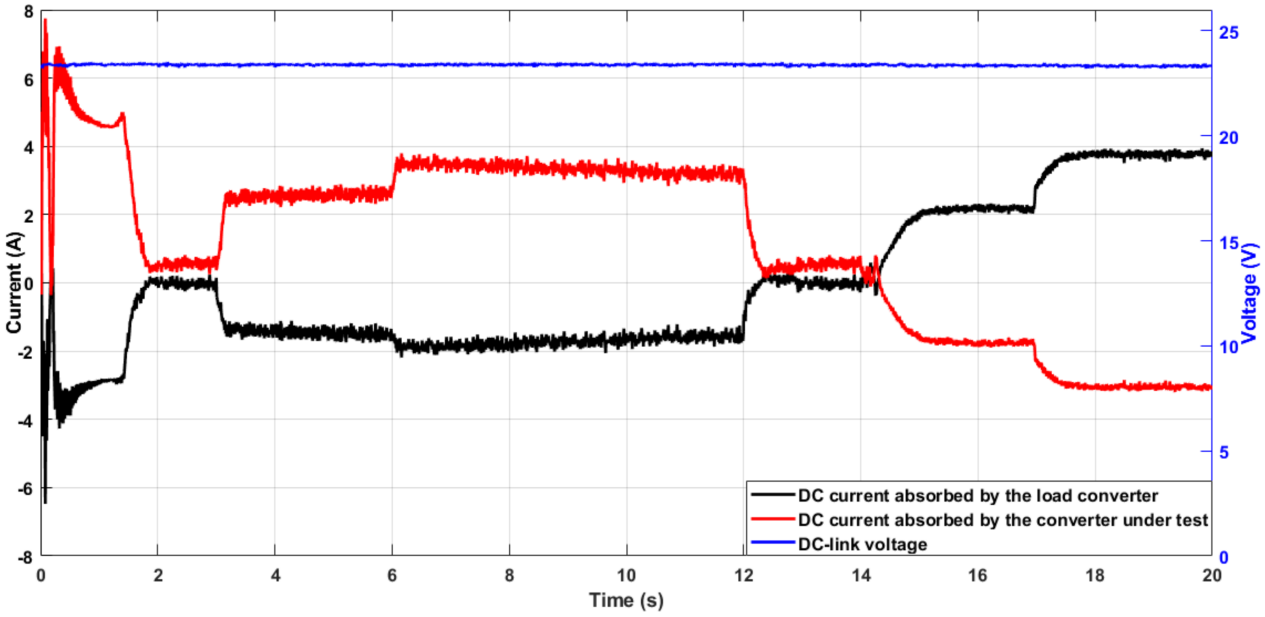

Figure 4.9: DC bus currents at the inputs of the two converters **Legend:** (red) of the tested converter, (black) of the load converter, (blue the DC-link voltage)

The total power loss in the system according to Eq.4.3 is $P_{loss} = 24.773W$.

From Eq.4.1 the output power can be calculated as follows:

$$P_{out} = P_{in} - P_{loss} = 35.2W \tag{4.7}$$

the output power can be expressed as a product of the output current I_{out} and the DC-link voltage as:

$$P_{out} = I_{out} Vdc \tag{4.8}$$

Finally, the output current can be calculated as:

$$I_{out} = P_{out}/V_{dc} = 1.46A \tag{4.9}$$

which is in agreement with the value in figure 4.9.

In the regenerative mode, i.e. starting from $t = 14s$, a reverse power flow establishes. In figure 4.9 the DC currents are different than at $t = 4s$ due to different values of the speed and torque, therefore the values of the losses are different.

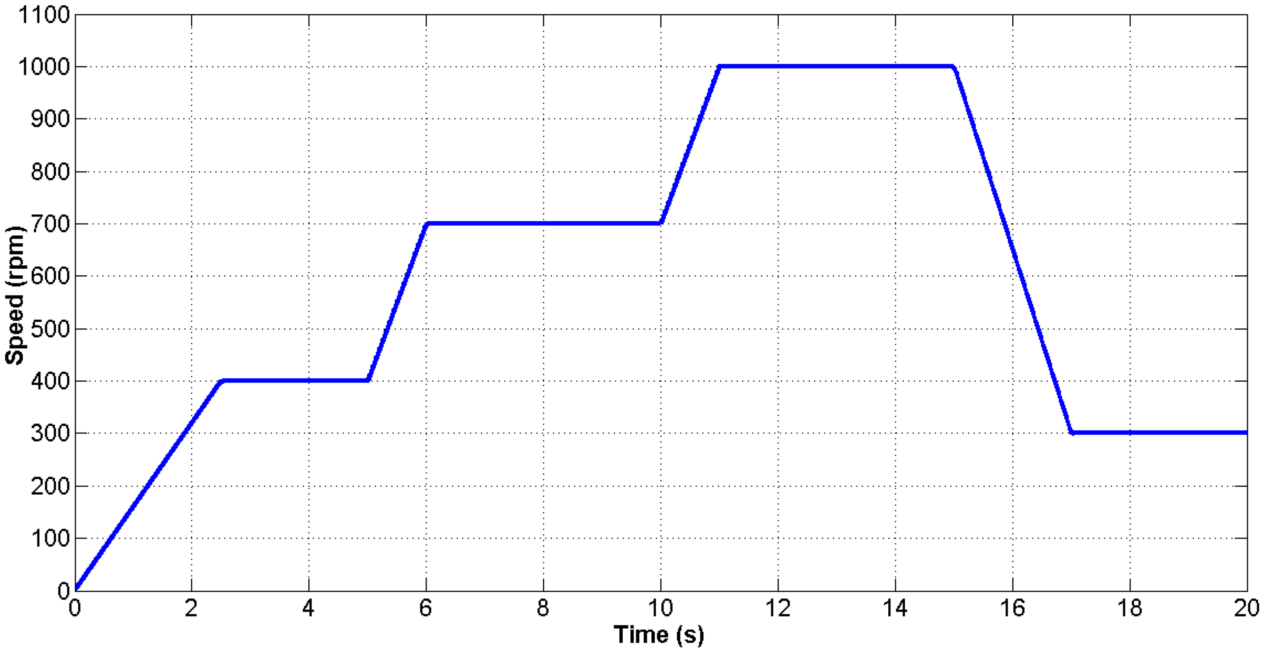

Figure 4.10: Reference speed cycle under a constant slope angle θ=+0.1rad

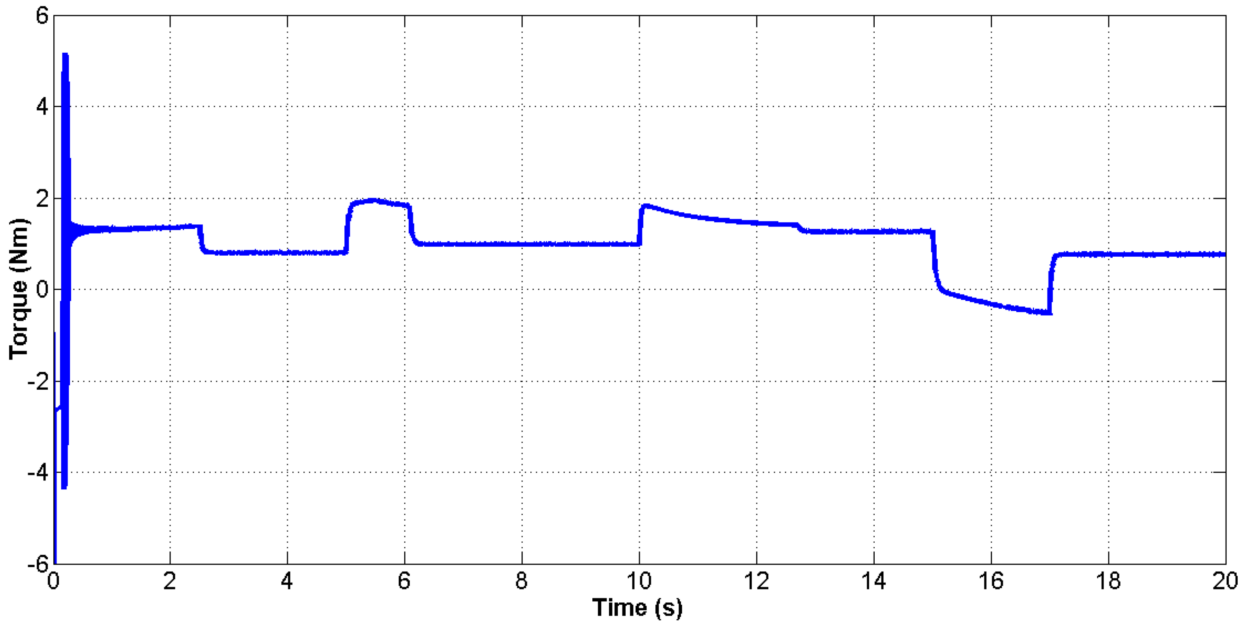

Figure 4.11: Load torque developed by the vehicle considering the reference speed cycle shown in figure 4.10.

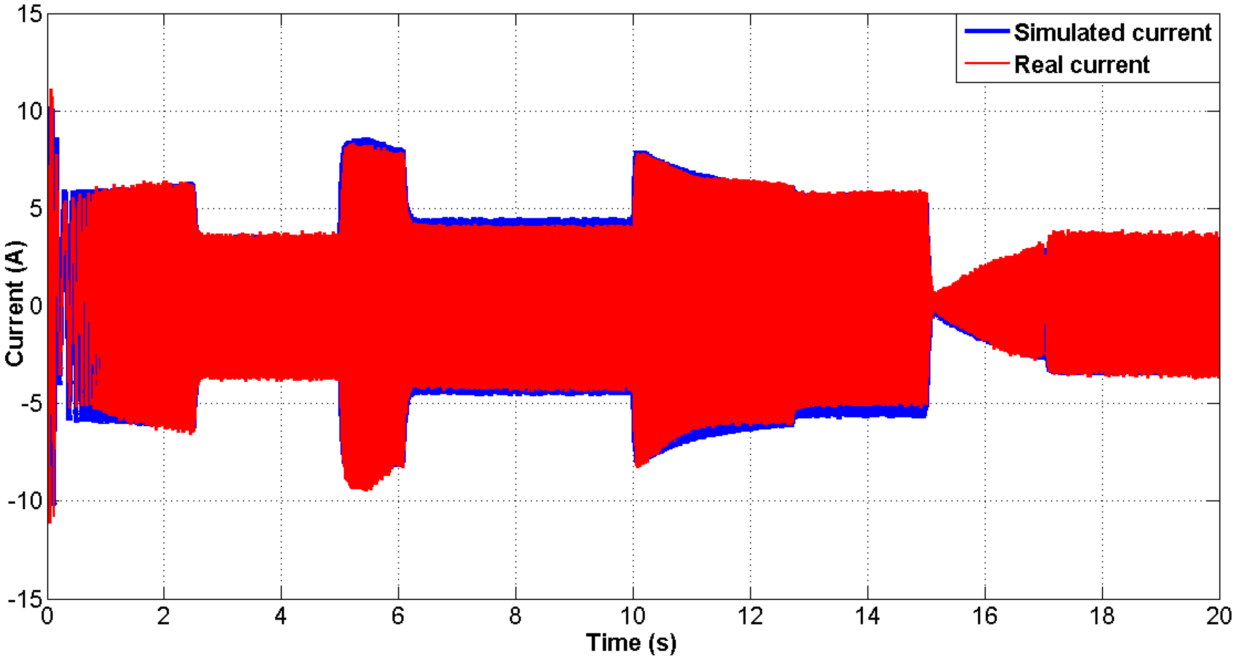

Figure 4.12: Simulated and emulated phase current under variable reference speed according to the cycle shown in figure 4.10. **Legend:** (blue) simulated, (red) emulated

Operation under constant road slope and variable speed

Let us consider the case where the vehicle is running under the following conditions:

- a constant road slope angle θ=+0.1rad,
- a speed cycle including a start-up, two accelerations, and a deceleration, as illustrated in figure 4.10.

The simulated load torque yielded by the vehicle model is shown in figure 4.11. The resulting simulated and emulated armature phase currents are shown in figure 4.12.

- at constant speed operation, the vehicle load torque is constant,
- during accelerations, the load torque is increased and the amplitudes of the simulated and real currents follow its absolute value,
- during decelerations, the load torque decreases and takes negative values starting from time equal to 13s. This offers the possibility of regenerative mode by transforming the kinetic energy into electricity that could be stored in the battery of an electric or a hybrid vehicle.

4.2.2 Case Study B Full scale testing system (ECE Urban Driving Cycle)

In case study B, the full-scale emulator was used to test a commercial drive. The industrial test bench system shown in 4.15, is developed in Loccioni group research labs. It has the same architecture of the test system used in case study A, and described in the previous chapters, but with high power level and a DC voltage up to 475V. The load drive used in the emulator is a custom drive. The tested inverter is provided by Loccioni customers from different automotive companies interested in the new testing facility.

The Economic Commission for Europe (ECE) standard driving cycle shown in figure 4.13 is an Urban Driving Cycle, also known as UDC. It was introduced for the first time in 1970 as part of ECE vehicle regulations. The cycle has been designed to represent typical driving conditions of busy European cities, and is characterized by low engine load, and low energy consumption .

It represents an urban vehicle driving in a traffic congestion obviously including frequent stops. When the engine starts, the car pauses for $11s$, then slowly accelerates to $15km/h$ in $4s$, cruises at constant speed for $8s$, brakes to a full stop in $5s$, then stops for 21s. At $49s$, the car slowly accelerates to $32km/h$ in $12s$, cruises for $24s$, slowly brakes to a full stop in $11s$, then pauses for another $21s$. At $117s$, the car slowly accelerates to $50km/h$ in $26s$, cruises for $12s$, decelerates to 35 km/h in $8s$, cruises for another $13s$, brakes to a full stop in $12s$, then pauses for $7s$. The cycle ends on $195s$ after a theoretical distance of 994.03 meters.

The full-scale was tested under the ECE driving cycle. The response of the system is shown in figure 4.14, where the simulated and emulated currents are compared. As in the previous case, the system is able to emulate correctly the behaviour of the IPM PMSM motor drive. The use of a standardized driving cycle validates the test bench by reproducing the real driving conditions of the EV in the virtual environment. Regeneration is correctly achieved during the braking stage.

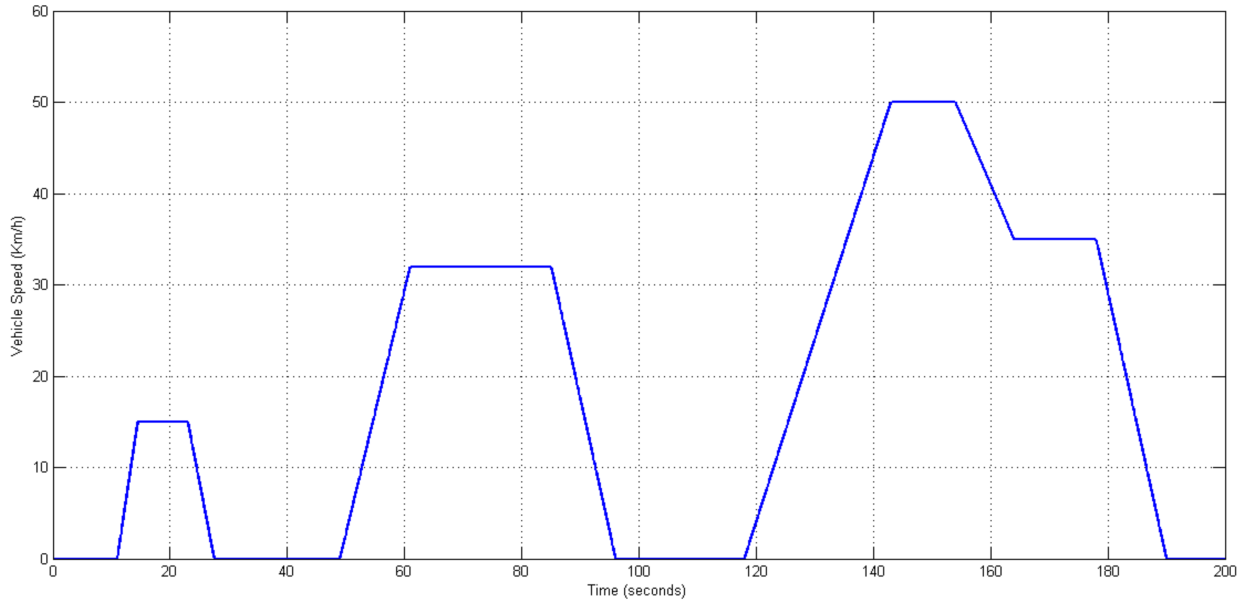

Figure 4.13: Reference speed ECE cycle.

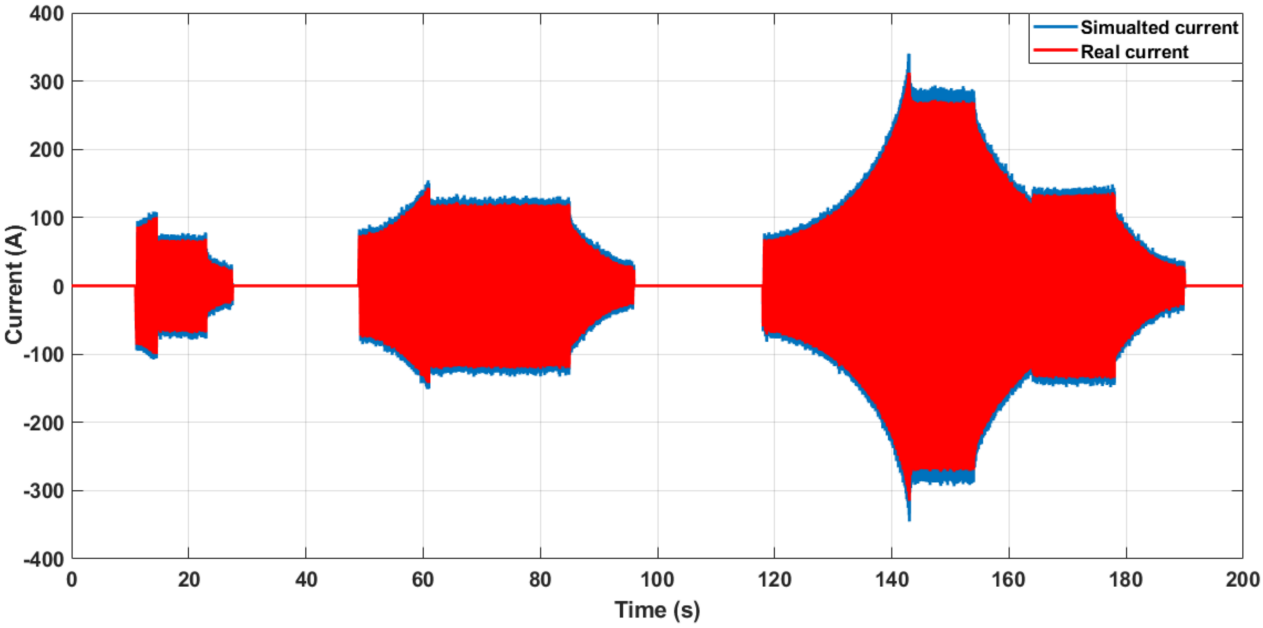

Figure 4.14: Simulated and real current variation during the Reference speed cycle shown in figure 4.13: (blue) simulated current generated by the PXI, (red) real current measured at the input of the load inverter.

Figure 4.15: The experimental industrial testing facility for electric drives for commercial EVs implemented in Loccioni

4.3 Conclusion

The experimental section showed the results of different tests carried out on the developed platform. In order to validate the proposed setting, different urban driving cycles have been emulated. Two case studies have been considered and implemented on a laboratory environment:

- Case study A a low power test bench system developed in chapter 2 and chapter 3, as a proof of concept. It has been tested with the following driving conditions:
  - a start-up cycle;
  - constant driving conditions (speed and slope);
  - constant speed and variable road slope;
  - constant road slope angle and variable speed.

- Case study B an industrial full-scale testing facility, developed in Loccioni group Laboratory, using the same concept and architecture as the case study A but with a high power factor. The tested inverter has been tested under the ECE urban driving cycle wich present typical driving conditions of busy European cities.

In both cases, a significant agreement between the simulation and emulation results has been found confirming the accuracy of the proposed testing facility.

The experimental results have shown that the proposed virtual machine can replicate the PMSM traction motor behaviour, during simulated vehicle driving cycles. In such a way, an inverter can be tested at actual power levels and under different driving conditions without the requirement of a real machine. Different machines and vehicles can be emulated by software. Only the parameters of the motor and vehicle model needs to be changed. It has also been shown with experimental results that the machine emulator is able to emulate both driving cycles of an electric vehicle which are the acceleration cycle and the regenerative braking cycle.

General Conclusion

The works synthesized in the present dissertation enabled the mastery of the HIL simulation, applied to the test of a variable speed drive dedicated to automotive propulsion chains. These latter involve different technological areas, including electric machines, power electronic converters, micro-informatics platforms, and automatic control strategies. This makes their simulation followed by their emulation crucial steps for their development. Accounting for the complexity of variable speed drives, their testing could be successfully achieved using the HIL simulation.

Our works have been initiated by a state of the art regarding the HIL method. An overview of the HIL-based RT simulation systems has been introduced, with emphasis on the RT simulation concept, the required HIL components and modules, the HIL main categories, and so on. Then a literature review exploring the historical development of the HIL technique and its recent applications in various sectors has been presented.

In the second chapter the industrial need to develop automotive inverter test systems has been highlighted. Two main types of automotive inverter test bed systems have been introduced. The first type represent the classical testing solution called the dayno test bench, where real mechanical components of the vehicle powertrain are included in the test system. The second type of inverter test bed systems, which is less known, is the HIL virtual testing facility. Where the electric machine and the remaining mechanical components of the vehicle power train are emulated with a power electronic emulator, also known as the electric machine emulator. The general architecture and the characteristics of both test solutions have been described.

A literature review of the HIL electric machine emulator test solution has been presented. Then a new HIL containing a machine emulator dedicated to automotive inverter testing has been proposed and described in details. The proposed emulator is connected to the inverter under test, and it is basically composed of a second inverter and a three phase inductor emulating a traction machine of an electric or hybrid vehicle. It has been shown that the proposed emulator is theoretically able to emulate both driving mode of an electric vehicle. In other words using the proposed emulator, it is possible to emulate an acceleration cycle as well as a regenerative braking cycle.

The value of the choke has been chosen following an analytical study aiming to minimize the current ripple, without introducing excessive delay in the current variation. The stability of the system has been demonstrated through the analysis of the transfer functions of the power system components. The stability range was assessed in terms of proportional gains of the PI regulators.

In the third chapter, our works have been achieved by the implementation of the HIL experimental bench dedicated to automotive electric drive tests. The required hardware used to implement the HIL test system has been presented. It consists in a NI PXI system, provided by the "National Instruments", used to simulate the control model in RT and to generate RT signals to control the inverter under test and the emulator.

The implemented test bench system consists in:

- a power system made up of two DC-AC converters connected through their AC sides by a three phase inductor. One among the converter is playing the role of an automotive inverter. The second is emulating the traction motor of an electric vehicle,

- a control system which is built around a NI PXI interface in which is embedded a real-time simulation HIL system. The communication with the power system is achieved through two analog signals: (i) the "speed" which is applied to the inverter under test, and (ii) the "torque" which is applied to the inverter emulating the traction motor.

The control system integrates in real-time the equations of three models:

- the PMSM (IPM or SPM) synchronous motor;
- the vector control;
- the vehicle dynamics.

The simulation control system has been implemented in the NI PXI interface. It considers a PMSM machine fed by a vector-controlled voltage source inverter and driving the wheels of an electric vehicle. The load torque considered in the mechanical equation of the PMSM is provided by the vehicle dynamics model.

The fourth chapter was devoted to the experimental test results. The results of different tests have been carried out on the developed platform. In order to validate the proposed setting, different urban driving cycles have been emulated. Two case studies have been considered and implemented on a laboratory environment. The first case has been implemented as a proof of concept. The second case has been developed on an industrial full-scale testing facility. In both cases, a significant agreement between the simulation and emulation results has been found. Furthermore, the regenerative braking capability exhibited by the developed platform has been highlighted and discussed.

Test results obtained considering the emulation of different accelerating and braking cycles have highlighted the potentialities of the developed test bench.

The implementation of the vehicle model in the control system adds more flexibility to the system in comparison to other similar solutions, allowing to emulate not only the electrical machine but also the whole vehicle powertrain and road conditions. Therefore it is possible to implement any kind of EV and road condition by simply changing the RT emulator parameters.

The proposed platform is characterised by the simplicity of the hardware used to build the machine emulator which makes the test system suitable for industrial applications on the basis of its cost-effectiveness, high-performances and power consumption.

$$\mathbf{M} = \begin{bmatrix} 2.4 \cdot 10^{-12} & K_{p1} - K_{Kp2} + 2.2 \cdot 10^{-12} & 1.44 * K_{p1} - 1.44 * K_{p2} \\ 4.4 \cdot 10^{-8} & 2.4 * K_{p1} - 2.4 * K_{p2} + 0.3 & 0 \\ A & 1.44 * K_{p1} - 1.44 * K_{p2} & 0 \\ B & 0 & 0 \\ 1.44 * K_{p1} - 1.44 * K_{p2} & 0 & 0 \end{bmatrix}$$

$$A = 9.27 \cdot 10^{-5} * K_{p1} - 3.17 \cdot 10^{-4} * K_{p2} + 2.07 \cdot 10^{-4}$$

$$B = \frac{(6.4 \cdot 10^{-8} * K_{p2} - 6.4 \cdot 10^{-8} * K_{p2}) + (2.4 * K_{p1} - 2.4 * K_{p2} + 0.3) * (A)}{A}$$

Bibliography

[1] J. Bélanger, P. Venne, and J.-N. Paquin, "The what, where, and why of real-time simulation," *Planet RT*, pp. 37–49, 01 2010.

[2] T. Berry, A. R. Daniels, and R. W. Dunn, "Real time simulation of power system transient behaviour," in *1991 Third International Conference on Power System Monitoring and Control*, 1991, pp. 122–127.

[3] M. D. Omar Faruque, T. Strasser, G. Lauss, V. Jalili-Marandi, P. Forsyth, C. Dufour, V. Dinavahi, A. Monti, P. Kotsampopoulos, J. A. Martinez, K. Strunz, M. Saeedifard, Xiaoyu Wang, D. Shearer, and M. Paolone, "Real-time simulation technologies for power systems design, testing, and analysis," *IEEE Power and Energy Technology Systems Journal*, vol. 2, no. 2, pp. 63–73, 2015.

[4] J. J. Sanchez-Gasca, R. D'Aquila, W. W. Price, and J. J. Paserba, "Variable time step, implicit integration for extended-term power system dynamic simulation," in *Proceedings of Power Industry Computer Applications Conference*, 1995, pp. 183–189.

[5] P. M. Menghal and A. J. Laxmi, "Real time simulation: Recent progress challenges," in *2012 International Conference on Power, Signals, Controls and Computation*, 2012, pp. 1–6.

[6] H. Fathy, Z. Filipi, J. Hagena, and J. Stein, "Review of hardware-in-the-loop simulation and its prospects in the automotive area - art. no. 62280e," *Proceedings of SPIE - The International Society for Optical Engineering*, vol. 6228, 05 2006.

[7] A. Wagener, T. Schulte, P. Waeltermann, and H. Schuette, "Hardware-in-the-loop test systems for electric motors in advanced powertrain applications," in *SAE Technical Paper*. SAE International, 04 2007.

[8] A. Bouscayrol, "Different types of hardware-in-the-loop simulation for electric drives," in *2008 IEEE International Symposium on Industrial Electronics*, 2008, pp. 2146–2151.

[9] W. Li, G. Joos, and J. Belanger, "Real-time simulation of a wind turbine generator coupled with a battery supercapacitor energy storage system," *IEEE Transactions on Industrial Electronics*, vol. 57, no. 4, pp. 1137–1145, 2010.

[10] S. Grubic, B. Amlang, W. Schumacher, and A. Wenzel, "A high-performance electronic hardware-in-the-loop drive–load simulation using a linear inverter (linverter)," *IEEE Transactions on Industrial Electronics*, vol. 57, no. 4, pp. 1208–1216, 2010.

[11] R. Isermann, J. Schaffnit, and S. Sinsel, "Hardware-in-the-loop simulation for the design and testing of engine-control systems," *Control Engineering Practice*, vol. 7, no. 5, pp. 643 – 653, 1999. [Online]. Available: http://www.sciencedirect.com/science/article/pii/S0967066198002056

[12] M. M. Sullivan, "Hybrid simulation of the apollo guidance and navigation system," *SAGE Journals, SIMULATION*, vol. 7, no. 1, pp. 25–33, 1966. [Online]. Available: https://doi.org/10.1177/003754976600700114

[13] F. J. Carrol and C. H. Spenny, "Apollo command and service module stabilization and control system design survey," *NASA technical note, Manned Spacecraft Center, Electronic Research Center, Cambridge*, December 1968.

[14] P. Sarhadi and S. Yousefpour, "State of the art: hardware in the loop modeling and simulation with its applications in design, development and implementation of system and control software," *International Journal of Dynamics and Control*, vol. 3, 01 2014.

[15] J. Drosdol and F. Panik, "The daimler-benz driving simulator a tool for vehicle development," in *SAE International Congress and Exposition*. SAE International, feb 1985. [Online]. Available: https://doi.org/10.4271/850334

[16] T. Suetomi, A. Horiguchi, Y. Okamoto, and S. Hata, "The driving simulator with large amplitude motion system," in *SAE Technical Paper*. SAE International, 02 1991. [Online]. Available: https://doi.org/10.4271/910113

[17] M. Karpenko and N. Sepehri, "Hardware-in-the-loop simulator for research on fault tolerant control of electrohydraulic flight control systems," in *IEEE 2006 American Control Conference*, 2006, pp. 7 pp.–.

[18] H. Spangenberg and H. Friehmelt, "Hardware-in-the-loop simulation with flight control actuators," *AIAA Modeling and Simulation Technologies Conference and Exhibit*.

[19] M. Jones, "The use of the open-loop onset point (olop) to predict rotorcraft pilot-induced oscillations," *CEAS Aeronautical Journal, Springer*, 2019.

[20] N. Anderson, B. Hagenauer, R. Erickson, and S. Bhandari, "Flight-testing of a uav aircraft for autonomous operation using piccolo ii autopilot," *AIAA Atmospheric Flight Mechanics Conference and Exhibit*. [Online]. Available: https://arc.aiaa.org/doi/abs/10.2514/6.2008-6568

[21] M. Shaqura and C. Claudel, "A hybrid system approach to airspeed, angle of attack and sideslip estimation in unmanned aerial vehicles," in *2015 International Conference on Unmanned Aircraft Systems (ICUAS)*, 2015, pp. 723–732.

[22] N. Gans, W. Dixon, R. Lind, and A. Kurdila, "A hardware in the loop simulation platform for vision-based control of unmanned air vehicles," *Mechatronics*, vol. 19, no. 7, pp. 1043 – 1056, 2009, special Issue on Hardware-in-the-loop simulation. [Online]. Available: http://www.sciencedirect.com/science/article/pii/S0957415809001263

[23] Z. Zhang, W. Yang, Z. Shi, and Y. Zhong, "Hardware-in-the-loop simulation platform for unmanned aerial vehicle swarm system: Architecture and application," in *2020 39th Chinese Control Conference (CCC)*, 2020, pp. 58–64.

[24] H. Min, Z. Guoqiang, and G. Yudong, "Thruster control for micro-satellite attitude and hardware-in-the-loop demonstration," in *2012 International Conference on Industrial Control and Electronics Engineering*, 2012, pp. 588–591.

[25] K. S. Badaruddin, J. C. Hernandez, and J. M. Brown, "The importance of hardware-in-the-loop testing to the cassini mission to saturn," in *2007 IEEE Aerospace Conference*, 2007, pp. 1–9.

[26] P. Tobbe, A. Matras, D. Walker, H. Wilson, C. Fulton, N. Alday, K. Betts, R. Hughes, and M. Turbe, "Real-time hardware-in-the-loop simulation of ares i launch vehicle."

[27] J. Leitner, "A hardware-in-the-loop testbed for spacecraft formation flying applications," in *2001 IEEE Aerospace Conference Proceedings (Cat. No.01TH8542)*, vol. 2, 2001, pp. 2/615–2/620 vol.2.

[28] R. Skjetne and O. Egeland, "Hardware-in-the-loop testing of marine control systems," *46th Conference on Simulation and Modeling (SIMS),Trondheim, Norway*, 10 2005.

[29] K. Marouani, H. Guendouz, B. Tabbache, F. Khoucha, and A. Kheloui, "Experimental investigation of an emulator "hardware in the loop" for electric naval propulsion system," in *IEEE 21st Mediterranean Conference on Control and Automation*, 2013, pp. 125–130.

[30] A. Hwang, S. Yoon, T. Kim, D. Kwon, C. Choi, and H. Cho, "Verification of unmanned underwater vehicle with velocity over 10 knots guidance control system based on hardware in the loop simulation," in *IEEE OCEANS 2009*, 2009, pp. 1–5.

[31] M. Woolsey and R. Jarnagin, "Design, implementation, and refinement of a hardware-in-the-loop simulator for a hovering auv," in *IEEE Oceans 2012*, 2012, pp. 1–4.

[32] H. Li, M. Steurer, K. L. Shi, S. Woodruff, and D. Zhang, "Development of a unified design, test, and research platform for wind energy systems based on hardware-in-the-loop real-time simulation," *IEEE Transactions on Industrial Electronics*, vol. 53, no. 4, pp. 1144–1151, 2006.

[33] A. Helmedag, T. Isermann, A. Monti, N. R. Averous, M. Stieneker, and R. W. De Doncker, "Multi-physics power hardware in the loop test bench for on-shore wind turbine nacelles," in *2013 IEEE ECCE Asia Downunder*, 2013, pp. 221–226.

[34] B. Lu, X. Wu, H. Figueroa, and A. Monti, "A low-cost real-time hardware-in-the-loop testing approach of power electronics controls," *IEEE Transactions on Industrial Electronics*, vol. 54, no. 2, pp. 919–931, 2007.

[35] A. Kuperman, Y. Horen, and S. Tapuchi, "A differential state-space approach to simultaneous emulation of uncertainties and disturbances in voltage-controlled brushless motors," *IEEE Transactions on Industrial Electronics*, vol. 57, no. 2, pp. 727–734, 2010.

[36] C. Carstensen and J. Biela, "10kv/30ka unipolar arbitrary voltage source for hardware-in-the-loop simulation systems for hvdc circuit breakers," in *Proceedings of the 2011 14th European Conference on Power Electronics and Applications*, 2011, pp. 1–10.

[37] H. Temeltas, M. Gokasan, S. Bogosyan, and A. Kilic, "Hardware in the loop simulation of robot manipulators through internet in mechatronics education," in *IEEE 2002 28th Annual Conference of the Industrial Electronics Society. IECON 02*, vol. 4, 2002, pp. 2617–2622 vol.4.

[38] C. Qi, F. Gao, X. Zhao, Q. Wang, and Q. Sun, "Distortion compensation for a robotic hardware-in-the-loop contact simulator," *IEEE Transactions on Control Systems Technology*, vol. 26, no. 4, pp. 1170–1179, 2018.

[39] A. Martin and M. R. Emami, "Dynamic load emulation in hardware-in-the-loop simulation of robot manipulators," *IEEE Transactions on Industrial Electronics*, vol. 58, no. 7, pp. 2980–2987, 2011.

[40] I. Tejado, J. Serrano, E. Pérez, D. Torres, and B. M. Vinagre, "Low-cost hardware-in-the-loop testbed of a mobile robot to support learning in automatic control and robotics," *IFAC-PapersOnLine*, vol. 49, no. 6, pp. 242 – 247, 2016, 11th IFAC Symposium on Advances in Control Education ACE 2016. [Online]. Available: http://www.sciencedirect.com/science/article/pii/S2405896316303901

[41] L. Chu, Y. Hou, M. Liu, J. Li, Y. Gao, and M. Ehsani, "Development of air-abs-hil-simulation test bench," in *2007 IEEE Vehicle Power and Propulsion Conference*, 2007, pp. 691–695.

[42] Jae-Cheon Lee and Myuug-Won Suh, "Hardware-in-the loop simulator for abs/tcs," in *Proceedings of the 1999 IEEE International Conference on Control Applications (Cat. No.99CH36328)*, vol. 1, 1999, pp. 652–657 vol. 1.

[43] Jihoon Roh, Kangwon Lee, Jongil Lee, Seungkyu Oh, Hyoungsoo Kim, and Jinhee Jang, "Development of hil simulator for the sensitivity analysis of factors influencing esc performance," in *2009 ICCAS-SICE*, 2009, pp. 4058–4062.

[44] Lifu Li and Jing Hong, "Hardware-in-loop simulation method for electronic stability program based on virtual integrated technology," in *2009 IEEE International Conference on Information and Automation, Zhuhai, Macau, China*, 2009, pp. 1188–1192.

[45] X. Yang and G. Zhu, "Si and hcci combustion mode transition control of an hcci capable si engine," *IEEE Transactions on Control Systems Technology*, vol. 21, no. 5, pp. 1558–1569, 2013.

[46] X. Jie, W. Feng, Y. Dongwei, Z. Yongguang, and G. Qiang, "An application of real-time engine model in hils simulation and testing platform based on simulink," in

2010 International Conference on Digital Manufacturing Automation, vol. 1, 2010, pp. 176–180.

[47] T. Kim, B. Lee, B. Lee, H. Song, and S. Shin, "Hils-based analysis of characteristics and performance of internal combustion engine vehicles with varying battery types," in *2016 IEEE Transportation Electrification Conference and Expo, Asia-Pacific (ITEC Asia-Pacific)*, 2016, pp. 326–331.

[48] J. Mamala, S. Brol, and G. Graba, "Hardware-in-the-loop type simulator of spark ignition engine control unit," in *2013 International Symposium on Electrodynamic and Mechatronic Systems (SELM)*, 2013, pp. 41–42.

[49] C. Bernard, S. Bolognani, L. Peretti, and M. Zigliotto, "Steering chain hil simulator for steer-by-wire systems," in *2006 12th International Power Electronics and Motion Control Conference*, 2006, pp. 1784–1789.

[50] G. Zhu, H. Yang, and F. Yu, "Controller design for an automobile steer-by-wire system," in *2019 IEEE 28th International Symposium on Industrial Electronics (ISIE)*, 2019, pp. 1492–1497.

[51] S. Končar, Z. Lukač, N. Stojanović, and I. Kolak, "Development of automotive video logger hil device for adas/ad algorithms development and testing," in *2020 Zooming Innovation in Consumer Technologies Conference (ZINC)*, 2020, pp. 295–300.

[52] U. Zivkovic, O. Dekic, Z. Lukac, and M. Milosevic, "Hil based solution for adas software development and verification," in *2019 IEEE 9th International Conference on Consumer Electronics (ICCE-Berlin)*, 2019, pp. 396–399.

[53] S. Zhao, L. Zhang, Y. Shen, and Y. Zhai, "Research on benchmarking of smart camera based on hardware-in-loop (hil)," in *2020 IEEE 4th Information Technology, Networking, Electronic and Automation Control Conference (ITNEC)*, vol. 1, 2020, pp. 1819–1823.

[54] J. Sobotka and J. Novak, "Digital vehicle radar sensor target simulation," in *2020 IEEE International Instrumentation and Measurement Technology Conference (I2MTC)*, 2020, pp. 1–5.

[55] A. S. Abdelrahman, K. S. Algarny, and M. Z. Youssef, "A novel platform for power-train modeling of electric cars with experimental validation using real-time hardware in the loop (hil): A case study of gm second generation chevrolet volt," *IEEE Transactions on Power Electronics*, vol. 33, no. 11, pp. 9762–9771, 2018.

[56] J. Adit, "Powertrain and chassis hardware-in-the-loop (hil) simulation of autonomous vehicle platform," in *SAE Technical Paper*. SAE International, 09 2017.

[57] A. Soltani and F. Assadian, "A hardware-in-the-loop facility for integrated vehicle dynamics control system design and validation," *IFAC-PapersOnLine*, vol. 49, no. 21, pp. 32 – 38, 2016, 7th IFAC Symposium on Mechatronic Systems MECHATRONICS 2016. [Online]. Available: http://www.sciencedirect.com/science/article/pii/S2405896316320973

[58] K. Enisz, D. Fodor, I. Szalay, and L. Kovacs, "Reconfigurable real-time hardware-in-the-loop environment for automotive electronic control unit testing and verification," *IEEE Instrumentation Measurement Magazine*, vol. 17, no. 4, pp. 31–36, 2014.

[59] V. Josef, G. Robert, K. Petr, L. František, and M. Karel, "Hardware-in-the-loop simulation for automotive parking assistant control units," in *Proceedings of the 16th International Conference on Mechatronics - Mechatronika 2014*, 2014, pp. 325–330.

[60] Y. Fan and F. Jiang, "Hardware-in-the-loop simulation of electronic control unit used on automated mechanical transmission," in *2010 2nd International Conference on Computer Engineering and Technology*, vol. 3, 2010, pp. V3–642–V3–644.

[61] M. Z. M. Nasir, A. Dwijotomo, M. A. Abdullah, and N. Tamaldin, "Development motor control unit for electronic steering system test rig," in *2014 IEEE 10th International Colloquium on Signal Processing and its Applications*, 2014, pp. 42–47.

[62] J. Lu, Y. Guo, and H. Wang, "Rapid prototyping real-time simulation platform for digital electronic engine control," in *2008 2nd International Symposium on Systems and Control in Aerospace and Astronautics*, 2008, pp. 1–5.

[63] B. Soner, A. Içke, A. C. Mert, U. Basaran, S. T. Impram, and I. Sahin, "Development of an electronic control unit for pmsm drives in automotive applications," in *2015 9th International Conference on Electrical and Electronics Engineering (ELECO)*, 2015, pp. 680–684.

[64] M. Kloc, R. Weigel, and A. Koelpin, "Making real-time hardware-in-the-loop testing of automotive electronic control units wireless," in *2016 International Conference on Advanced Technologies for Communications (ATC)*, 2016, pp. 407–412.

[65] D. J. Verburg, A. C. M. van der Knaap, and J. Ploeg, "Vehil: developing and testing intelligent vehicles," in *Intelligent Vehicle Symposium, 2002. IEEE*, vol. 2, 2002, pp. 537–544 vol.2.

[66] R. Rothe and K. Hameyer, "Life expectancy calculation for electric vehicle traction motors regarding dynamic temperature and driving cycles," in *2011 IEEE International Electric Machines Drives Conference (IEMDC)*, 2011, pp. 1306–1309.

[67] J. Fan, C. Zhang, Z. Wang, Y. Dong, C. E. Nino, A. R. Tariq, and E. G. Strangas, "Thermal analysis of permanent magnet motor for the electric vehicle application considering driving duty cycle," *IEEE Transactions on Magnetics*, vol. 46, no. 6, pp. 2493–2496, 2010.

[68] F. Xu, L. Chen, and N. Narayanachar, "Traction inverter evaluation method based on driving cycles for electric and hybrid electric vehicles," in *2016 IEEE Energy Conversion Congress and Exposition (ECCE)*, 2016, pp. 1–6.

[69] M. Paulweber and K. Lebert, *Powertrain Instrumentation and Test Systems*. Springer International Publishing, 2016.

[70] N. Othman and H. Daniyal, "Investigation on chassis dynamometer with capability to test regenerative braking function," *International Journal of Power Electronics and Drive Systems (IJPEDS)*, vol. 6, pp. 657–664, 09 2015.

[71] S. Van Sterkenburg, E. Rietveld, F. Rieck, B. Veenhuizen, and H. Bosma, "Analysis of regenerative braking efficiency — a case study of two electric vehicles operating in the rotterdam area," in *2011 IEEE Vehicle Power and Propulsion Conference*, 2011, pp. 1–6.

[72] K. M. Rahman and S. E. Schulz, "High-performance fully digital switched reluctance motor controller for vehicle propulsion," *IEEE Transactions on Industry Applications*, vol. 38, no. 4, pp. 1062–1071, 2002.

[73] K. M.Rahman and S. E. Schulz, "Design of high-efficiency and high-torque-density switched reluctance motor for vehicle propulsion," *IEEE Transactions on Industry Applications*, vol. 38, no. 6, pp. 1500–1507, 2002.

[74] H. J. Slater, D. J. Atkinson, and A. G. Jack, "Real-time emulation for power equipment development. ii. the virtual machine," *IEE Proceedings - Electric Power Applications*, vol. 145, no. 3, pp. 153–158, 1998.

[75] A. Monti, S. D'Arco, Y. Work, and A. Lentini, "A virtual testing facility for elevator and escalator systems," in *2007 IEEE Power Electronics Specialists Conference*, 2007, pp. 820–825.

[76] T. Boller and R. M. Kennel, "Virtual machine — a hardware in the loop test for drive inverters," in *2009 13th European Conference on Power Electronics and Applications*, 2009, pp. 1–5.

[77] A. Monti, S. D'Arco, and A. Deshmukh, "A new architecture for low cost power hardware in the loop testing of power electronics equipments," in *2008 IEEE International Symposium on Industrial Electronics*, 2008, pp. 2183–2188.

[78] S. Uebener and J. Böcker, "Application of an e-machine emulator for power converter tests in the development of electric drives," in *European Electric Vehicle Congress (EEVC)*, 2012, pp. 1–9.

[79] G. M. Casolino, M. AlizadehTir, A. Andreoli, M. Albanesi, and F. Marignetti, "Software-in-the-loop simulation of a test system for automotive electric drives," in *IECON 2016 - 42nd Annual Conference of the IEEE Industrial Electronics Society*, 2016, pp. 1882–1887.

[80] K. Saito and H. Akagi, "A power hardware-in-the-loop (p-hil) test bench using two modular multilevel dscc converters for a synchronous motor drive," *IEEE Transactions on Industry Applications*, vol. 54, no. 5, pp. 4563–4573, 2018.

[81] O. Vodyakho, M. Steurer, C. S. Edrington, and F. Fleming, "An induction machine emulator for high-power applications utilizing advanced simulation tools with graphical user interfaces," *IEEE Transactions on Energy Conversion*, vol. 27, no. 1, pp. 160–172, 2012.

[82] M. A. Masadeh, K. S. Amitkumar, and P. Pillay, "Power electronic converter-based induction motor emulator including main and leakage flux saturation," *IEEE Transactions on Transportation Electrification*, vol. 4, no. 2, pp. 483–493, 2018.

[83] K. S. Amitkumar, R. S. Kaarthik, and P. Pillay, "A versatile power-hardware-in-the-loop-based emulator for rapid testing of transportation electric drives," *IEEE Transactions on Transportation Electrification*, vol. 4, no. 4, pp. 901–911, 2018.

[84] T. Wu, M. Misra, Y. Jhang, C. Yang, and Y. Xu, "A variable dc bus voltage based power hardware-in-the-loop emulation of electric motors with wide variation in interface filter inductance," in *2018 International Power Electronics Conference (IPEC-Niigata 2018 -ECCE Asia)*, 2018, pp. 3884–3889.

[85] Y. Boukadida, A. Masmoudi, G. M. Casolino, F. Marignetti, A. Andreoli, and M. Albanesi, "Automotive propulsion drive emulation using two cascaded inverters," in

2018 Thirteenth International Conference on Ecological Vehicles and Renewable Energies (EVER), 2018, pp. 1–7.

[86] Y. Boukadida, F. Marignetti, G. M. Casolino, A. Masmoudi, A. Andreoli, and M. Albanesi, "Emulation and testing for automotive propulsion drive using two cascaded inverters," *IEEE Transactions on Industry Applications*, vol. 56, no. 2, pp. 1766–1783, 2020.

[87] R. Krishnan, *Electric Motor Drives: Modeling, Analysis, and Control*. Upper Saddle River: Prentice Hall, 02 2001.

[88] M. Dagbagi, A. Hemdani, L. Idkhajine, M. W. Naouar, E. Monmasson, and I. Slama-Belkhodja, "Adc-based embedded real-time simulator of a power converter implemented in a low-cost fpga: Application to a fault-tolerant control of a grid-connected voltage-source rectifier," *IEEE Transactions on Industrial Electronics*, vol. 63, no. 2, pp. 1179–1190, 2016.

[89] F. Montano, T. Ould-Bachir, and J. P. David, "An evaluation of a high-level synthesis approach to the fpga-based submicrosecond real-time simulation of power converters," *IEEE Transactions on Industrial Electronics*, vol. 65, no. 1, pp. 636–644, 2018.

[90] M. Wetzel and M. Dewey, "The pxi standard — a summary of updates and enhancements to the pxi specifications," in *2019 IEEE AUTOTESTCON*, 2019, pp. 1–4.

[91] S. Morimoto, M. Sanada, and Y. Takeda, "Effects and compensation of magnetic saturation in flux-weakening controlled permanent magnet synchronous motor drives," *IEEE Transactions on Industry Applications*, vol. 30, no. 6, pp. 1632–, 1994.

[92] S. Carpiuc and C. Lazar, "Fast real-time constrained predictive current control in permanent magnet synchronous machine-based automotive traction drives," *IEEE Transactions on Transportation Electrification*, vol. 1, no. 4, pp. 326–335, 2015.

[93] Y. Boukadida, A. Masmoudi, G. M. Casolino, and F. Marignetti, "A simple assessment of the dynamics of the road vehicles," in *2018 Thirteenth International Conference on Ecological Vehicles and Renewable Energies (EVER)*, 2018, pp. 1–6.

[94] I. Husain, "Electric and hybrid vehicles design fundamentals," *CRC Press*, 01 2005.

[95] R. Rajamani, *Vehicle Dynamics and Control*, ser. Mechanical Engineering Series. Springer US, 2006.

[96] H.Pacejka, *Tire and Vehicle Dynamics*. ELSEVIER SCIENCE AND TECHNOLOGY Imprint Butterworth-Heinemann Ltd, 01 2002.